An Automated Tissue Digester for Pancreatic Islet Production

by

Zhongliang Lu

A dissertation submitted to the Graduate Faculty of
Auburn University
in partial fulfillment of the
requirements for the Degree of
Doctor of Philosophy

Auburn, Alabama
December 14, 2013

Keywords: Pancreas Digestion, Islets of Langerhans, Tissue Digester,
Time-exposure Photography, CFD Simulation, Uniform Shear Environment

Approved by

Thomas R. Hanley, Chair, Professor of Chemical Engineering
Mario R. Eden, Department Chair, Professor of Chemical Engineering
Steve R. Duke, Associate Professor of Chemical Engineering
Allan E. David, Assistant Professor of Chemical Engineering
Paul W. Todd, Chief Scientist, Techshot Inc.
Robert C. McCarthy, President, VitaCyte LLC.

Abstract

Pancreatic digestion is the primary step in preparing islets of Langerhans for clinical transplantation for restoring euglycemia in Type-1 diabetes patients. The yield of islets from the traditional method developed by Ricordi et al. tends to be variable and depends on several parameters. Operator function (shaking the vessel by hand) also produces variability from case to case and can cause damage to the recovered islets. The purpose of this dissertation is to design an automated digestion unit through the incorporation of an automated horizontally rotating bioreactor (the modified Dynacult reactor or MDR) consisting of a rotating outer cylindrical shell and a counter-rotating core both with hemispherical baffles. The new design is capable of producing reproducible operating parameters for the consistent preparation of islets.

Using computational fluid dynamics (CFD), a discrete phase model (DPM) is used to predict the flow patterns in the MDR and Ricordi chamber. CFD analysis and comparison of flow variable contours between above two digesters indicates that MDR has predictable, controllable fluid shear environment and optimized differential rotation mode at 120 ml/min velocity inlet and 100 rpm rotation speed. The superiority of the MDR model is demonstrated through the comparison of simulation data with that of Ricordi chamber, in which are found higher and lower extremes of shear rate, Reynolds' number and energy dissipation rate. These characteristics of the newly designed digester can be applied to an automatic mode (controlled rotation speed) instead of manual (shaking) operation.

The particle dispersion test reveals that the particles will move along a certain path controlled by the action of different hydrodynamic forces. Localized turbulent flow can be seen through the transparent shell wall. The complete mixing process occurs in the intermediate region between adjacent vanes and double walls without any sedimentation of particles. In particle tracking tests, a new application in the Image-Pro Premier software called "Fiber Separation and Measurement App" is introduced to accomplish the automatic identification of particle streaks that are formed using digital photography with a slow shutter speed such as 1/40 s. High shutter speed has little impact on the distribution of streak lengths while the lower shutter speed will cause streaks that allow measurements in the low velocity zone of a log scale histogram. Almost 100 per cent of particle velocity determined by the experiment is distributed in the numerical range of velocity 0.01 m/s to 0.2 m/s at 1/40s, chosen as the optimal shutter speed. Lengths of particle streaks give good agreement between experimental and numerical results.

A pig pancreas infused intraductally with collagenase enzyme blend is digested by using both MDR and Ricordi chamber in a parallel test in order to compare the islet yield and other relevant parameters between them. Then, the experimental data such as mean islet diameter and islet equivalent quantification (IEQ) are categorized and presented as two-series histograms for further analysis and comparison. In the example test the donor sow had an exceptionally large pancreas and smaller islets than typical one (many of them are less than 100 μm). The MDR digestion proceeded more rapidly and uniformly than that in the Ricordi chamber, and there is clear evidence that excessive digestion occurred in the MDR. In addition, the digestion process in the MDR is more extensive than in the Ricordi chamber. Exocrine tissue is digested to smaller fragments and there are no islets attached to exocrine tissue in the MDR while 32.61 per

cent of the islets are still embedded in or mantled by larger tissue pieces in the Ricordi chamber digests. The main advantages of the MDR digester are recovery of cleaner islets that are easier to purify from the surrounding tissue, higher average shear rate for more rapid, uniform digestion, and lack of extremes in shear rate and energy dissipation rate.

Acknowledgments

Table of Contents

List of Figures

List of Tables

Chapter 1 - Introduction

1.1 - Treatment of diabetes

According to CDC reports in 2008, 24 million Americans, eight per cent of the population, are diabetic. Three or more per cent of the U. S. population have type 1 diabetes and are dependent on frequent insulin injections. Diabetes costs the US economy $132 billion per year, $92 billion in direct medical costs. It has been suggested that large quantities of pure viable donor islets are necessary for transplantation to treat type 1 diabetes, which afflicts over 800,000 in the U.S alone. Islet transplantation can prevent the development of diabetic complications because of the role played by C-peptide, a by-product of insulin processing. Hence, biological replacement of destroyed or functionally impaired β cells with normal islet transplants remains the best option to achieve glycemic control and prevents the development of disabling complications. Still, major obstacles remain for routine use of islet transplants as a treatment option. These obstacles include the shortage of pancreas from human donors and the need to prevent transplant rejection by the use of immunosuppressive drugs, which are often toxic to β cells and cause other adverse effects in transplant recipients. The ultimate goal in transplantation is the unlimited availability of organs or tissue to be transplanted in a simple procedure that requires no immunosuppressive drugs.

Isolation of the islets is the primary step in preparing the islets for the transplantation. For decades, patients with diabetes have been treated with porcine insulin, and the pig is regarded as the ideal source of islet cells for clinical xenotransplantation. Porcine tissue has advantages for islet transplantation not only because of adequate tissue availability, but also because porcine insulin has proven effective in humans. In addition, human islet production is expensive and limited by the number of available donor pancreas. The swine model offers a

unique advantage when compared to human sources: the possibility of standardization of the isolation procedure. It is possible to use pigs of the same age group, always with the same pancreas retrieval procedure. In contrast, standardizing pancreas retrieval from cadaver donors is difficult, since many variables can interfere with the condition of the gland at the time of isolation.

Successful isolation of intact and viable porcine islet cells can be difficult because of their highly fragile nature. Also, currently accepted procedures include operator dependent steps leading to variability among treatments and among treatment centers. To date, state of the art tools are the Ricordi Chamber employing a blend of enzymes produced at various times by Roche, Serva or Boehringer-Mannheim. Hence, this combination of tools is seldom the same from center to center and sometimes from treatment to treatment. The strong operator dependence of these tools begs for standardization.

1.2 - Methods of pancreas digestion

The two main isolation methods are 'semi-automated' and 'manual'. Both methods rely on prompt and careful removal and transfer of the donor pancreas to allow isolation to commence. Each method involves exocrine digestion with high-activity collagenase (Liberase). In 1988 Ricordi developed a semi-automated method in which the infused pancreas was placed into a sealed chamber during the digestion phase and shaked constantly to enhance dispersion of the pancreas. This is a standardized method, generally provides higher islet yields and is used for clinical transplant purposes although it is not suitable for all donor pancreata. The manual method is less expensive and more adaptable and enables islets to be isolated for research from most donor pancreata.

In most cases, the method is a semiautomatic procedure that requires specially designed isolation chambers, and involves collagenase digestion with mechanical disruption of pancreatic tissue. These procedures are usually performed with either recirculation or continuous agitation of the digestion medium, and result in significant fragmentation of the harvested porcine islets. Consequently, the islets often have poor response to glucose stimulation.

The first description of a repeatable technique for mass human islet isolation was the subsequent adaptation of the technique within a digestion filtration chamber originally developed and patented by Scharp and Lacy and adapted to the human pancreas by Ricordi that made the technique more efficient and practical for clinical use. In the Ricordi method, the digestion chamber contains five or six stainless steel balls. The chamber is hand-shaken, enabling the balls to interact with the pancreatic tissue and to break down the interlobular fibrous tissue to release the islets. Recently, a yield of 2279 islets per gram pancreas with 79 per cent purity was achieved, a definite improvement on previous methods. The technique relies on the intraductal injection of collagenase into the pancreatic gland and subsequent warm incubation to remove the fine framework of collagen between acini and islets within the pancreatic tissue.

However, the thicker collagen making up the interlobular and ductal framework is more difficult to digest and remains relatively unaffected by the injected collagenase and must be broken down by mechanical means. Intuitively, it would seem that shaken balls are not ideal for breaking down the interlobular fibrous tissue, as the balls are unlikely to be particularly effective in separating tissue. Moreover, the impact of the balls on the tissue might be expected to actually damage the islets, thus affecting viability and resulting in them being not as effective for the treatment of diabetes after transplantation. Therefore, an urgent need exists to develop simple,

reproducible and reliable procedures for the isolation of intact and viable porcine islet cells that would be easily adaptable in a basic research laboratory.

1.3 - Dissertation objectives

The main objective of this dissertation is to build an automated system that is capable of performing in an automated and cost-effective fashion in order, to introduce rigorous standards into the preparation of pancreatic islets for transplantation. In the first task, fluid mechanical models of pancreas disruption will be developed. Before the digester is tested, a mathematical model will be developed to describe the complex phenomena related to the dissociation of pancreas, taking into account the main features of the digester used for disruption and the variation of particulate size. This model includes the complex interplay between the decreasing size of the tissue and the structure of the convective field inside the vessel. In the mathematical model, computational fluid dynamics (CFD) is a necessary tool in order to simulate the complicated process.

In the second task, a prototype digester will be constructed to test models. To validate the mathematical model, experimental measurements will be made in a novel bioreactor. The bioreactor consists of a cylindrical vessel of circular cross-section rotating about its axis with constant angular speed. The rotation rate of the bioreactor may be adjusted during the course of an experiment to ensure that the tissue particles are maintained in 'free-fall'. The system can be used as a differential digestion method, where the vessel is initially seeded with a perfused pancreas in HBSS solution. As the bioreactor turns, the tissue fragments continually fall through the solution and, over a period of time, the pancreas 'self-dissociates' to form three-dimensional tissue particulates.

In the third task, test digestions will be performed using porcine pancreata. The first experiment will be done in the optimal condition determined by preliminary tests. Then, other tests can be carried out in surrounding range of optimized condition to further make sure its validity. Due to the high cost of porcine pancreas, the availability of organs is limited. VitaCyte LLC will provide a relatively inexpensive organ procurement and digestion manipulation. VitaCyte also has research experience using enzyme blends and has collected reliable data from the Ricordi method which can be used to compare with the new obtained results.

The most important strategy is to recognize two technical components: the digester mechanical design and the utilization of enzyme blends. VitaCyte will provide pure enzyme blends that are optimized at the time of the tests. Thus we perform comparative fluid mechanical calculations using dimensionless numbers and computational fluid dynamics to identify variations in mixing and shear rates in Ricordi chambers and Techshot's digester design; then a trial digester will be built at small scale for concept testing and finally for testing in tissue digestions at increasing levels of fidelity. The availability of an automated, controllable digester combined with an established, documented enzyme digestion system allow us to cooperate on the digestion protocol and should produce results that can be compared and collated in order to identify and eliminate other variables from the islet production process. Based these results, further scale-up design will be presented.

2. The configuration design and Computational Fluid Dynamics Simulation of an Automated Tissue Digester for Pancreatic Islet Production

2.1 - Abstract

An automated digestion unit capable of producing reproducible operating parameters is needed for the consistent preparation of islets. This research focuses on the incorporation of an automated horizontally rotating digester consisting of a rotating outer cylindrical shell and a counter-rotating core both with hemispherical baffles (Also called modified Dynacult reactor or MDR). The specified spacing between shell and core walls is one variable under investigation, along with the selection of rotation speeds and inlet flow rate. This configuration is designed to enhance the turbulent effect and contact area between tissue fragments and walls. In the digestion process, the rotation of the inner core is adjusted for optimum dissociation, and independently the exterior wall rotation is optimized to maintain particles in suspension without centrifuging them.

In the process of computational fluid dynamics (CFD) simulation, a discrete phase model (DPM) is used to predict the flow patterns in the MDR and Ricordi chamber. CFD analysis and comparison of flow variable contours between above two digesters indicate that MDR has predictable, controllable fluid shear environment and optimized differential rotation mode at 120 ml/min velocity inlet. At the same time, the dimension of the novel digester is also optimized as 3'' (0.0762m) body length, 0.375'' (0.00953m) spacing between double cylinder walls with uniform baffle diameter of 0.5'' (0.0127m) at 100 rpm rotation speed in opposite direction as a confirmed operation mode in order to minimize shear rate and energy dissipation rate per volume. The superiority of the MDR model is performed

through the comparison of simulation data with that of Ricordi chamber. These characteristics of the newly designed digester can be applied to an automatic mode instead of manual operation.

Key words: **automated horizontally rotating digester, modified rotating reactor, Ricordi chamber, computational fluid dynamics, Discrete Phase Model**

2.2 - Introduction

Large quantities of pure viable islets are necessary to treat diabetes which afflicts over 800,000 population in the U.S. Isolation of the islets is the primary step in preparing islets for transplantation. Moskalewski in 1965 used collagenase digestion of the pancreas and was the first to obtain large number of islets. Lacy and Kostianovsky in 1967 improved islet yield by cannulation of the pancreatic duct and injection of Hanks solution, which mechanically distended and disrupted the gland before digestion. After the successful application of islet transplantation in the small animal, attempts were made to the large animal. In 1981, Horaguchi and Merrel described a new technique for the isolation of islets from dog pancreas, but it could not be applied to other larger animals or the human pancreas. Noel et al. in 1982 modified the technique of Horaguchi by injecting collagenase in two separate sections, adding a calcium chelator (EGTA) into the duct. In 1984 Gray et al. modified the previous technique and applied it to the human and monkey pancreas. Warnock et al., from the same group in Edmonton, compared the method of perfusion with single intraductal injection of collagenase. Finally, Ricordi et al. in 1988 further developed a semi-automated method for the isolation of human pancreatic islets, which was a definite improvement on existing methods. In the Ricordi digestion, the pancreas and glass balls are placed into the chamber, creating a closed-loop recirculation and dissociation system operated by intermittent manual shaking of the vessel.

Moreover, the tissue dissociation enzymes (TDEs) used to disrupt pancreas is also important in the process, including isoforms, classI (C1) and class II (C2) collagenase from *C. histolyticum* in place of purified collagenase used in the earlier report (Vosscheperkeuter,

1997). The effects of enzymes alone or in combination and in the presence or absence of neutral protease were assessed for their ability to reduce collagen or glycoprotein staining. The results showed that C1+C2 were more effective than C2>C1>neutral protease in reducing the collagen histochemical staining. Comparison of these same enzymes to decrease glycoprotein staining showed C1+C2 was more effective than either class alone. The addition of neutral protease to the individual or combined collagenase isoforms accelerated the kinetics of loss of collagen staining but did not change the pattern where C1+C2>C2>C1 (Robert C. McCarthy et al., the report of VitaCyte LLC). Little is known about the exact mechanism by which collagenase and neutral proteases degrade the ECM to release cells from the pancreatic tissue. However, it is clear that both classes of collagenase and neutral proteases are required since neither enzyme alone is sufficient to maximize the yield of islets (Wolters, 1992).

However, the yield of islets was still variable (Iwashita, 1996). One of the most important reasons is the collagenase, essential for islets release from the surrounding tissues, can cause damage to islets by both warm ischemic injury and enzymatic disruption. The problem is further compounded by the variable activation degree of native proteolytic enzymes within acinar cells. Therefore, an automated system that is capable of introducing rigorous standards into the preparation of islets must be established to eliminate the uncertainty. By utilizing an established enzyme digestion system and by creating a reproducible, controllable tissue digester, two of the major variables in islet production are eliminated.

In the new design, Techshot's Dynacult bioreactor will be introduced as the prototype

of digester consisting of the following components: the shell cylinder, the core cylinder, two identical hubs, two O-rings, two rotary unions, six rotary seals, two drive pulleys, the filter mask, the filter, the core rotator shaft, and the bioreactor rotator shaft. The motors selected for the bioreactor have been tested and are able to rotate the bioreactor at maximum speed 160rpm (Paul, 2004). The Dynacult reactor has wide application as documentation in micro gravity research (Ivan, 2006). One advantage is that the fluid flow within the vessel can be carefully controlled, enabling the shear stress experienced by the islets to be optimized when the islets rotate with the fluid flow simultaneously. All above features lay a good foundation for the new digester design. The modification of this reactor was accomplished by introducing vanes to enhance turbulence. The details of digester design and subsequent results of FLUENT simulations will be illustrated by diagrams. The effects of rotation speed of double walls, inlet flow rate, specific area of whole device, shear rate, and energy dissipation rate per volume on digester performance are tested in this study.

2.3 - Materials and Methods

2.3.1 The design of new digester

The modified Dynacult reactor (MDR) incorporates hemispherical vanes to create turbulence similar to that created by moving glass balls inside the Ricordi chamber. Contrary to Ricordi chamber, the MDR provides a controllable shear rate that allows for a controllable and more reproducible digestion environment. In addition, the digestion is automated as the cylinder walls are controlled by motors in contrast to the manual operation of the Ricordi chamber. To create the MDR for the "half-ball" vanes, shell and core were rinsed by 70% ethanol, and all

surfaces were cleaned. A small spoon of silicone sealant was spreaded on the flat surface of the vanes, which were then placed one by one onto the core correctly with slight adjustment of position if necessary. This cementing process was repeated on the inner side of the transparent wall; the sealant was evenly distributed on contact interfaces by slightly pressing down the vanes. The new digestion system will be ready to use after at least 24 hours drying. When the bioreactor is operating, the rotation of the core is independent of the exterior wall. The operator may choose to rotate the core at the same rate and in the same direction as the wall, hold it stationary; or rotate it in opposite directions. With the progress of tissue dissociation, the vanes reduce the tissue fragment size and allow maximum islet release and production. Eight combinations of dimensions of MDR were selected for FLUENT simulation, which are showed in figure 2.1(Only the fluid region is extracted for study).
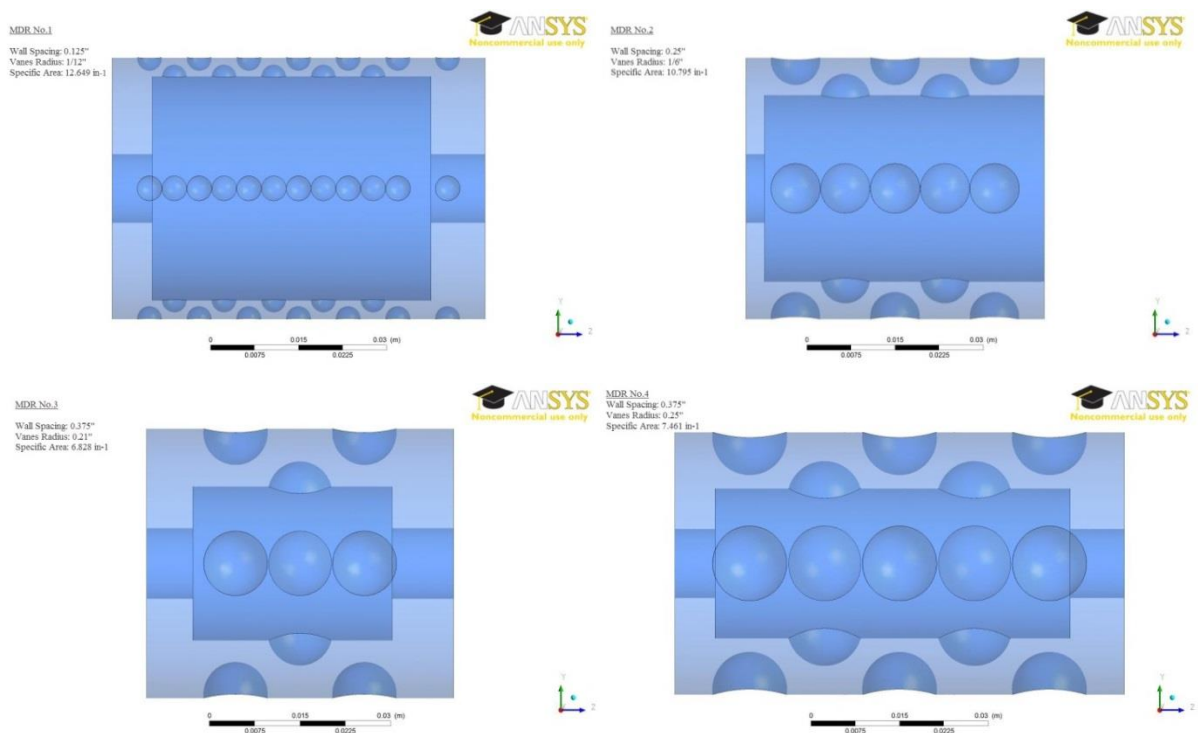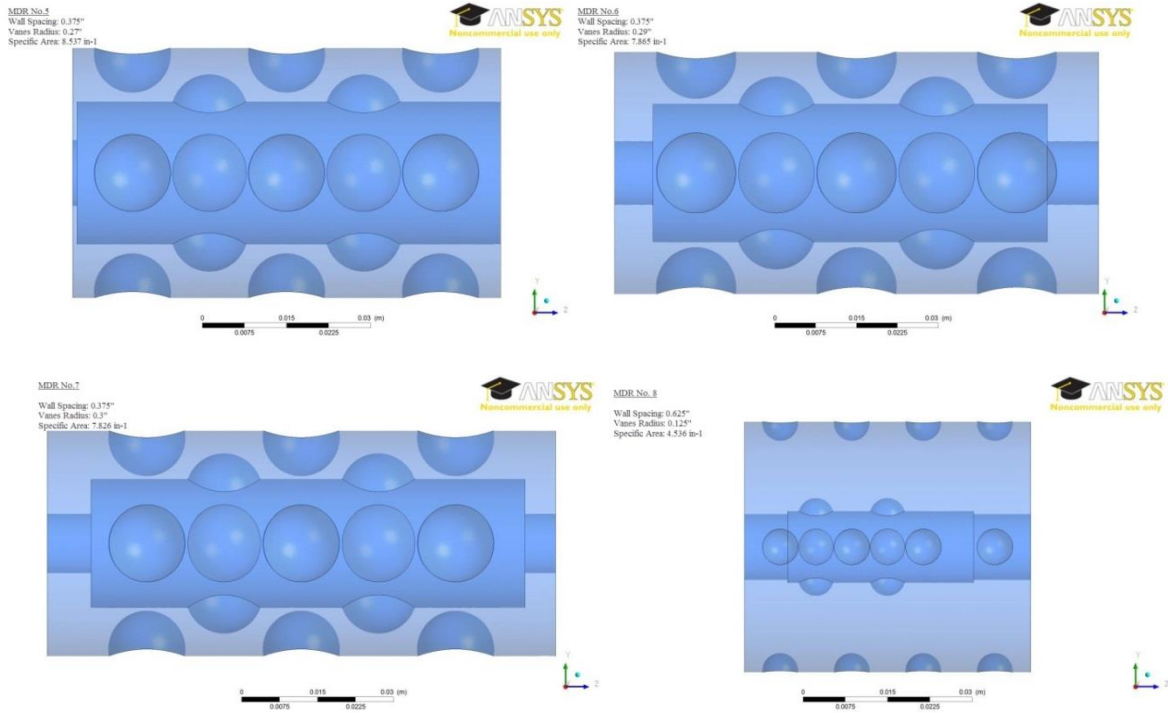
Figure 2.1 – Geometry drawings of eight combinations of dimensions of the MDR

2.3.2 Mechanical analysis of the rotation of MDR shell and core

The left sprocket rotates the core cylinder while the right sprocket rotates the outer shell maintaining particles in suspension. The shear rate between the vanes can be varied independently of outer cylinder rotation speed (delos Santos, 1994). Firstly, fluid flow is near solid body if the inner and outer cylinder walls rotate at the same angular velocity, which avoids the large shear stress and allows introduction of controlled homogenous shear fields. At the same time, the radial velocity gradient and the associated shear effects are also minimized. But the baffles or diverters on the wall invariably cause inhomogeneity in the shear field while cylinders are rotating in opposite directions. Secondly, the HBSS buffer solution is gently mixed by rotation. The mixing is the result of a secondary flow pattern induced by particle sedimentation through the fluid media or by laminar flows established

when differential rotation rates are chosen for the vessel components. Hemispherical vanes disrupt the tissue by both local turbulence at their surface and the high speed created between the vessel walls and the vanes (Goodwin, 1996). Finally, there is no headspace. Due to complete filling of the chamber, the potent sources of extra shear such as turbulence and secondary bubble formation are not created in the enzymatic medium (Todd, 1998). In sum, this kind of digester provides fluid dynamic operation characterized by solid body rotation about a horizontal axis, optimally reduced fluid shear and turbulence (Hammond, 2001).

The analysis of forces created during rotation indicates that gravity must be balanced by equal or opposite mechanical forces. These forces produce shear. In a horizontally rotating vessel, trajectory of the circular particle motion is determined by the sedimentation rate and vessel rotation speed. As the fluid rotates in the vessel, the gravitational vector acting on a tissue particle can be separated into radial and tangential components. That is, the diameter of particle spirals in suspension is determined by the terminal velocity, the angular velocity of the vessel, gravity, and the radial particle migrating velocity (Gao, 1997). At high rotation speeds, centrifugal forces lead to wall impacts, and the particles remain on the outer cylinder wall. At low rotation speeds, the gravity-induced deviations predominate and the spirals are extremely large, with many wall impacts. At its extension, as the rotations approach zero the spirals are so large that the particles sediment on the bottom of the vessel. These effects define the practical operating range for the new tissue digester (Hammond, 2001).

Gao et al. analyzed and calculated the movement of a particle in double-wall reactor. The results showed that if the density of the particle was larger than that of the surrounding medium, the particle would migrate towards the outer cylinder wall and collide with it. The

shear stress coming from liquid acting on the particle increases with the density difference between the particle and liquid. Qiu et al. in 1999 recorded the motion tracks of particles and the results revealed that the migrating speed in radial direction decreased with increasing particle radius. If the density of a particle was lighter than that of medium, the particle would finally come to the center of the circle. Then, the forces acting on a small piece of tissue particle and its movement in the rotating digester were analyzed. The tracks of a tissue fragment were calculated under different inner and outer cylinder rotating speeds, different particle sizes and density difference between enzymatic medium and the particle (Liu, 2004).

2.3.3 Computational Fluid Dynamics (CFD) simulation

FLUENT simulates fluid flow by using a discrete-phase Reynolds stress model. The results for both the MDR and the Ricordi chamber are compared. Velocity inlet boundary conditions assume velocities normal to inlet surface, the outlet pressure is set at 0 Pa gauge, and the no-slip condition is assumed at all walls. In addition, FLUENT's preprocessor "Mechanical" is used to generate flow-field meshes. An unstructured mesh consisting of tetrahedral volumetric elements in three dimensions is used in the entire domain with discrete control volumes. The operation mode is optimized by investigating rotating speed, inlet flow rate and vessel dimensions, each separately considered as a variable while others are held constant. The distribution of hydrodynamic numbers and relevant parameters is then displayed by contours generated by CFD-post. Therefore, the optimal operation condition can be determined by comparing all the parameter values and distribution diagrams under different examined conditions.

2.3.4 Mesh generation

"Mechanical", a CFD pre-processor, is used to create a volume mesh in the fluid domain before solving the discretized governing equations. Figure 2.2 shows a MDR mesh consisting of tetrahedral and hexahedral elements from the view of the rotating walls and sample inlet. Figure 2.3 shows the Ricordi chamber mesh with two motion styles. The common meshing procedure includes:

(1) Set target physics preference as CFD. This will be automatically set if the mesh is generated as part of the physics based system.

(2) Set meshing methods as automatic/tetrahedrons with patch conforming by using global setting.

(3) Specify mesh sizing setting such as edge sizing and face sizing.

(4) Create named selections that will be shown as the names of boundary conditions in FLUENT.

(5) Preview mesh and adjust settings if necessary.

(6) Generate mesh, and then check mesh quality.
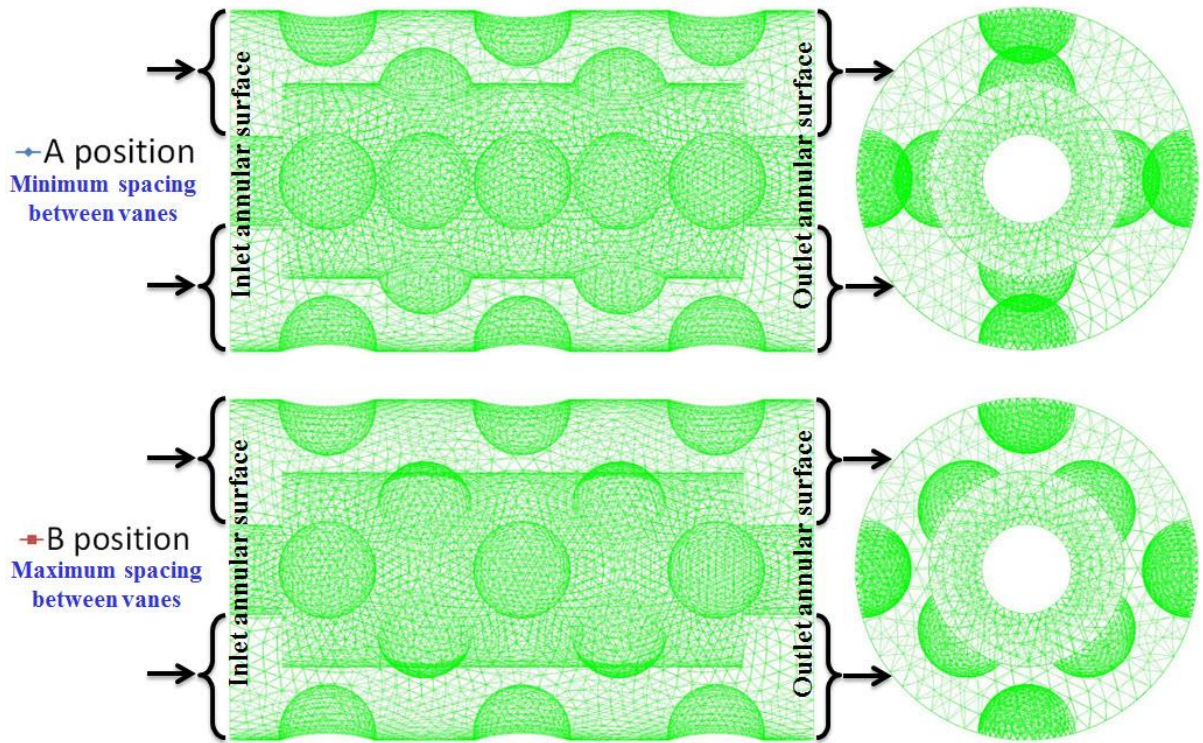
Figure 2.2 – MDR grid profile in two critical vane positions

$V_z = -0.921534*\sin(16.755161*t)$
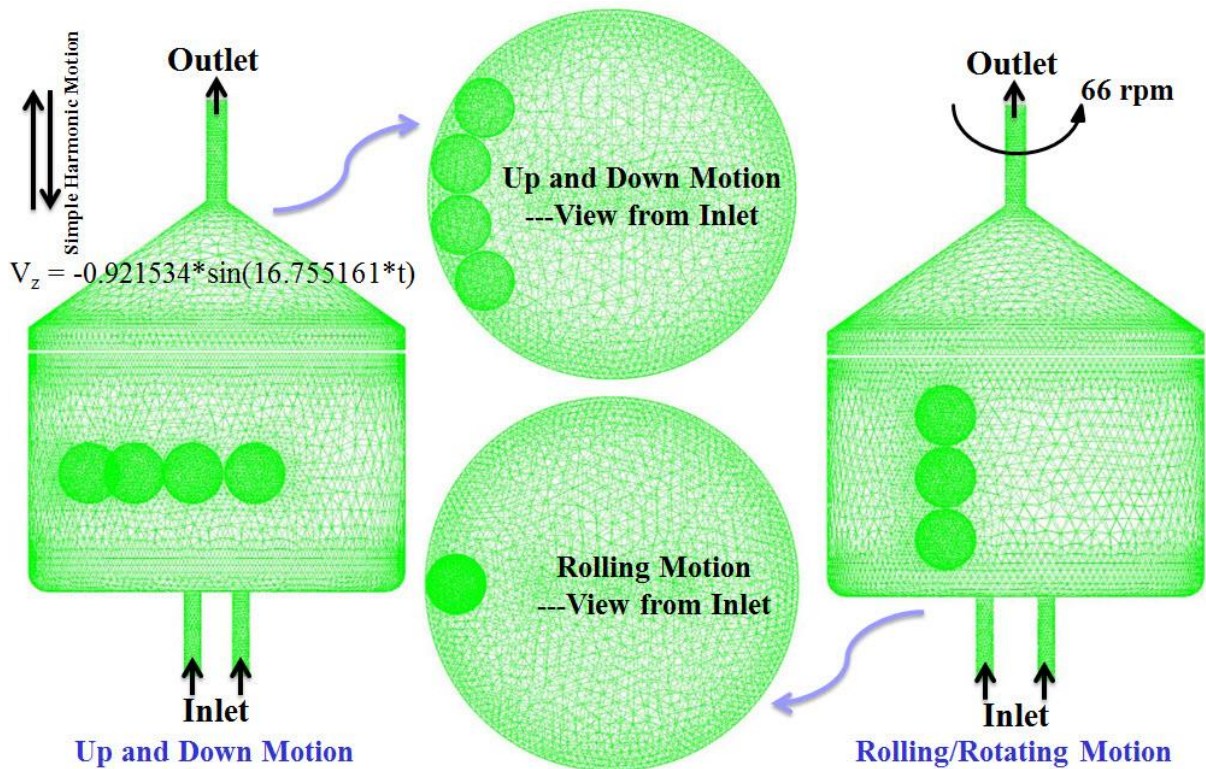
Figure 2.3 – Ricordi chamber grid profile in two styles of shaking operations

Mesh Quality has to be considered because poor quality may lead to inaccurate solution and/or slow convergence. Several Mesh Quality Metrics are involved in order to quantify the quality, including the skewness and aspect ratio as the primary metric. FLUENT requires higher mesh quality, resolution and good mesh distribution to avoid numerical diffusion. However, in worst scenarios FLUENT can tolerate poor mesh quality. The overall mesh quality metrics may be obtained in mechanical meshing under the statistics object.

2.3.5 Theory of FLUENT and calculation

The commercial software FLUENT has been used to simulate the fluid flow in rotating bioreactors by solving numerically the set of governing mathematical equations including conservation of mass and momentum. This software uses a control-volume approach to integrate the governing equations over each cell in the mesh. Flow in a MDR is characterized as turbulent because of higher rotational velocities in opposite directions. When the equations of motions are solved, the acceleration of the fluid is augmented by additional terms that appear in the momentum equation. Moreover, the equations are formulated in absolute velocity formulation.

The fluid is assumed to be incompressible and of uniform density and viscosity. The solution is independent of the azimuthal direction and can be obtained in a radial-axial plane. The flow pattern can be visualized using the intersections of stream surfaces with a radial-axial plane. For the steady-state solution, these lines would coincide with fluid element's paths viewed in a plane rotating in the azimuthal direction with the fluid element. These lines are called streamlines, although they are not tangent to the local velocity vectors (only the

radial and axial components). It should always be remembered that the primary fluid motion is in the azimuthal direction.

In this study, Reynolds Stress Model (RSM) is used in the simulation of MDR digestion process, the Reynolds stress transport equations are defined as:

$$\frac{DR_{ij}}{Dt} = P_{ij} + \Phi_{ij} - \varepsilon_{ij} + \frac{\partial J_{ijk}}{\partial x_k} \tag{1}$$

Where P_{ij} is generation: $P_{ij} = \rho(\overline{u_\iota u_k}\frac{\partial U_j}{\partial x_k} + \overline{u_j u_k}\frac{\partial U_i}{\partial x_k})$

Φ_{ij} is pressure-strain redistribution: $\Phi_{ij} = \overline{-P'(\frac{\partial u_\iota}{\partial x_j} + \frac{\partial u_j}{\partial x_\iota})}$

ε_{ij} is dissipation: $\varepsilon_{ij} = 2\mu\overline{\frac{\partial u_\iota}{\partial x_k}\frac{\partial u_j}{\partial x_k}}$

J_{ijk} is turbulent diffusion: $J_{ijk} = \overline{P'u_\iota}\delta_{jk} + \overline{P'u_j}\delta_{ik} + \rho\overline{u_\iota u_j u_k} - \mu\frac{\partial}{\partial x_k}(\overline{u_\iota u_j})$

Reynolds stress tensor R_{ij} is a symmetric, second-order tensor; it comes from averaging the convective acceleration term in the momentum equation. It provides the averaged effect of turbulent convection which is highly diffusive and represents a combination of mixing due to turbulent fluctuation and smoothing by averaging. Although RSM is more difficult to converge than 2-equation models and requires substantially more modeling for the governing equations in which the pressure-strain is most critical and difficult one among them, this model is most suitable for highly anisotropic, three dimensional flows complex with strong streamline curvature, swirl and rotation. Furthermore, RSM is able to address the limitations and weakness of eddy viscosity models (EVMs) including the following aspects: (1) Linear algebraic stress-strain relationship results in poor performance where stress transport is important, including non-equilibrium flows, separating and reattaching flows, etc. (2) Inability to account for extra strain due to streamline curvature, rotation, and highly skewed flows, etc. (3) Poor performance where turbulence is highly

anisotropic (e.g., in flows normal stresses play an important role) or 3D effects are present. In order to avoid these shortcomings, transport equations for the six distinct Reynolds stress components are derived by averaging the products of velocity fluctuations and Navier-Stokes equations. A turbulent dissipation rate equation is also needed. But RSMs still do not always provide indisputable superior performances over EVMs. In general, RSM is the most physically sound model with effects of curvature, swirl, and rotation are directly accounted for in the transport equations for the Reynolds stresses.

In the near-wall region, the turbulent boundary layer is very thin and the solution gradients are very high, but accurate calculations in the near-wall region are paramount to the success of the simulation. For equilibrium turbulent boundary layers, standard wall functions (which are based on Launder-Spaulding law-of-the-wall, Equation (2) are chosen as near-wall treatment in order to promote convergence. Velocity profile and wall shear stress obtained from the log law are used to set the boundary values of stresses for the wall-adjacent cells. The benefit of wall functions is to allow the use of a relatively coarse mesh in the near-wall region thereby reducing the computational cost. In the standard wall functions, wall adjacent cells should have y^* values between 30 and 300–500 and the mesh expansion ratio should be no larger than around 1.2.

$$u^* = \begin{cases} y^* & (y^* < y_v^*) \\ \frac{\ln(Ey^*)}{k} & (y^* > y_v^*) \end{cases} \tag{2}$$

$$\text{Where } u^* = \frac{u_p C_\mu^{1/4} k_p^{1/2}}{u_\tau^2}; \quad y^* = \frac{\rho C_\mu^{1/4} k_p^{1/2} y_p}{\mu}$$

As a comparison, the FLUENT simulation is also performed on a Ricordi chamber. It is not necessary to use RSM but rather realizable k-ε Model. The standard k-ε model needs to be modified to satisfy the following condition: k equation is unchanged but a new

formulation is applied on μ_t and ε, C_μ is variable; dissipation rate (ε) equation is derived from

the mean-square vorticity fluctuation, which is fundamentally different from the standard k-ε

model; several realizable conditions are enforced for Reynolds stress. The benefits of

realizable k-ε model includes: accurately predicts the spreading rate of both planar and round

jets; it is likely to provide superior performance for flows involving rotation, boundary layers

under strong adverse pressure gradients, separation, and recirculation. The new ε-transport

equation is shown in Equation (3):

$$\rho\frac{D\varepsilon}{Dt} = \frac{\partial}{\partial x_j}\left[\left(\mu + \frac{\mu_t}{\sigma_\varepsilon}\right)\frac{\partial\varepsilon}{\partial x_j}\right] + C_1 S\rho\varepsilon - C_2\frac{\rho\varepsilon^2}{k+\sqrt{v\varepsilon}} \tag{3}$$

Where $C_1 = \max\left[0.43, \frac{\eta}{\eta+5}\right]$, $\eta = \frac{Sk}{\varepsilon}$, $C_2 = 1.0$

In which turbulent viscosity is defined as: $\mu_t = \rho C_\mu\frac{k^2}{\varepsilon}$, $C_\mu = \frac{1}{A_0+A_s\frac{U^*k}{\varepsilon}}$

And the relevant parameters: A_0=4.04; $A_s = \sqrt{6}\cos\phi$; $\phi = \frac{1}{3}\cos^{-1}(\sqrt{6}W)$;

$$U^* = \sqrt{S_{ij}S_{ij} + \Omega_{ij}\Omega_{ij}};\ W = \frac{S_{ij}S_{jk}S_{ki}}{\tilde{S}};\ \tilde{S} = \sqrt{S_{ij}S_{ij}}$$

The hydrodynamic parameters are calculated by using the following formula from

Equations (4) ~ (9):

$$\text{Cell Reynolds Number: } Re = \frac{\rho ud}{\mu} \tag{4}$$

$$\text{Turbulent Intensity:} I = \frac{\sqrt{\frac{2}{3}k}}{U};\quad U = \sqrt{U_x^2 + U_y^2 + U_z^2} \tag{5}$$

$$\text{Shear Stress: } \tau = \mu\frac{du}{dx} = \mu\gamma \tag{6}$$

$$\text{Shear Rate: } \gamma = \frac{du}{dx} = \frac{\Delta v_z}{\Delta x} \tag{7}$$

$$\text{Energy Dissipation Rate per Volume:} \frac{P}{V} = \mu\gamma^2 \tag{8}$$

$$\text{Kolmogoroff Length: } l_e = \left(\frac{\rho v^3}{P/V}\right)^{1/4} = (\frac{\mu^3/\rho^2}{P/V})^{1/4} \tag{9}$$

Where ρ is the density of medium (kg/m^3); u is velocity magnitude; d is the (cell

volume) $^{1/3}$ in 3D cases (m); μ is the effective viscosity (N·s/m^2); k is the turbulence kinetic

energy (m^2/s^2); U (m/s) can be computed from the three mean velocity components U_x, U_y and U_z; P is the power consumption (w) in the process, V is volume of chamber (m^3); υ is the liquid kinematic viscosity (m^2/s).

When the cultisphers particles get involved in the study of flow streamlines, the Discrete Phase Model (DPM) can set up the injection properties to generate the particle pathlines. Particle equation of motion is shown in equation (10):

$$m_p \frac{du_p}{dt} = F_{drag} + F_{pressure} + F_{virtual\ mass} + F_{gravity} + F_{other} \tag{10}$$

In which, drag force: $F_{drag} = \frac{\rho A_p}{2} C_D \|u - u_p\|(u - u_p) = \frac{3}{4} m_p \frac{\rho}{\rho_p} \frac{C_D}{d_p} \|u - u_p\|$

Pressure force: $F_{pressure} = \int_A - p\ dA = \int_V - \nabla p\ dV = -\frac{m_p}{\rho_p} \nabla p$

Virtual mass force: $F_{virtual\ mass} = \frac{m_p}{2} \frac{\rho}{\rho_p} \frac{d(u - u_p)}{dt}$

Gravitation: $F_{gravity} = m_p \frac{\rho_p - \rho}{\rho_p} g$

Particle acceleration and location are also expressed as below:

$$\frac{du_p}{dt} = \alpha + \beta(u_f - u_p) \qquad and \qquad \frac{dx_p}{dt} = u_p$$

When particles enter a turbulent eddy, they try to follow it for the time they are crossing the eddy. This effect leads to lateral dispersion which must be considered in modeling. Particle cloud model is the cloud tracking with local variations in flow properties getting averaged inside the particle cloud, smooth distribution of particle coupling source terms, and independent cloud trajectory calculation for each diameter size.

2.3.6 Boundary conditions

Three different boundary conditions used in the primary phase are velocity inlet, pressure-outlet and rotational walls. Velocity inlet boundary conditions are used to define the

flow velocity along with all flow properties at the inlet. Pressure-outlet boundary conditions are used to model flow exits where the details of the flow velocity and pressure are not known prior to solution of the flow problem. For turbulent flows at the rotational wall, the no-slip shear condition is enforced at the walls. Additionally, discrete phase boundary conditions for DPM should be set to escape for velocity-inlet and pressure-outlet to reflect rotating walls boundary conditions. This sort of boundary condition is illustrated in figure2.4:
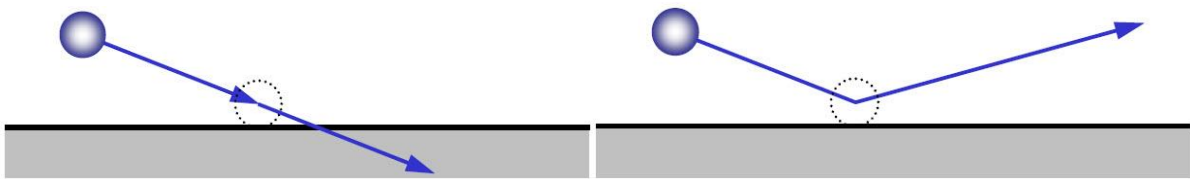
Figure 2.4 – (Left) Escape boundary condition–Particle leaves the flow domain;

(Right) Reflect boundary condition–Particle bounces off the wall with certain coefficient of restitution.

2.3.7 Solvers

In FLUENT, two solver technologies are available: pressure-based and density-based. Two algorithms also exist under the pressure–based solver: a segregated algorithm and a coupled algorithm. In general, the coupled algorithm significantly improves the convergence speed over the segregated algorithm; however, the memory requirement for the coupled algorithm is more than that for the segregated algorithm. When selecting a solver and an algorithm we must consider the following issues: the model availability for a given solver; solver performance for the given flow conditions; the size of the mesh under consideration. In our study, pressure-based is chosen as the solver because it is applicable for a wide range of flow regimes from low speed incompressible flow to high-speed compressible flow. In

addition, pressure-velocity coupling refers to the numerical algorithm which uses a combination of continuity and momentum equations to derive an equation for pressure when using the pressure-based solver. The SIMPLE scheme is used to obtain a relationship between velocity and pressure corrections to obtain the pressure field.

The DPM model has its own equations which are separate from the FLUENT solver. The particle equation of motion with sub models has unique numerical algorithms with their specific convergence behavior and settings. A coupled flow simulation will never converge if the particle algorithms are failing. Additionally, some sub models contain some stochastic behavior. Therefore, care should be taken in order to ensure a smooth distribution of source terms. During the coupling procedure, particles are computed including the source terms every N^{th} flow iteration. For the next N flow iterations the particle source terms are kept constant and considered in the flow equations. The flow solution may change due to heterogeneous phase of particles. This process is repeated until convergence is achieved. The figure 2.5 illustrates the DPM coupling procedure in steady state:
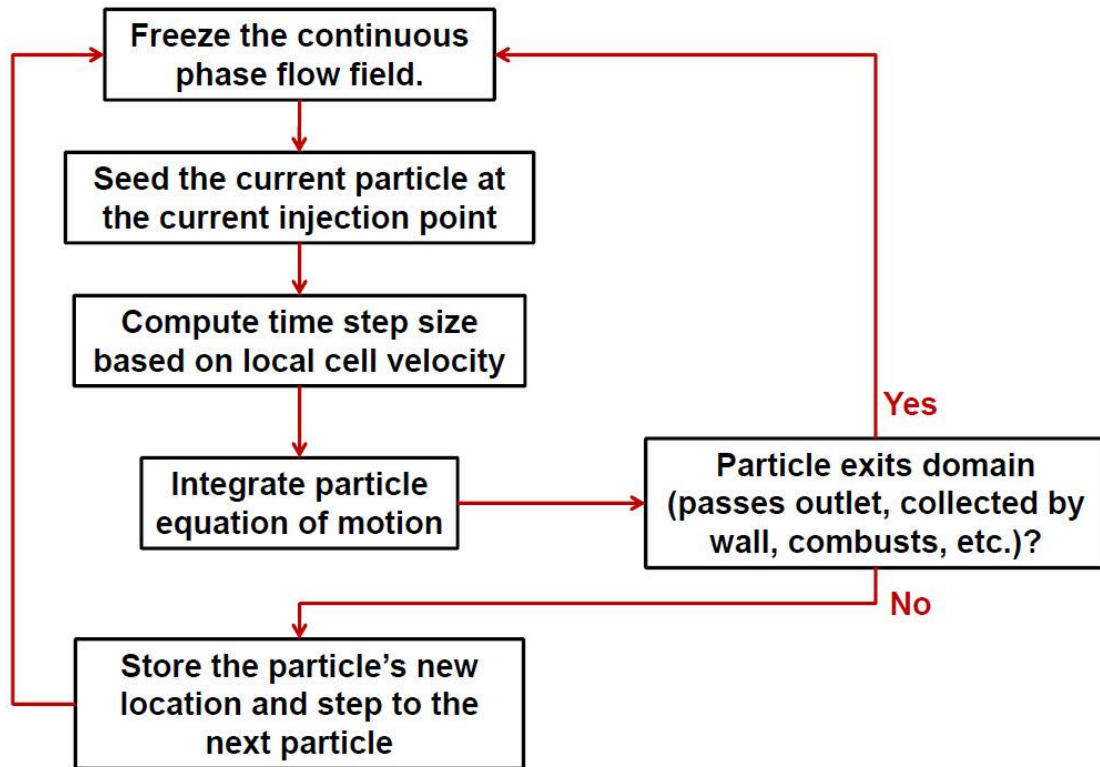
Figure 2.5 – DPM coupling flow chart under steady state

2.3.8 Spatial discretization

Discretization is replacing the differential equations that govern fluid flow with a set of algebraic equations which are solved at distinct points. This process involves two main steps: (1) converting the continuum partial differential equations into algebraic formulas and (2) converting the continuous physical domain into nodes, faces, or cells where the algebraic equations will be solved. Discretization of partial differential equations can be accomplished in ways that can be used to solve problems in fluid mechanics: finite differences (discretization of partial differential form of equations) and finite volumes (discretization of equations in the integral form). In general, the finite volume method is more common to use in spatial discretization. The conservation principles are applied to a fixed region or space known as the control volume. By using this approach, either control volumes are established

first and grid points are placed at the center of the volumes (cell-centered method) or grid points are established first and then the boundaries of the control volume are fixed (vertex-centered method) (Tannehill et al., 2004).

In this study, the finite volume method using the cell-centered approach is used to convert the governing equations into an algebraic form that is then solved numerically. The cell-centered method is to solve the flow properties at the cell centers; the values at the interfaces used to obtain cell fluxes are obtained by interpolating the cell-centered values with an upstream direction bias. This method is called an upwind scheme. In addition, second-order accurate upwind methods are used as the option of momentum, turbulent kinetic energy, turbulent dissipation rate, and Reynolds stress.

2.3.9 Simulation procedure

The following guidelines can be used in a successful CFD simulation:

1. Examine the quality of mesh: perform a mesh check to avoid problems due to incorrect mesh connectivity. As a general rule, the value of maximum skewness should be below 0.95. If there are mesh problems, we may have to re-mesh the geometry.

2. Scale the mesh and check length units: all the physical dimensions are initially assumed to be in SI units. The mesh might be scaled according to the established unit system.

3. Employ the appropriate physical models: in this study, the RSM and realizable k-ε model are used in simulation of MDR and Ricordi chamber, respectively.

4. Use node-based gradients with unstructured tetrahedral meshes: the node-based averaging scheme is known to be more accurate than the default cell-based scheme for unstructured meshes, most suitable for triangular and tetrahedral meshes.

5. Monitor convergence with residuals history: residual plots can show when the residual values have reached the specified tolerance. At the same time, check if the residuals have reduced by at least three orders of magnitude.

6. Run the CFD simulation using second order discretization for better accuracy rather than a faster solution. A converged solution is not necessarily a correct one. Always inspect and evaluate the solution by using available data, physical principles and so on. The second-order upwind discretization scheme should be used for final results.

7. Monitor values of solution variables to make sure that any changes of the solution variables from one iteration to the next are negligible.

8. Verify that property conservation is satisfied: after the simulation, note if overall property conservation has been achieved. At a minimum, the net imbalance should be less than 1% of smallest flux through domain boundary.

9. Check for mesh dependence: we should ensure that the solution is grid-independent and use mesh adaption to modify the mesh or create additional meshes for the grid-independence study. A systematic procedure for obtaining a grid-independent solution is described as follows: generate a new, finer mesh; continue calculation until convergence; compare the results obtained on the different meshes; repeat the procedure if necessary.

10. Check to see that the solution makes sense based on engineering judgment: If flow features do not seem reasonable, the physical model and boundary conditions should be reconsidered.

2.4 - Results and Discussion

2.4.1 MDR configuration and operation modes

The configuration of the MDR is illustrated in Figure 2.6. The dimensions are listed in Table 2.1. In order to imitate the turbulent environment caused by glass balls in the Ricordi chamber, the "half-ball baffle" vane is employed to dissociate the pancreatic tissue. In earlier testing all vanes were cemented onto the annular wall evenly distributing four in one circle. The base system, including a stationary base that is mounted to the experiment enclosure and a mobile base that can be repositioned between experiments in order to vary the length of the bioreactor, has been designed to allow the shell, core, and rotational speeds to be changed (Paul, 2004).
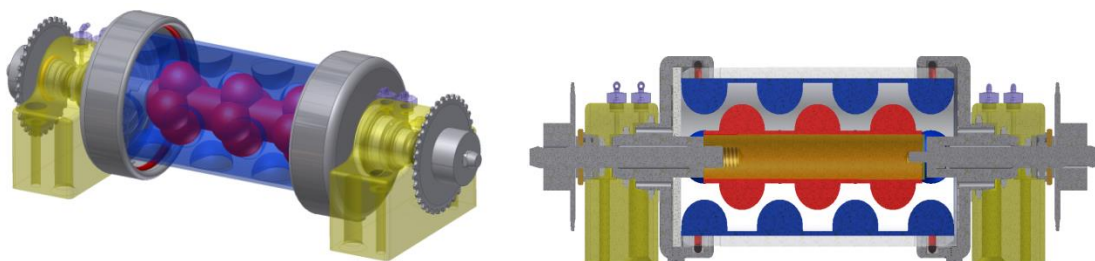
Figure 2.6 – The Modified Dynacult Digester Design

Table 2.1 – Dimensions of Tissue Digester (Unit: inch)

No.	Shell diameter	Core diameter	Shell length	Core length	Shell shaft	Core shaft	Wall distance	Ball radius	No. of balls on shell	No. of balls on core	Specific Area (in^{-1})
1	OD=2, ID=1.75	1.5	2.5	1.87	0.362	0.268	0.125	0.0833	7	5	12.6
2	OD=2, ID=1.75	1.25	2	1.88	0	0.125	0.25	0.167	3	2	10.8
3	OD=2, ID=1.75	1	2	1.3	0.4	0.3	0.375	0.21	2	1	6.83
4	OD=2, ID=1.75	1	3	2.37	0.362	0.268	0.375	0.25	3	2	7.46
5	OD=2, ID=1.75	1	3	2.97	0	0.031	0.375	0.27	3	2	8.54
6	OD=2, ID=1.75	1	3.5	2.85	0.372	0.278	0.375	0.29	3	2	7.87
7	OD=2, ID=1.75	1	3.95	3.37	0.237	0.341	0.375	0.3	3	2	7.83
8	OD=2, ID=1.75	0.5	2	1.3	0.4	0.3	0.625	0.125	4	2	4.54

Dimensions of Tissue Digester (Unit: m)

No.	Shell diameter	Core diameter	Shell length	Core length	Shell shaft	Core shaft	Wall distance	Ball radius	No. of balls on shell	No. of balls on core	Specific Area (m⁻¹)
1	OD=0.0508, ID=0.0445	0.0381	0.0635	0.0475	9.19E-03	6.81E-03	3.18E-03	2.12E-03	7	5	496
2	OD=0.0508, ID=0.0445	0.0318	0.0508	0.0478	0	3.18E-03	6.35E-03	4.24E-03	3	2	425
3	OD=0.0508, ID=0.0445	0.0254	0.0508	0.0330	0.0102	7.62E-03	9.53E-03	5.33E-03	2	1	269
4	OD=0.0508, ID=0.0445	0.0254	0.0762	0.0602	9.19E-03	6.81E-03	9.53E-03	6.35E-03	3	2	294
5	OD=0.0508, ID=0.0445	0.0254	0.0762	0.0754	0	7.87E-04	9.53E-03	6.86E-03	3	2	336
6	OD=0.0508, ID=0.0445	0.0254	0.0889	0.0724	9.45E-03	7.06E-03	9.53E-03	7.37E-03	3	2	310
7	OD=0.0508, ID=0.0445	0.0254	0.1	0.0856	6.02E-03	8.66E-03	9.53E-03	7.62E-03	3	2	308
8	OD=0.0508, ID=0.0445	0.0127	0.0508	0.0330	0.0102	7.62E-03	0.0159	3.18E-03	4	2	179

2.4.2 Distributions of hydrodynamic parameters for the Ricordi chamber

Manual shaking mode is divided into two motions: (1) rolling motion with the rotational axis parallel to central line of the Ricordi chamber at a maximum rotation speed of 66 rpm; (2) simple harmonic motion; velocity formula $V_z = -0.921534 * \sin(16.755161*t)$ (m/s). Figure 2.7 shows the distributions of four important hydrodynamic parameters in the

whole chamber and the symmetric plane, figure 2.8 displays velocity magnitude contours and

velocity vectors, and figure 2.9 shows the particle motion streamlines.

■ **Distributions of Cell Reynolds Number:**
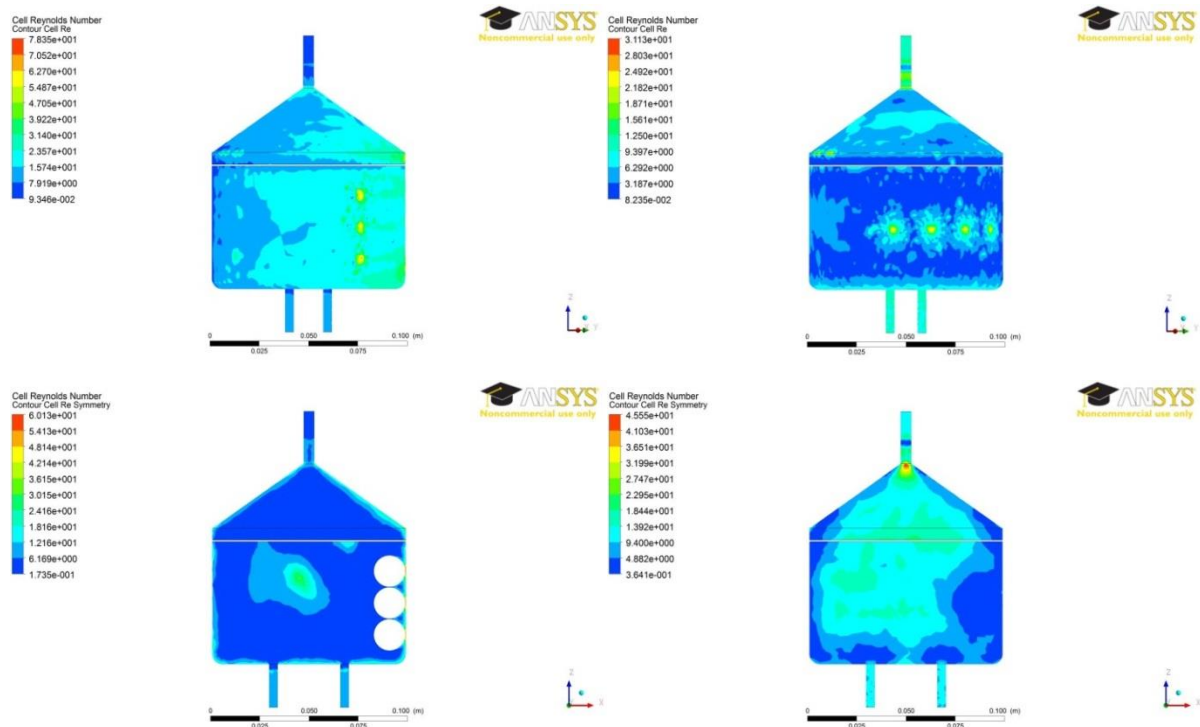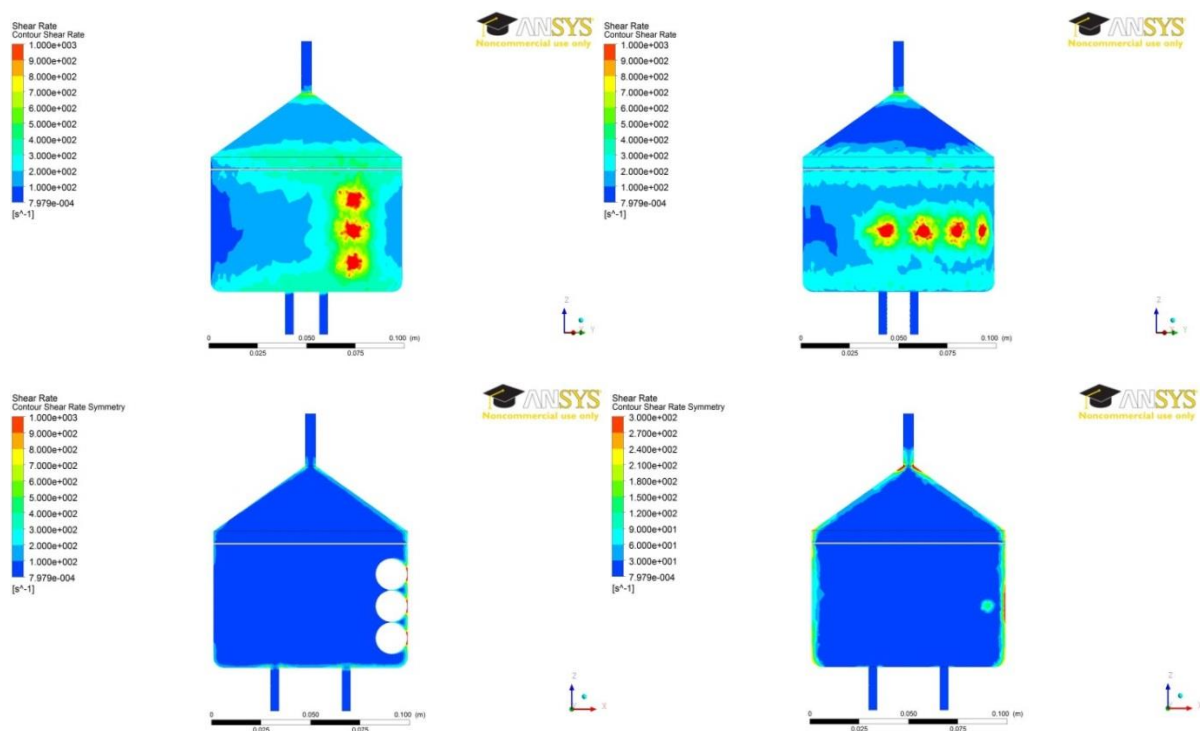
■ **Distributions of Shear Rate (s^{-1}):**

■ **Distributions of Energy Dissipation Rate per Volume (W/m^3):**
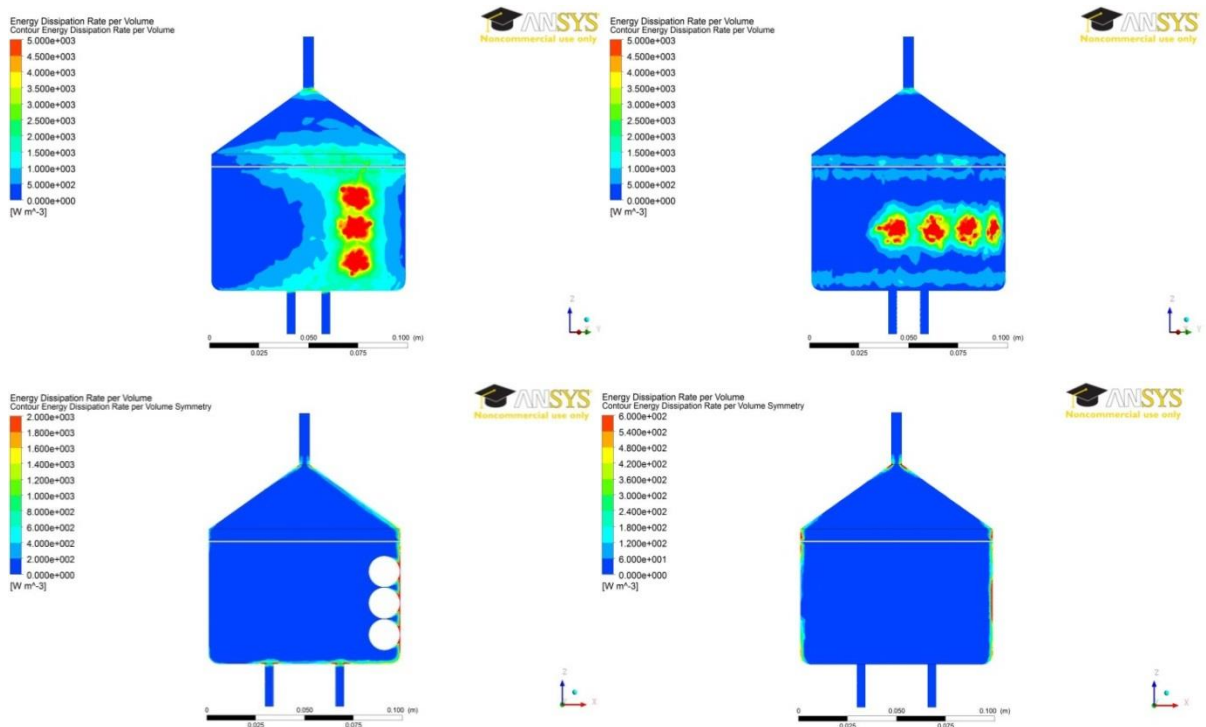
■ **Distributions of Kolmogoroff Length(m):**
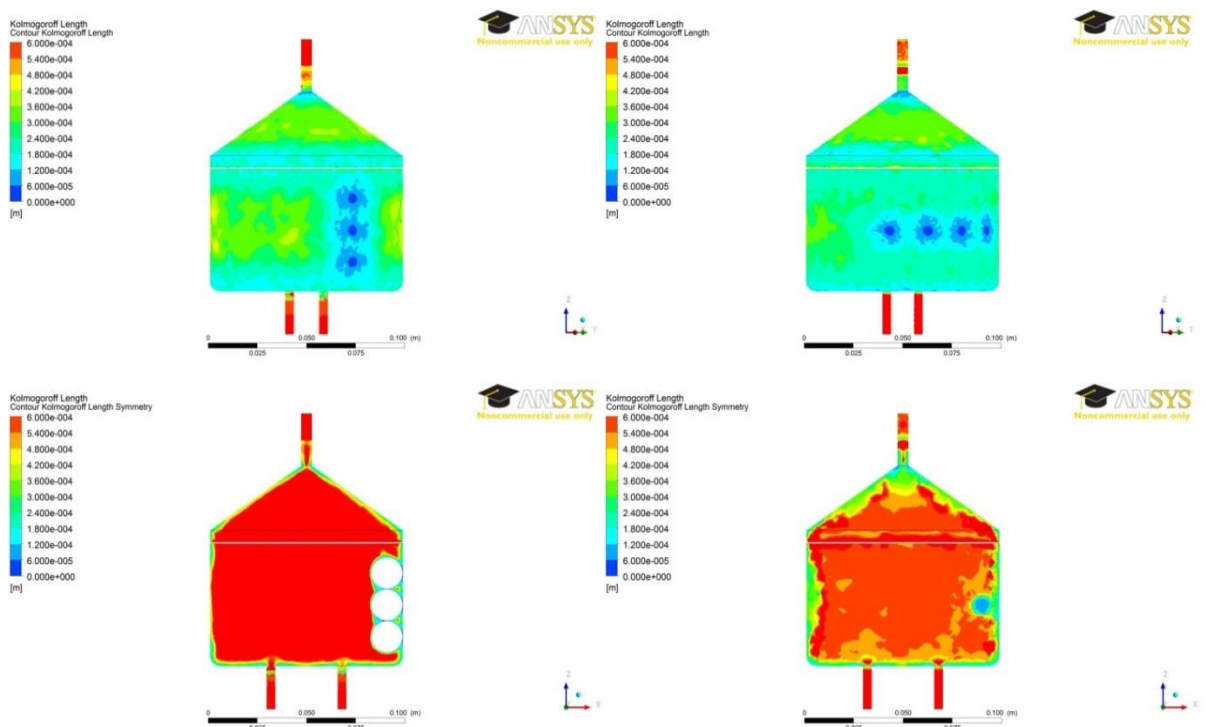
Figure 2.7 – The spatial distribution of hydrodynamic parameters for the Ricordi chamber.
(Left column – rolling motion; right column – up and down motion)
(Upper pair – volume; lower pair – central plane)
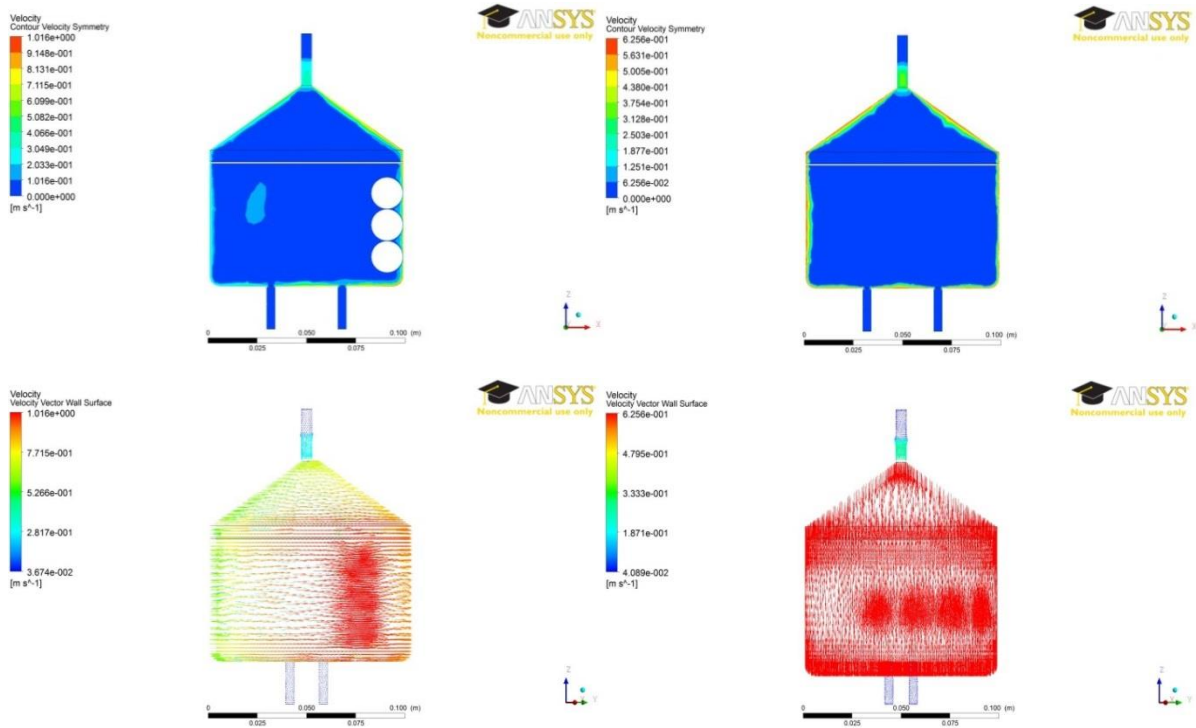
**Figure 2.8 – The velocity magnitude contours on central plane and velocity vectors.
(Left column – rolling motion; right column – up and down motion)**
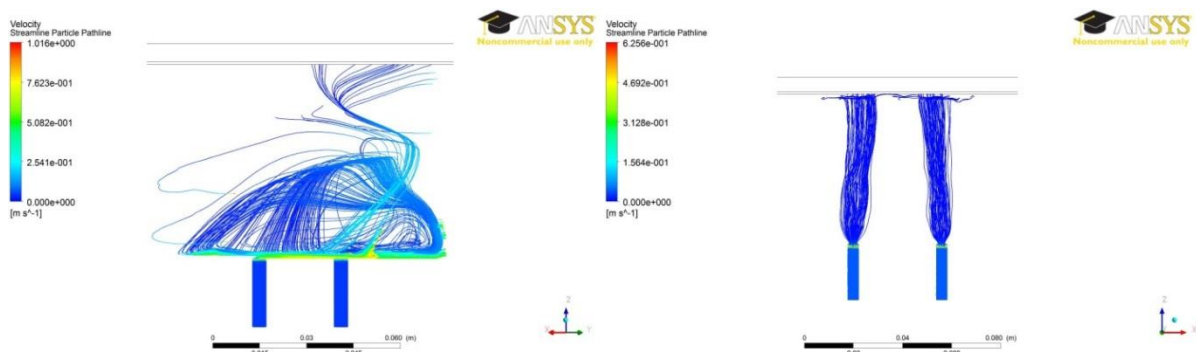
**Figure 2.9 – The particle streamlines coincide with fluid element's paths
(Left column – rolling motion; right column – up and down motion)**

Moreover, the percentage histogram is another important type of column chart used to show the area percentage of flow parameters. Figure 2.10 shows the percentage of relevant parameters located on the symmetric plane:

- **Percent of Cell Reynolds Number:**
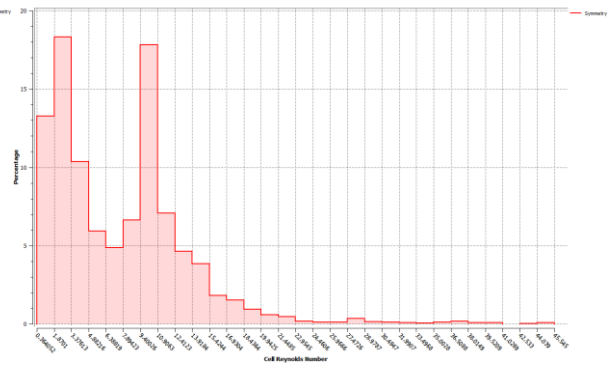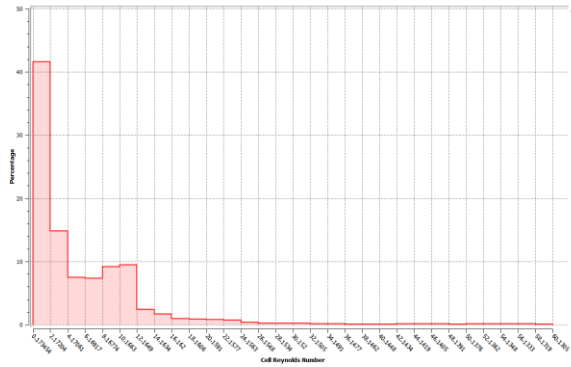
- **Percent of Shear Rate (s^{-1}):**
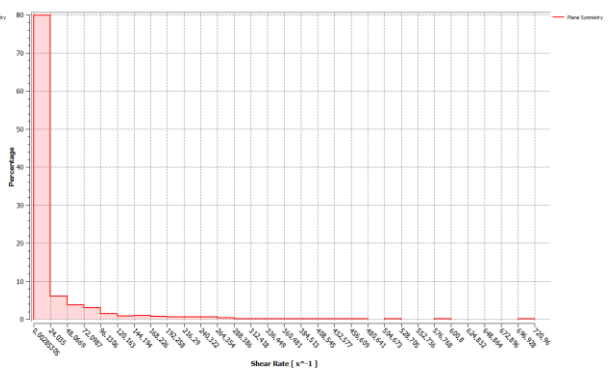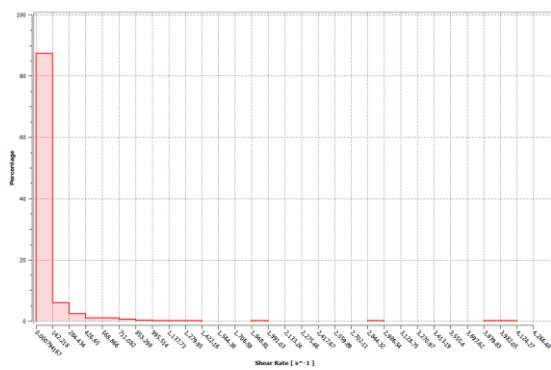
- **Percent of Energy Dissipation Rate per Volume (W/m^3):**
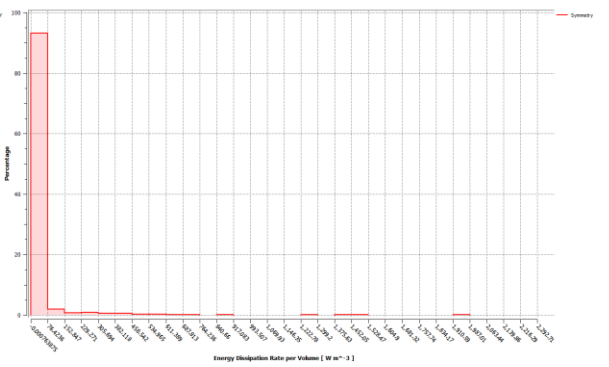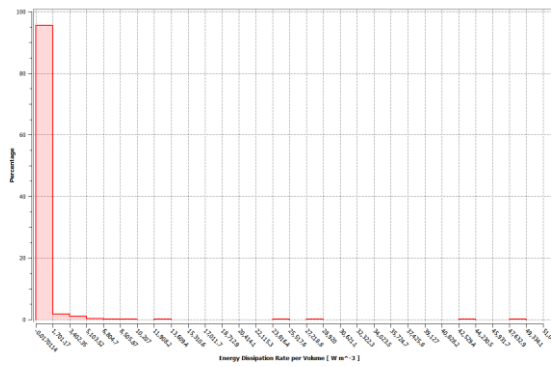
- **Percent of Flow Velocity(m/s):**
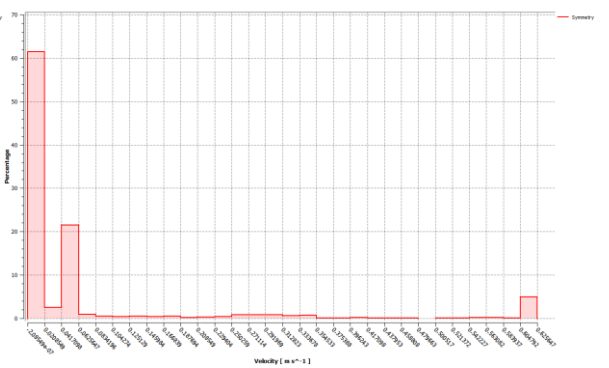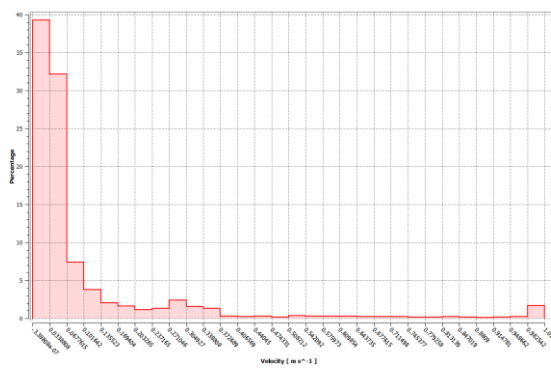
**Figure 2.10 – Histograms showing the distribution of flow parameters
on Ricordi chamber central plane
(Left column – rolling motion; right column – up and down motion)**

2.4.3 Distributions of hydrodynamic parameters in the MDR

Three important factors including the rotation speed of moving walls, inlet flow rate and vessel specific area were investigated independently for optimization; the double wall rotation position is assumed to have impact on shear environment. Firstly, the effect of rotation speed on shear rate, shear stress, and energy dissipation rate per volume (also noted as **P/V**) are plotted in figure 2.11 while the inlet flow rate and vessel specific area are kept constant (80ml/min and 7.46 in^{-1} (294m^{-1}), respectively).
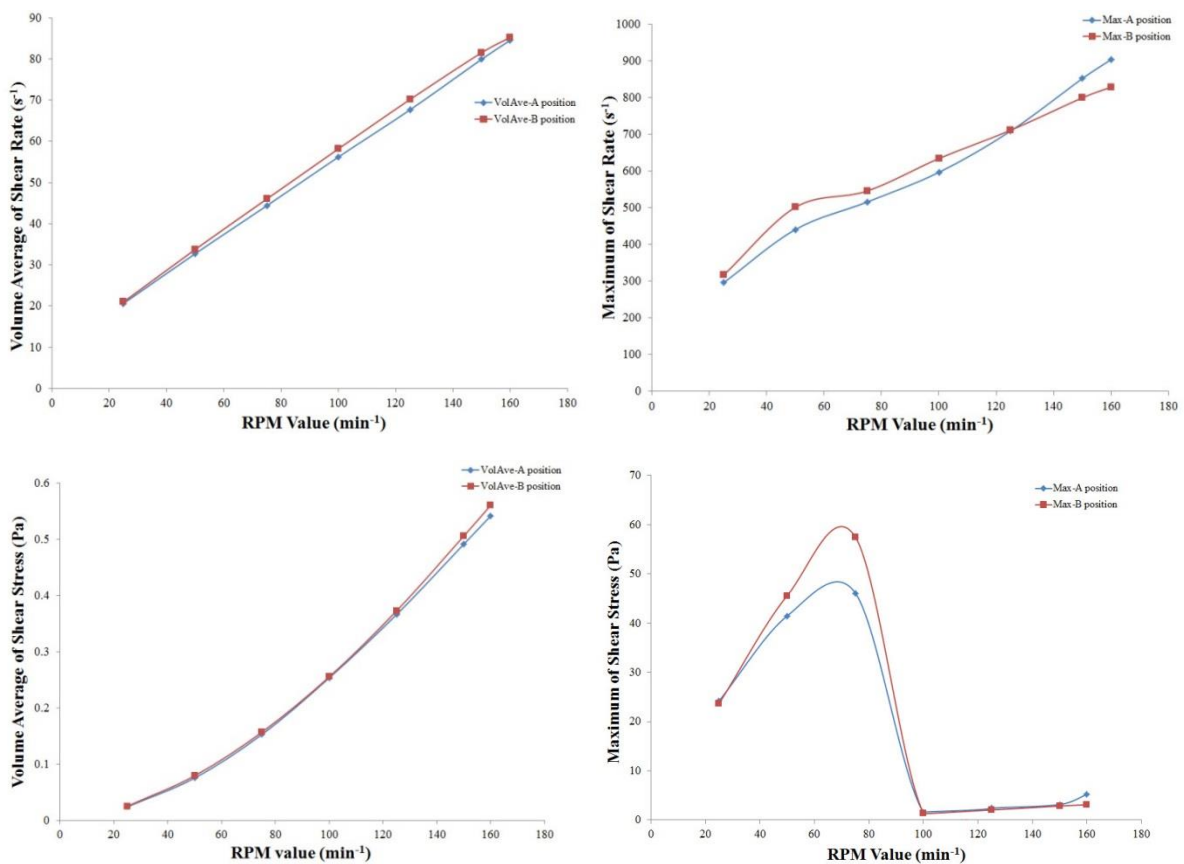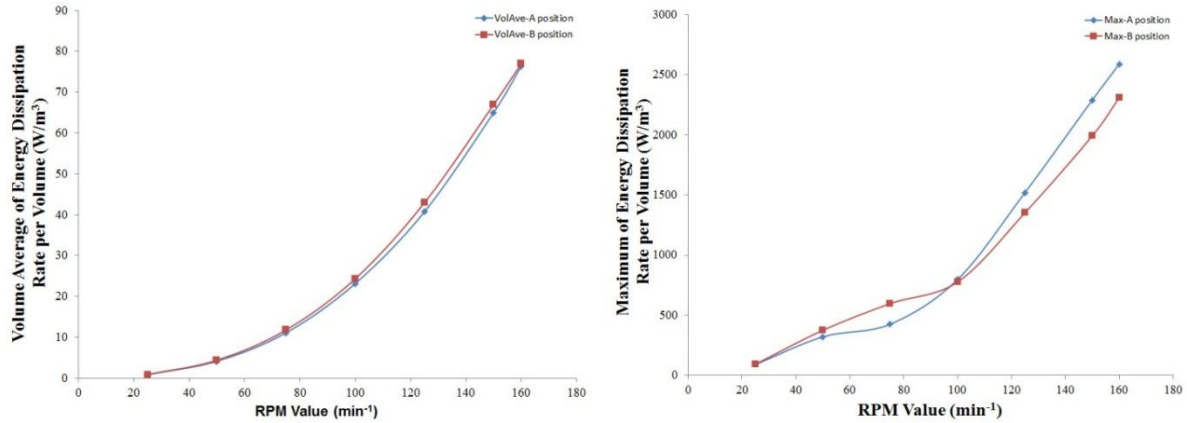
Figure 2.11 – Comparison of shear rate, shear stress and P/V as a function of double walls rotation speed under two critical vane positions (Position A and B) in the MDR

The above plots of hydrodynamic parameters versus RPM show that volume average or maximum shear rate and P/V are rising with RPM and reach the peak value at the upper-limit 160rpm. However, the relationship of the maximum shear stress with RPM shows a different profile with the minimum point at 100rpm. Based on the results of Ricordi chamber, the volume average of shear stress and P/V is around 0.487 Pa and 46.3 W/m^3, respectively. By comparing them with corresponding value in the plots for the MDR in figure 2.11, the rotation speed should be controlled under 125rpm for sake of lower shear environment. Additionally, the maximum shear stress in Ricordi chamber reaches 14.4 Pa so that the optimal RPM range is 100~160rpm, in this case, the maximum shear stress in MDR is lower than 14.4 Pa. Incorporation of above two RPM range determines the preferred rotation speed at about 100 rpm. It is also found that the cylinder wall rotation has little impact on flow parameters so that all the contours can be displayed at position A with minimum vane spacing.

Secondly, the effect of inlet flow rate on shear rate, shear stress, and P/V are plotted in figure 2.12 while the rotation speed and vessel specific area are kept constant (100rpm and

7.46 in^{-1} (294m^{-1}), respectively); Thirdly, the effect of specific area on shear rate, shear stress, and P/V are also plotted in figure 2.13 while the rotation speed and inlet flow rate are kept constant (100rpm and 120ml/min, respectively). Finally, the optimal inlet flow rate 120 ml/min and vessel dimension 4 (see Table 2.1, the specific area is 7.46 in^{-1} (294m^{-1})) are obtained by similar comparison under corresponding variable gradients.
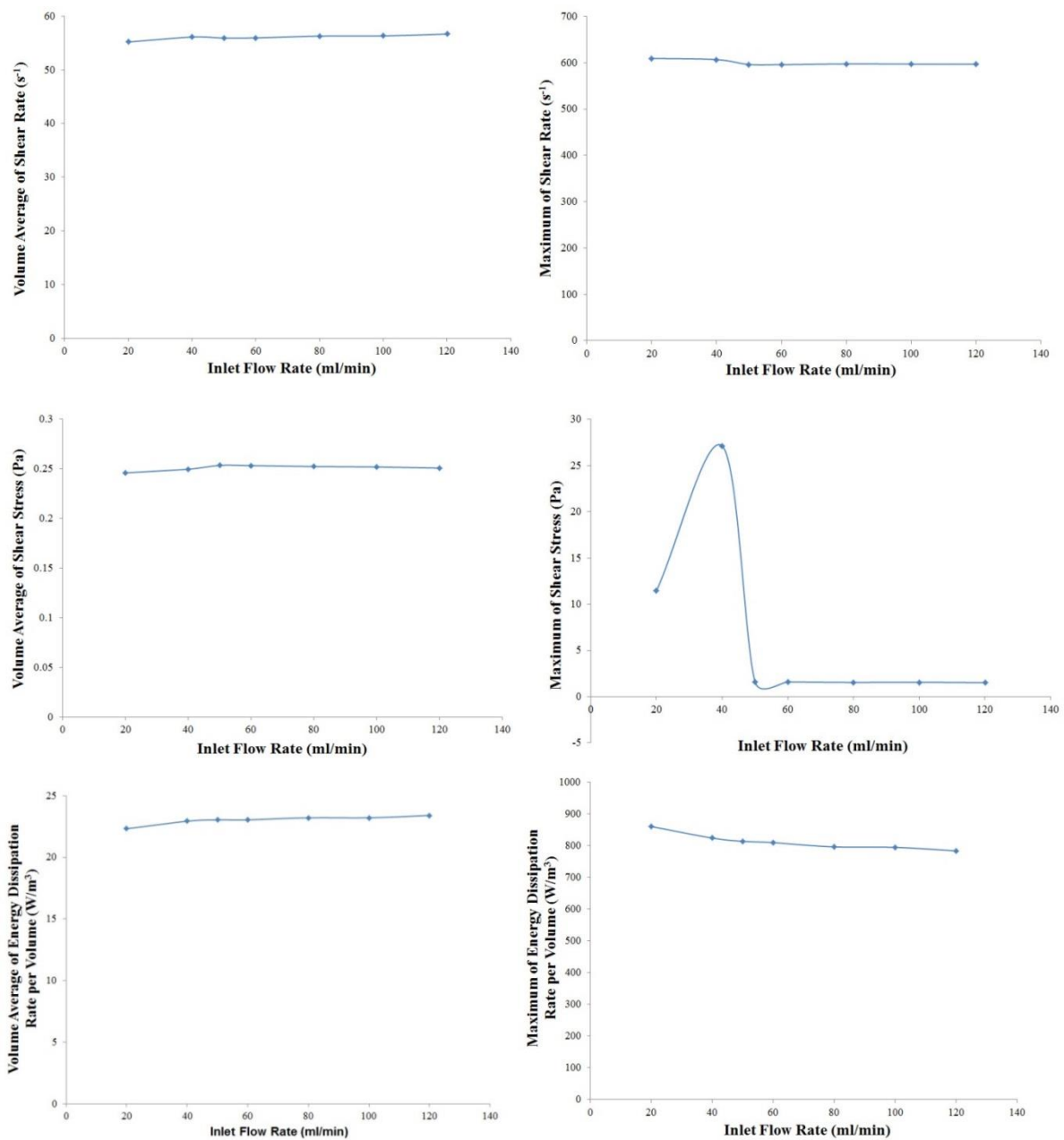
Figure 2.12 – The shear rate, shear stress and P/V as a function of MDR inlet flow rate
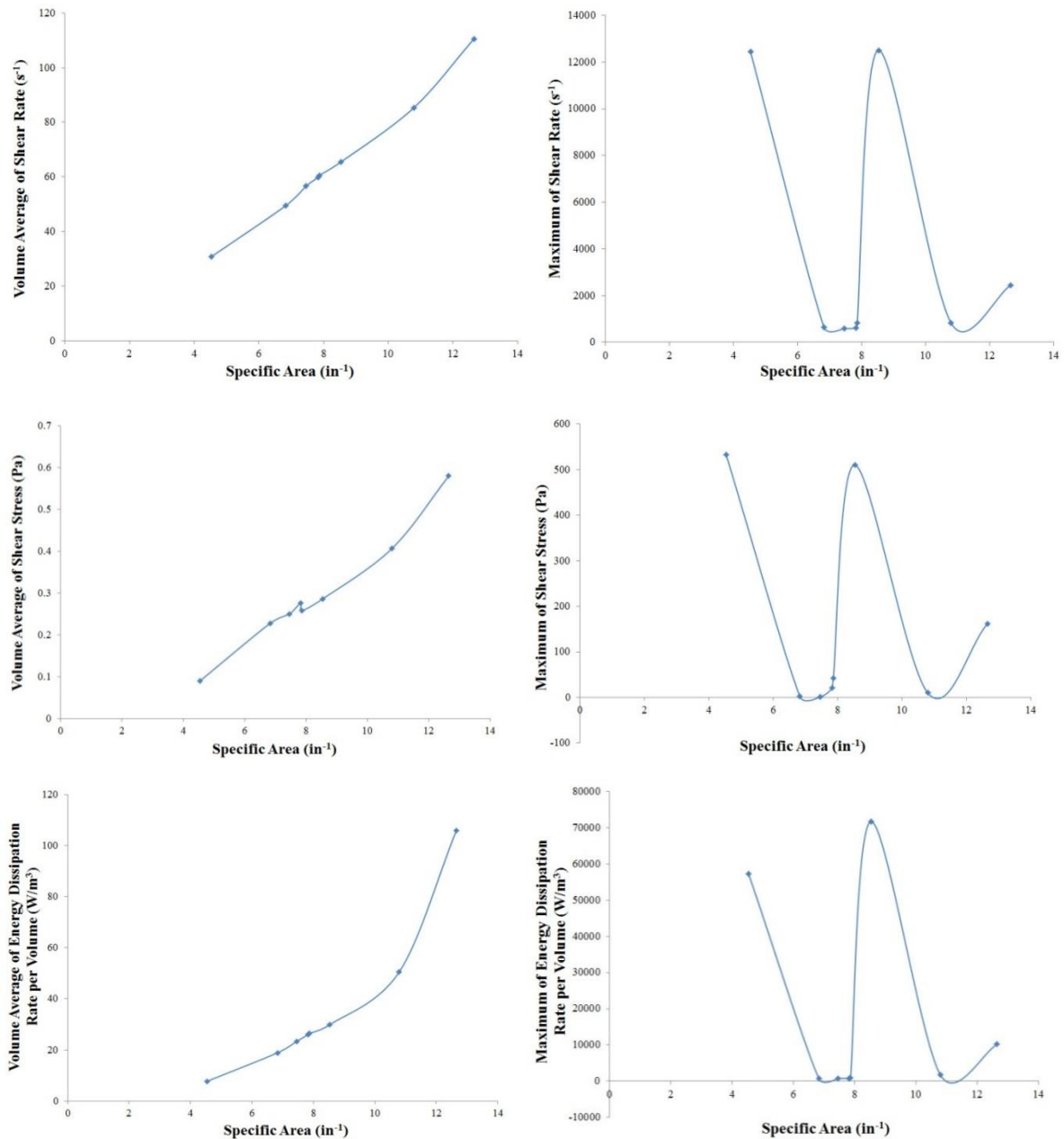
Figure 2.13 – The shear rate, shear stress and P/V as a function of MDR specific area

Totally, 35 combinations of triple variables were verified by FLUENT simulation and displayed by CFD-post. Under optimal operation condition and vessel dimension, the distributions of hydrodynamic parameters in the whole MDR and the symmetric plane, velocity magnitude contours and velocity vectors, particle motion streamlines are shown in figure 2.14, figure 2.15 and figure 2.16, respectively.

■ Distributions of Cell Reynolds Number:
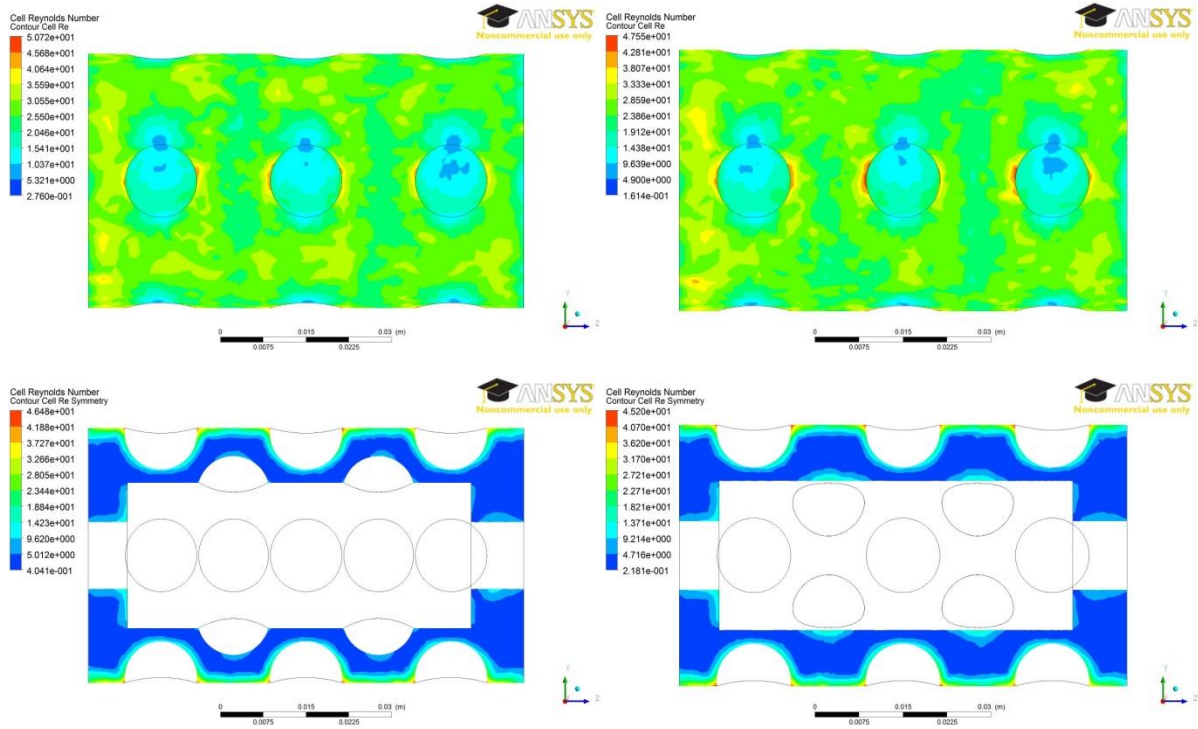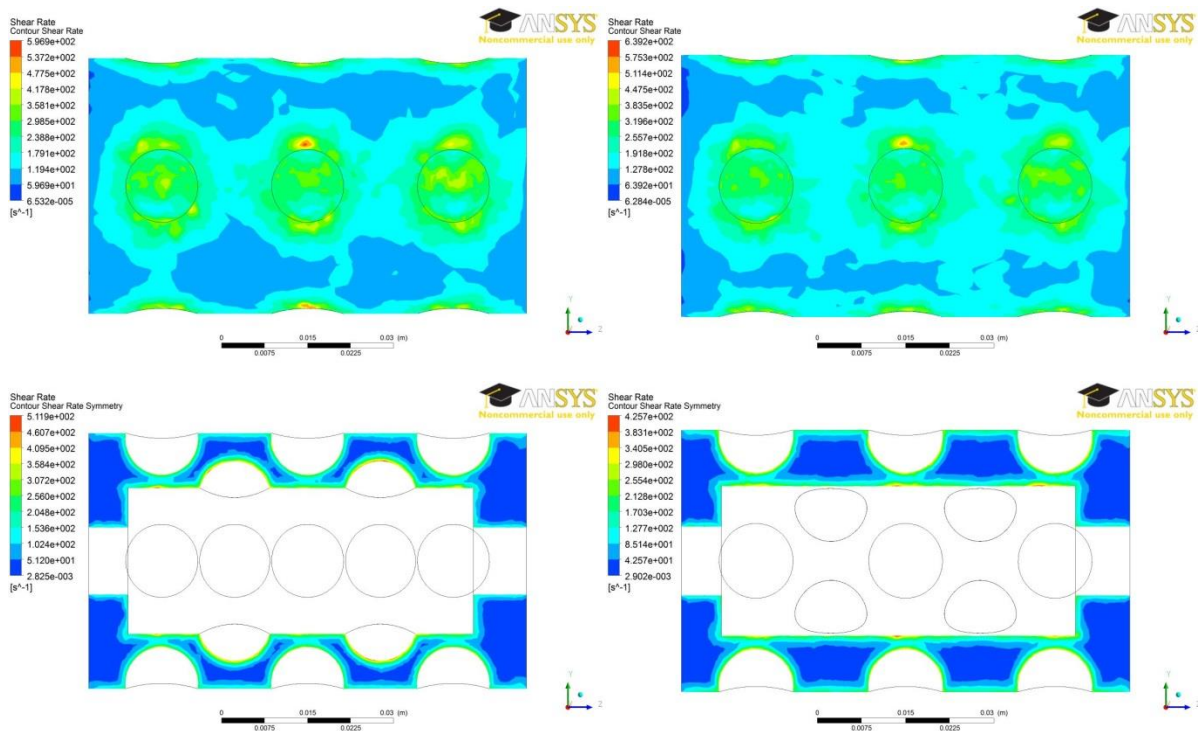
■ Distributions of Shear Rate (s⁻¹):

■ **Distributions of Energy Dissipation Rate per Volume (W/m³)**
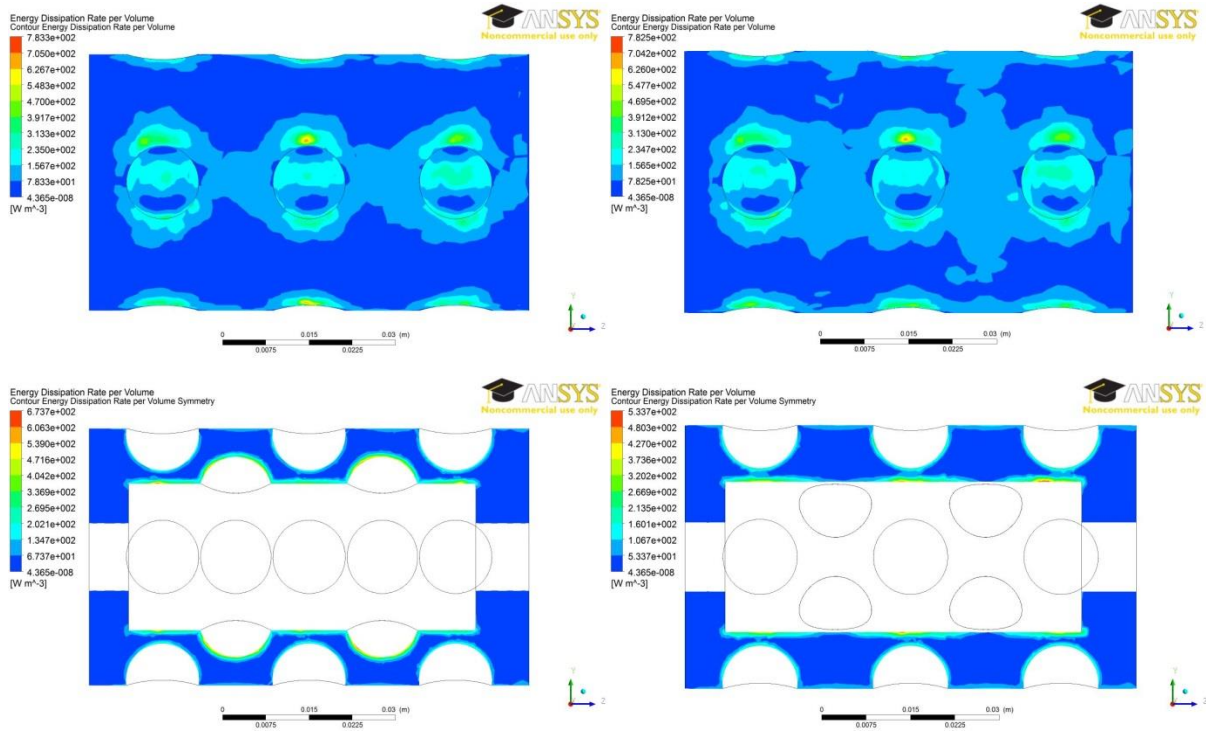
■ **Distributions of Kolmogoroff Length (m)**
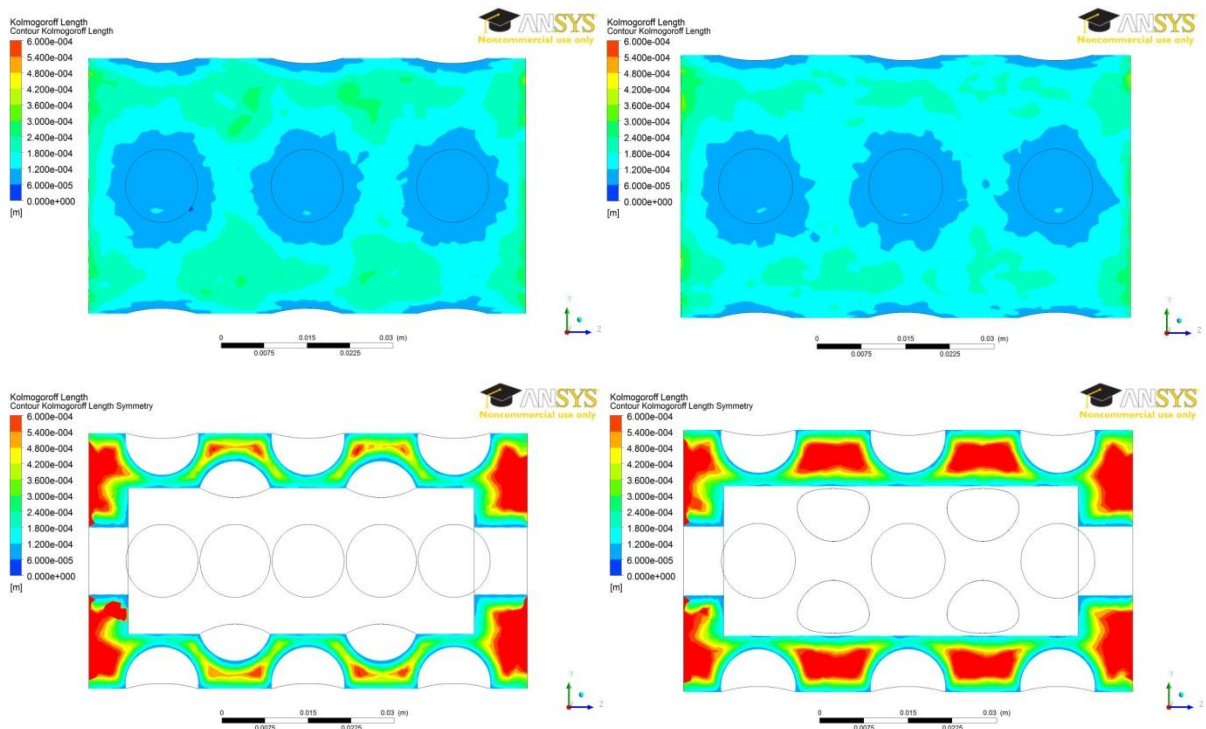
Figure 2.14 – Spatial distributions of hydrodynamic parameters for the MDR
(Left column – A position; right column – B position)
(Upper pair – volume; lower pair – central plane)
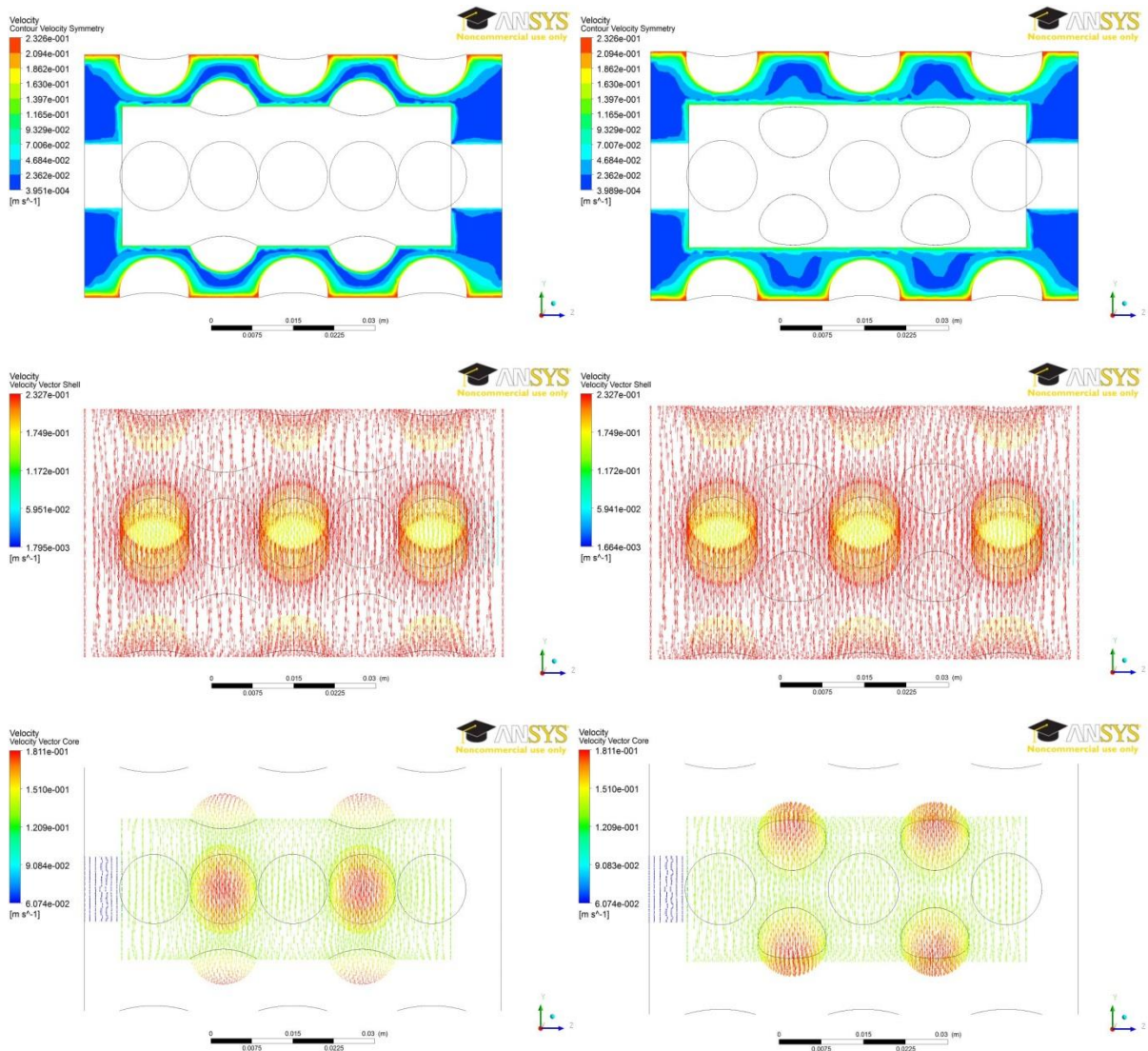
Figure 2.15 – Velocity magnitude contours on central plane and velocity vectors on the outer and inner cylinder walls (Left column – A position; right column – B position)
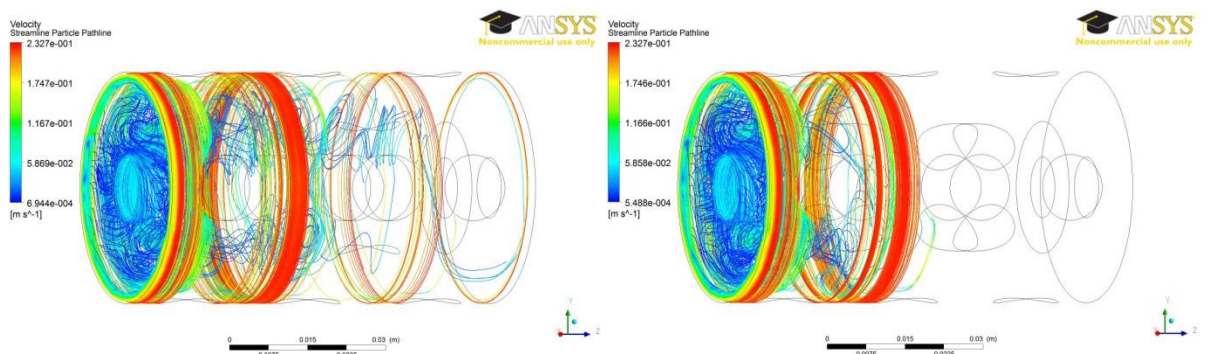
Figure 2.16 – The particle streamlines coincide with fluid element's paths (Left column – A position; right column – B position)

The percentage distributions of relevant parameters located on the MDR central plane are also shown in figure 2.17:

- **Percent of Cell Reynolds Number:**
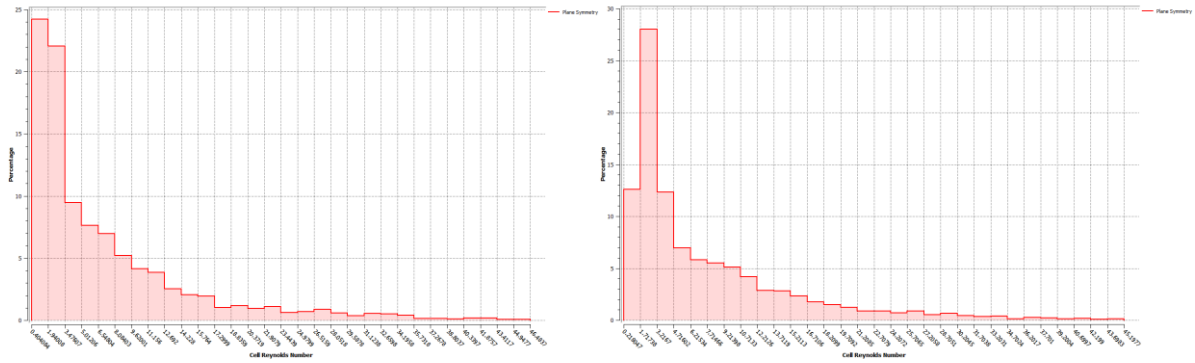
- **Percent of Shear Rate (s^{-1}):**
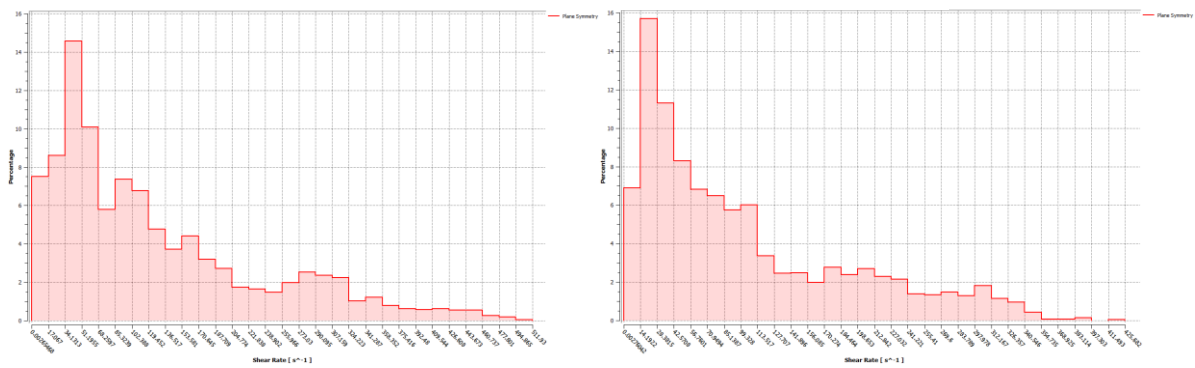
- **Percent of Energy Dissipation Rate per Volume (W/m^3):**
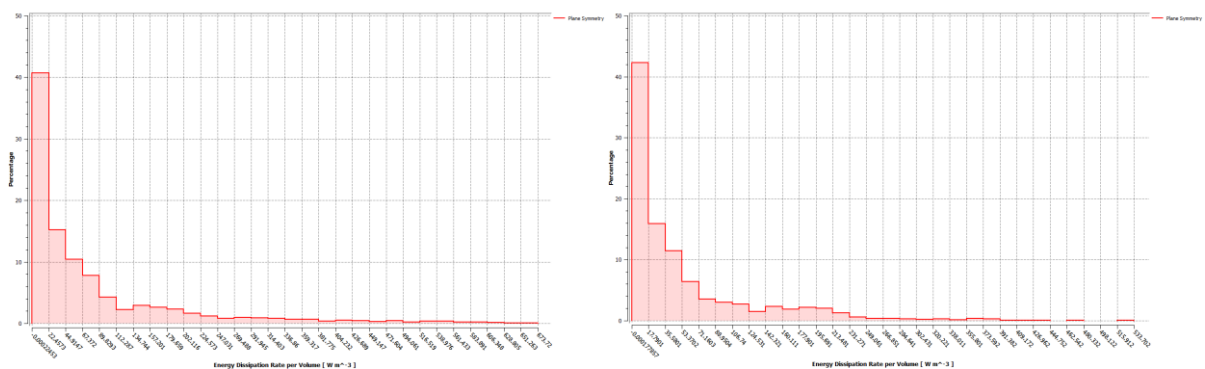
■ **Percent of Flow Velocity (m/s):**
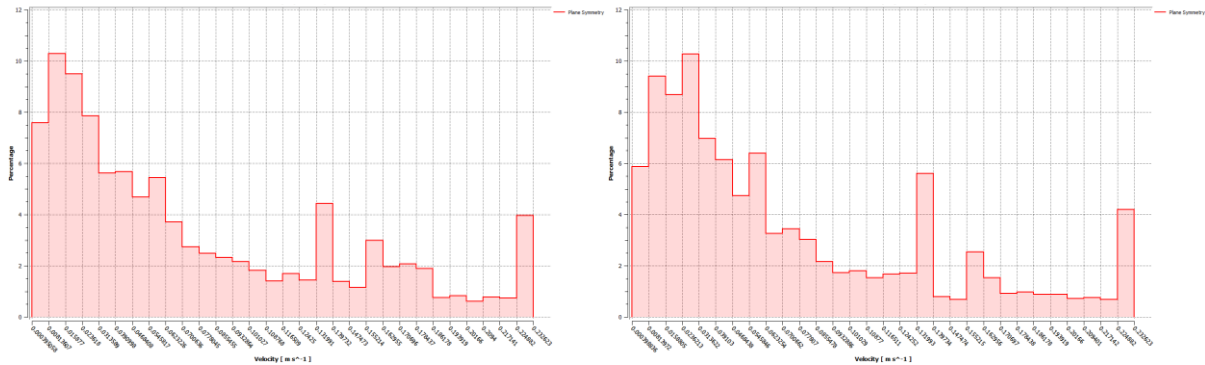
**Figure 2.17 – Histograms showing the percentage of flow parameters
on the MDR central plane
(Left column – A position; right column – B position)**

2.4.4 Comparison of results between Ricordi chamber and MDR

Three flow parameters, including shear rate, shear stress, and energy dissipation rate per volume, are summarized as volume average, minimum and maximum value in Table 2.2.

Table 2.2 – Numerical simulation results for Ricordi chamber and MDR

Digester type Flow parameters		Ricordi chamber		MDR	
		Rolling motion	Up & down motion	A position	B position
Shear Rate **(s^{-1})**	VolAve	28.3	17.6	49.5	48.1
	Min	0.000798	0.00219	0.000498	5.78E-05
	Max	4361	3364	651	620
Shear Stress **(pa)**	VolAve	0.487	0.131	2.28E-01	2.14E-01
	Min	2.40E-05	1.42E-05	3.96E-06	3.97E-06
	Max	14.4	13.0	2.23	1.27
P/V (W/m^3)	VolAve	46.3	20.5	18.9	17.4
	Min	1.92E-08	3.61E-07	4.36E-08	2.06E-08
	Max	57880	30879	736	755

P/V - energy dissipation rate per volume; VolAve - volume average value of corresponding

parameters. Spacing between two adjacent vanes is minimum at A, maximum at B

The comparison of above parameters indicate that volume average shear stress and

P/V for the MDR are lower than that for Ricordi chamber, with lower maximum values as

well. Moreover, the maximum of shear rate has the same results as that of shear stress and

P/V. However, volume average of shear rate shows the opposite results. The table clearly

demonstrates the absence of extreme conditions in the MDR.

2.4.5 The potential problems and alternative strategy for MDR design

Existing technologies of pancreatic digestion have fundamental limitations. The

design of the MDR, including the spacing between vanes and the rotational rates of the outer

and inner modules, may need to be studied in greater details if we are unable to either

suspend tissue during the digestion or if we are unable to separate islets from acinar tissue.

The complex interaction between the tissue fragments and the MDR walls/vanes may require

additional analysis resulting in a redesign. Problems with this design may require additional

CFD analysis in order to estimate the shear stress and the convection forces in the MDR. The

preliminary design of interacting hemispherical vanes may be altered. We also may only

allow one of these modules to implement in order to simplify the simulation. Nevertheless,

CFD analysis shows the proposed MDR design to be superior to the Ricordi method.

2.5 - Conclusions

The new design of the MDR digester succeeding partial feature of Ricordi chamber overcomes the deficiency of manual operation. This digester configuration is designed to enhance the turbulent effect and maximize contact area with more probability of collision and mixing between tissue fragments and vanes. FLUENT simulations confirm a more uniform and lower shear environment in the MDR within an appropriate range of operating parameters while both the shear and energy dissipation rates at the ball contact area in the Ricordi chamber are extremely larger than values in the MDR. However, the volume average value of shear rate for the Ricordi chamber is slightly lower than that for the MDR. Ricordi chamber fluid away from walls is near stationary. In addition, comparing MDR results between rotation position A and B indicates the cylindrical wall motion has little effect on the shear and energy dissipation rates. The MDR is worthy of further testing in particle-suspension and tissue digestion experiments.

2.6 - References

delos Santos B, Shiragami N, Unno H, Kariya M. 1994. A model for microcarrier motion inside a horizontally rotating bioreactor for animal cell culture. Bioprocess Engineering 11: 115-120.

Gao H, Ayyaswamy PS, and Ducheyne P. 1997. Dynamics of a microcarrier particle in the simulated microgravity environment of a rotating wall vessel, Microgravity Science and Technology X: 154–165.

Goodwin TJ, Wolf DA, Spaulding GF, and Prewett TL. 1996. Method for Producing Non-

Neoplastic, Three-Dimensional Mammalian Tissue and Cell Aggregates Under Microgravity Culture Conditions and the Products Produced Therefrom. US patent 5496722. 5 March.

Gray DWR, McShane P, Grant A, Morris PJ. 1984. A method for isolation of islets of Langerhans from the human pancreas. Diabetes 33: 1055-1061.

Hammond TG and Hammond JM. 2001. Optimized suspension culture: the rotating-wall vessel (Invited review). American Journal of Physiology. 281: F12–F25.

Horaguchi A, Merrell RC. 1981. Preparation of viable islet cells from dogs by a new method. Diabetes 30: 455-458.

Iwashita C, Asano T, Kenmochi T, Jingu K, Uematsu T, Nakagohri T, Hasegawa M, Maruyama M, Miyauchi H, and Isono K. 1996. Combined Method of Mechanical Chopper and Automated Two-Step Digestion Technique for Islet Isolation from Canine Pancreas. Transplantation Proceedings 28(1): 337.

Lacy PE, Kostianovsky M. 1967. Method for the isolation of intact islets of Langerhans from the rat pancreas. Diabetes 16: 35-39.

Liu T, Li X, Sun X, Ma X, Cui Z. 2004. Analysis on forces and movement of cultivated particles in a rotating wall vessel bioreactor. Biochemical Engineering 18: 97-104.

McCarthy, RC, Andrew GB, Michael LG, Francis ED. Tissue dissociation enzymes used for isolating islets for clinical transplantation: factors to consider in setting acceptance criteria. VitaCyte report.

Moskalewski S. 1965. Isolation and culture of the islets of Langerhans of the guinea pig. General and comparative endocrinology 5: 342-353.

Noel J, Rabinovitch A, Olson L, et al. 1982. A method for large scale high-yield isolation of canine pancreatic islets of Langerhans, Metabolism 31: 184-187.

Qiu QQ, Ducheyne P, Ayyaswamy PS. 1999. Fabrication, characterization and evaluation of bioceramic hollow microspheres used as microcarriers for 3D bone tissue formation in rotating bioreactors. Biomaterials 20: 989–1001.

Ricordi C, Lacy PE, Finke EH, et al. 1988. Automated method for isolation of human pancreatic islets. Diabetes 37: 413-420.

Rivera-Solorio I, Kleis SJ. 2006. Model of the mass transport to the surface of animal cells cultured in a rotating bioreactor operated in micro gravity. Biotechnology and bioengineering 94(3): 496.

McCarthy, RC, Andrew GB, Michael LG, Francis ED. Tissue dissociation enzymes used for isolating islets for clinical transplantation: factors to consider in setting acceptance criteria. VitaCyte report.

Tannehill JC, Anderson DA, Pletcher RH. 2004. Computational Fluid Mechanics and Heat Transfer. Taylor and Francis, second edition, ISBN 1-56032-046-X.

Todd P, Klaus DM, Stodieck LS, Smith JD, Staehelin LA, Kacena M, Manfredi B, and Bukhari A. 1998. Cellular responses to gravity: extracellular, intracellular and in-between. Adv Space Res 21: 1263–1268.

Todd P, Hodapp L, Jones A, Kennedy K, Popson T, Taylor E. 2004. Robotic Bioreactor for Cell Culture in Space Applications (Dynacult). Final Progress Report: 1-119.

Vosscheperkeuter GH, Vansuylichem PTR, Vonk MWA, Wolters GHJ, and Vanschilfgaarde R. 1997. Histochemical analysis of the role of class I and class II clostridium histolyticum

collagenase in the degradation of rat pancreatic extracellular matrix for islet isolation. Cell transplantation 6: 403-412.

Warnock GL, Ellis D, Rajotte RV, et al. 1988. Studies of the isolation and viability of human islets of Langerhans. Transplantation 45: 957-963.

Wolters G.H., Vos-Scheperkeuter G.H., Van Deijnen J.H., and Van Schilfgaarde R. 1992. An analysis of the role of collagenase and protease in the enzymatic dissociation of the rat pancreas for islet isolation. Diabetologia 35: 735-742.

3. Experimental Study of Particle Tracking in the MDR Digester

3.1 - Abstract

In the particle tracking test, we can automatically follow particles by using different colors and names to classify and organize the measurements, including the distance traveled, orientation of each track, and more. The key point in our project is to find an easier way to identify the particle streaks and measure the lengths for them. A new app in Image-Pro Premier software called "Fiber Separation and Measurement App" is introduced to realize the automatic identification process. The particle dispersion test reveals that the particles will move along a certain path controlled by the action of different hydrodynamic forces. Localized turbulent flow can be seen through the transparent shell wall. The complete mixing process occurs in the intermediate region between adjacent vanes and double walls without any sedimentary particles. When the inner core is stopped while only the outer shell keeps rotating at 50 rpm, this is more than adequate to suspend the particles. The particle streaks are formed using time-exposure photography by means of opening the camera shutter for a selected time interval. Almost 100 per cent of particle velocity determined by the experiment is distributed in the numerical range of velocity 0.01 m/s to 0.2 m/s. Finally, 1/40 s as the optimal shutter speed provided good agreement between experimental and numerical results.

Key words: **Particle tracking, particle streaks, Image-Pro Premier software, time-exposure photography, velocity histogram**

3.2 - Introduction

Confirmation of the predictions of chapter 2 depends on particle tracking, a topic for which interest has increased exponentially in recent years. It is impossible to manually follow hundreds to thousands of particles through many hundreds to thousands of image frames in live imaging process, so sophisticated approaches are needed for these tasks (Meijering, 2012). Although the first attempts to automate the tracking of particles by digital image processing date back at least 30 years, the development of more advanced tracking methods was rising rapidly in the past decade. There are generally two methods to solve the tracking problem of particles: 1) segmentation: the recognition of relevant objects and their separation from the background in every frame, and 2) linking: the association of segmented objects from frame to frame and making connections.

Quite a number of particle tracking tools already exist but there is no single criterion to decide which one is best for a given purpose. Most of tools assume the target objects to contrast significantly with the local background, and filtering of the images generally has a positive impact on their performance. In contrast with the mentioned commercial tools, many of which offer the most user-friendly interfaces and extensive functionality but may be prohibitively expensive, most free particle tracking tools are sufficient either as a plugin of the widely used image analysis platform or as a Matlab module. While all tracking tools generally perform well if the image data satisfies certain conditions, experimental constraints often force these conditions to be violated. In addition, some proteins or molecular complexes are hardly visible in bright field or phase-contrast microscopy and require fluorescent labeling and imaging. Since fluorescent proteins are two orders of magnitude smaller than the optical resolution of typical microscopes, they appear as diffraction limited spots in the images. The outcome of a recent

comparison study (Smal et al., 2010) suggest that better results can be obtained by specialized algorithms from mathematical morphology and supervised approaches.

A video microscope installed on the particle tracking velocimeter (PTV) is utilized to image the cultispher particles with various degrees of magnification, and a computer connected with PTV is used to capture and process the video image as illustrated in Figure 3.1.

Figure 3.1 – Image from Hyperflux PTV using cultisphers as tissue fragment surrogates.

Meijering (2012) defines the following velocity terms: (1) instantaneous velocity is computed as the displacement from one frame to the next, divided by the time interval. It is important to realize that this quantity is a vector, and its magnitude value is called speed, although the latter is also referred as velocity in some literature. (2) The mean curvilinear speed is calculated as the arithmetic mean of the instantaneous speeds. If the frame rate is constant, this is equal to computing the ratio of the total distance traveled to the total trajectory time. (3) Alternatively, if we use the net distance traveled, the ratio yields the mean straight-line speed. The velocity ratio of the latter (3) to the former (2) is a parameter used to calculate the linearity of forward progression. It is advisable to make velocity histograms instead of taking grand

averages (Qian et al., 1991; Bahnson et al., 2005), as they give more insight into the statistics of the dynamics. After a brief description of the time-exposure photography, we highlight the Image-Pro premier, a powerful software tool for particle-streak identification and measurement, and then discuss the strategy to calculate the particle velocity and plot the histograms.

3.3 - Image-Pro Premier software and its fiber app (Media Cybernetics internet source)

Image-Pro Premier is a sophisticated image processing software capable of removing background noise and enhancing hidden details with an extensive set of image processing filters. The filters can be previewed on the active image for instant results. In particle tracking, we can manually or automatically follow particles by using different colors and names to classify and organize the measurements, including the distance traveled, orientation of each track, and more. We can even track challenging objects that fade out of view and move out of the image workspace. Automation tools for image processing not only save time by eliminating repetitive steps, but more importantly, they minimize the chance of errors or inconsistencies.

The key point in our project is to find an easier way to identify the particle streaks and measure lengths for them. Most researchers end up manually counting and measuring the lengths, which is not only a time consuming process but also can cause inconsistencies. However, a new app in Image-Pro Premier called "Fiber Separation and Measurement App" is introduced to deal with this problem, it is possible to measure and classify overlapping streaks with one button click. At first, all the particle streaks should be assumed to be strip-like fibers. The fiber app is designed for applications where the entire fiber is visible in the image. Although our eyes can detect overlapping structures, most image processing software programs are unable

51

to automatically segment fibers. Multiple fibers are often lumped into one structure, resulting in inaccurate results. This app allows users to automatically detect, measure and classify overlapping fibers in an image. Not only does it offer a significant time savings, but also ensures that the same analysis techniques are applied consistently to all images. In addition, it can easily separate overlapping fibers and determine measurements such as length and thickness, and automatically classify the fibers by length and display in different colored groups. These results are also available to export to a report or Excel.
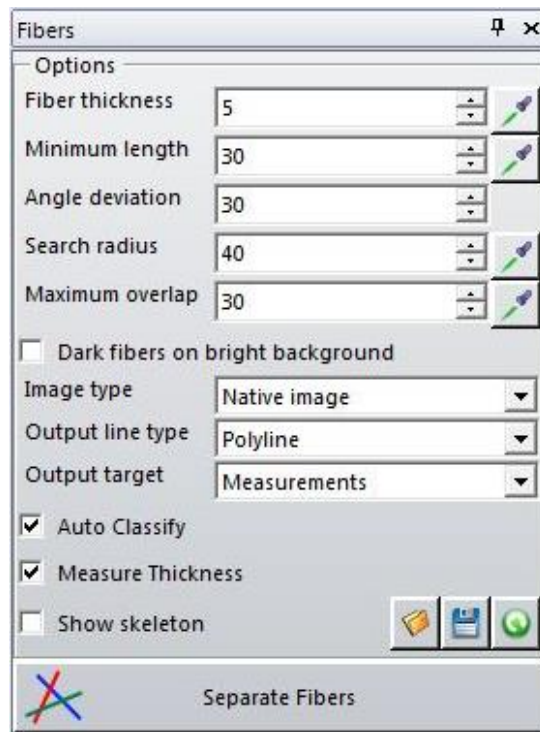
Figure 3.2 – The Overview of Fiber Separation Options in Image-Pro Premier

We may need to make some settings adjustments shown in Figure 3.2 when using the fiber app on a new image. This section will walk through the various parameters as follows. Fiber thickness defines the thickness of fibers in pixels used to extract a skeleton of the fibers. We can click the right eyedropper tool to draw across the thickest fibers we wish to analyze. The minimum length defines the minimum fiber length in pixels. Fibers shorter than this limit will

be ignored. The angle deviation defines how much the fibers can be bent. If the limit is small, only the straight fibers will be detected as separate. This parameter is used to connect branches in the node area. If the orientation of branch vectors differs for more than the given value, the branches will be considered separate. The search radius is the maximum size of the overlapping fiber area used to analyze how fibers are connected. The maximum overlap stands for the length or the area where two fibers can be overlapped, but still be separated if they have visibly separate end points.

The default type of fiber image is bright fibers on dark background. In our project this option should be changed by checking the "Dark fibers on bright background" box. The source image type can be divided into three categories: native image is the default option that is used in a gray-scale or color image. Binary Image is chosen if the binarization is required or a custom binarization algorithm is used. Skeleton is selected when the skeletonization is done using a custom algorithm. The output line type can be either polyline or start-end line. In case of polyline type the output will be a polygonal line following the skeleton branches. With start-end line type the output is a straight line connecting the first and the last point of the fiber. The output target is including measurements that are the default output, or annotation.

When it is set to measurements and the auto classify option is active, the fibers will be automatically classified by lengths and are displayed in different colors based on their classification grouping. It will also display a data histogram of the classified fibers. The annotation option will separate fibers and display an overlay, but will not output measurement data. In some cases the fiber thickness is necessary to measure. When this option is on, the average fiber thickness on the basis of the thickness of binarized fiber image is measured. The fiber thickness measurement is automatically added to the selected list of measurements and

reported in the data table and other data windows. We can activate the show skeleton checkbox to follow the fiber separation algorithm step by step. After all the relevant settings are adjusted, the separate fibers button on the bottom is clicked to output the measurements.

3.4 - Materials and Methods

3.4.1 The dimension of MDR device in the experiment

On the basis of section 2.4.3 in chapter 2, the targeted vessel dimension is optimized by CFD simulation (see Table 2.1, the specific area is 7.46 in^{-1} (294m^{-1})). The optimal dimensions of MDR are illustrated in figure 3.3. The diameters of outer and inner wall D=1.75'' (0.0445m) and d=1'' (0.0254m) are known, so that the radii of outer and inner wall are R = D/2 = 0.875'' (0.0222m) and r = d/2 = 0.5'' (0.0127m), respectively. The maximum of resulting gap width is d_{max} = R-r = 0.375'' (9.53E-03m); the minimum gap d_{min} = d_{max}-r_v = $\sqrt{d_{max}^2 + (2r_v)^2} - 2r_v$ = 0.125'' (3.18E-03m) (r_v is radius of the vane). In addition, the radius of hemispherical ball r_{hb}=0.25'' (6.35E-03m) (Diameter of half-ball is 0.5'' (0.0127m))

So, the maximum of core radius $r_1 = \sqrt{r^2 - r_{hb}^2} + r_{hb} = \sqrt{0.5^2\text{-}0.25^2} + 0.25 = 0.683''=0.0174m$

the minimum of shell radius $r_2 = \sqrt{R^2 - r_{hb}^2} - r_{hb} = \sqrt{0.875^2 - 0.25^2} - 0.25 = 0.589''=0.0150m$
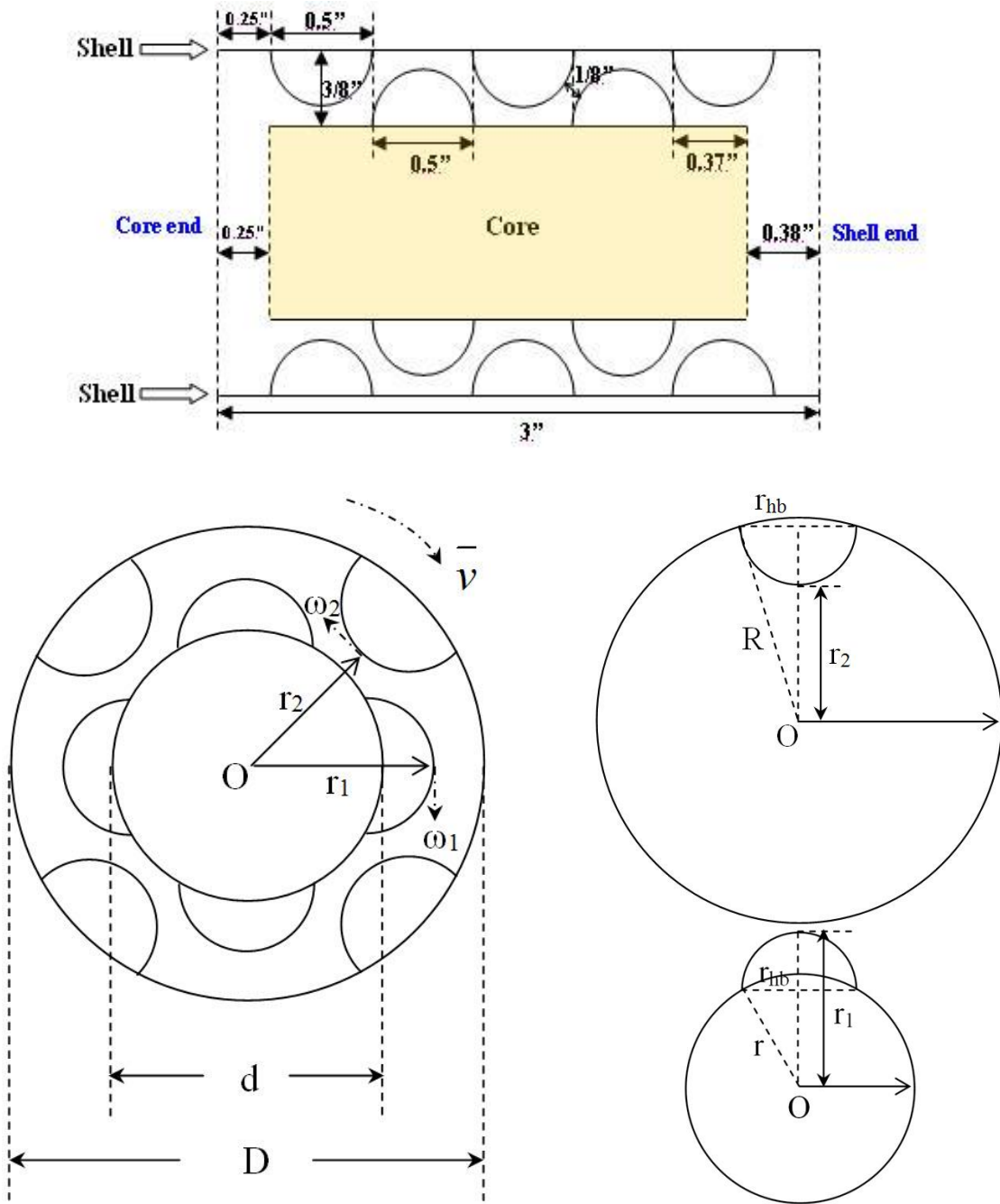
Figure 3.3 – The dimensions of MDR digester

3.4.2 Particle dispersion test using cultisphers

Two and one/half grams of cultispher particles (gelatin bead, size range from 130 to 380µm, Sigma-Aldrich, Saint Louis, MO) are weighed on the balance, then 250 ml phosphate

buffered saline (PBS) is added into the particles and soaked for two hours. After that, most of the particles are sedimented on the bottom of the beaker with only a small amount suspended. The fully hydrated cultispher particles are rinsed several times and mixed with certain amount of pure water to prepare the suspension with certain concentration. The motor is operated at four different voltage 6, 8, 10 and 12 volt (12 is nominal voltage). The corresponding rotation speed (rpm) is measured by RPM meter (Monarch Instrument, Amherst, NH).

In the dispersion process, particle suspension is pumped into the water-filled digester at flow rate 60 ml/min. Initially, only the shell is rotating as controlled by applied voltage, subsequently the double walls are rotating in opposite directions operated in a closed circulation at maximum rotation speed. The particle motion and collision are observed in detail. Finally, the time interval (dispersion time) is measured between when the particles are firstly seen and when particles completely fill into the vessel. All the particle motion process is recorded by digital camera.

3.4.3 Time-exposure experiments using stained acinar tissue

Fixed acinar tissue from University of Minnesota with 20 mL volume is diluted to 90 mL in phosphate buffered saline (PBS) to reach a final concentration of about 50,000 fragments/mL. The dye methylene-blue is used to stain tissue fragments/particles. The detailed process is as follows: add the same volume of methylene-blue into the acinar tissue suspension contained in a centrifuge tube, and then the tube is shaken slowly by putting it on the platform shaker. After about 4 hours, the tissue suspension is centrifuged under 2000 rpm for 10 min and the supernatant is removed. PBS solution is then added up to 45 ml level in this tube to rinse the tissue fragments, and remove the supernatant again after centrifugation under the same rotation

speed for 5 min. The rinse and centrifugation process is repeated for several times until the supernatant is clear (very light blue or close to no color). Finally, About 75 mL of the standard acinar tissue suspension is pumped into the PBS-filled MDR chamber at 120 mL/min of inlet flow rate while rotating the double walls in opposite directions at 50 rpm. Subsequently, the MDR is operated at the same rotation speed without inlet flow. The fragments' motion and collisions are recorded as time-exposure photography by Canon EOS 6D camera at a gradient of shutter speeds; 1/40, 1/25, 1/15, and 1/8 s. Finally, only inner core is stopped while outer shell keeps rotating, after 4 min or less operation the core rotation is switched on 50 rpm again.

3.4.4 Image post-processing

In the interface of Image-Pro Premier software, the picture is opened and zoomed in until only the particle area is shown in the screen. Then, the function of quick calibrate is used to adjust the whole dimension of MDR. Select the region of interest (ROI that includes particles) and click "best fit" button to change dark degree of the background color. The next important process is to use the 2D filters High-Gaussian to remove the noise and make the particle streaks easier to recognize. Copy the ROI and save as a new picture for further "Fibers App" identification. The relevant parameter settings are shown in Table 3.1, and the options of dark fibers on bright background and auto classify should be checked in the left square area. Press "separate fibers" button and then the lengths of particle streaks will be generated by this system.

Table 3.1 – The Overview of parameter settings in Image-Pro Premier

Fiber thickness	**2 pixel (5.29E-04m)**
Minimum length	**10 pixel (2.65E-03m)**
Angle deviation	**20**
Search radius	**10 pixel (2.65E-03m)**
Maximum overlap	**10 pixel (2.65E-03m)**
Image type	**Native image**
Output line type	**Start-end line**
Output target	**Measurements**

3.5 - Results and Discussion

3.5.1 The general description of particle motion and the mixing process in the MDR

For the cultispher particle dispersion test, all the particles are already inside the MDR device rather than pumping them into the vessel. The particle dispersion time and relevant phenomenon are summarized in Table 3.2:

Table 3.2 – The dispersion process for Cultisphers

Voltage (V)	RPM	Dispersion mixing time (s)	Particle suspension
6, shell only	7	22	Very few particles are suspended.
8, shell only	10	19	Suspended and sedimentary particles are nearly equal.
10, shell only	13	15	More particles are suspended.
12, shell only	17	13	More particles are suspended.
12, in opposite directions	17 (Shell end) 21 (Core end)	11	All the particles are suspended in turbulent flow.

The particle distribution is snapshotted from the top of cylinder walls when the mixing process is complete (Figure 3.4). When the outer shell is only rotating, more sedimentary particles accumulate onto top of the core with lower rotation speed while more and more particulates suspend into the liquid with increasing rotation speed. In addition, the sedimentary section becomes blurry and scattered. When the double walls of MDR are rotating in opposite directions at maximum speed, it is indicated that none of particles sediment on the core.
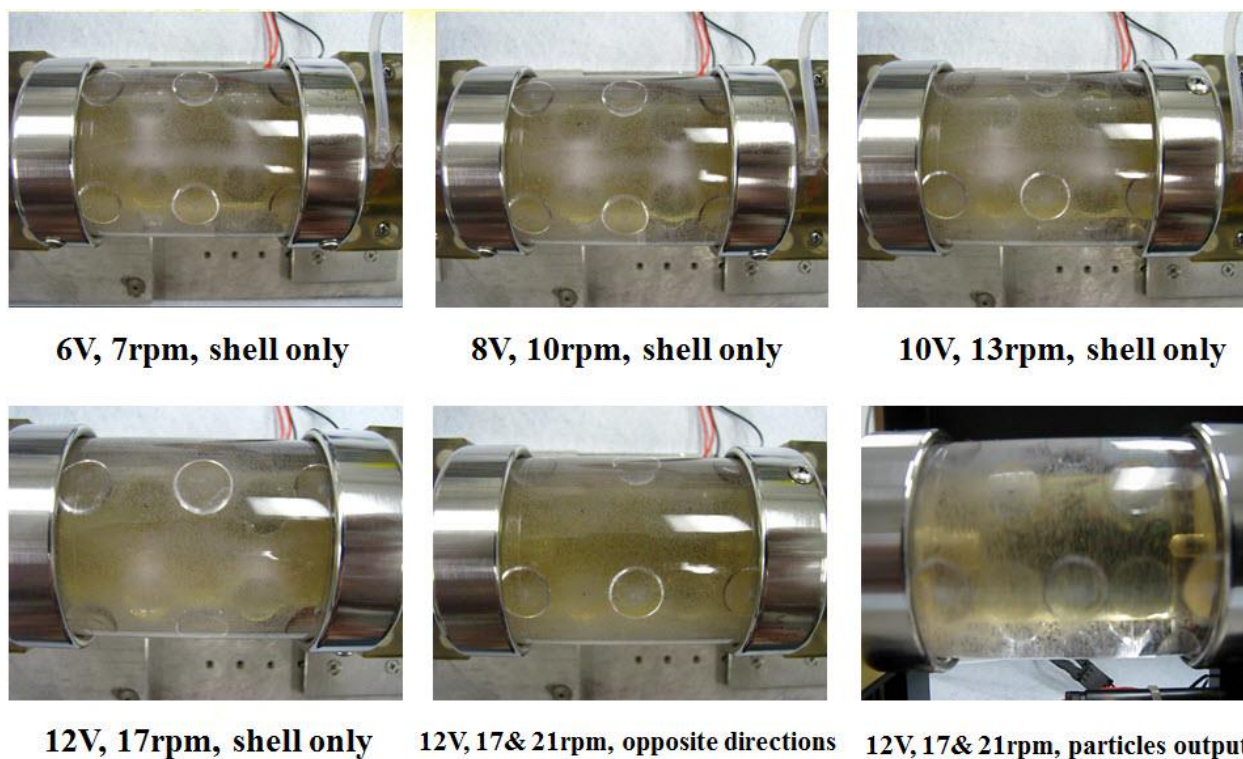
Figure 3.4 – The snapshots in cultisphers dispersion test

Effect of opposite rotation of the cylinder walls on the particles motion is described as follows: the particles will move along a certain path controlled by the action of different hydrodynamic forces. Localized turbulent flow can be seen through the transparent shell wall. The complete mixing process occurs in the intermediate region between adjacent vanes and double walls without any sedimentary particles while the particles near the walls will move with the shell/core in the same direction. When only inner core is stopped while outer shell keeps rotating, this is more than adequate to suspend the particles.

3.5.2 Comparison of particle streaks under different shutter speeds

The reason why the cultispher sample is not used in the time-exposure experiment is that it is more difficult to stain with methylene blue even if staying for a couple of days. The blue color fades rapidly when the stained cultispher particles are rinsed with water. Even in the white

background, it is impossible to identify the particle streaks using Image-Pro software due to the weak contrast. However, the fixed acinar tissue from University of Minnesota, which is judged to be 30 to 150 μm in diameter under microscope, is really a good material used to perform the particle test. All the tissue fragments are stained by methylene blue in order to enhance the effect of tracking.

An experimental analysis of the relative particle-to-fluid motion shows that fragments rapidly disperse over the entire chamber, and then begin to appear in the exit flow. The particle streaks are formed using time-exposure photography by means of opening the shutter of the camera for a longer time than normal. Figure 3.5 shows the pictures of particle streaks taken under different shutter speeds 1/40s, 1/25s, 1/15s, 1/8 s and corresponding length distributions generated by Image-Pro Premier. Note that the arrows shown in this picture do not represent velocity directions because they are scalar lengths automatically generated by the fiber-length software.
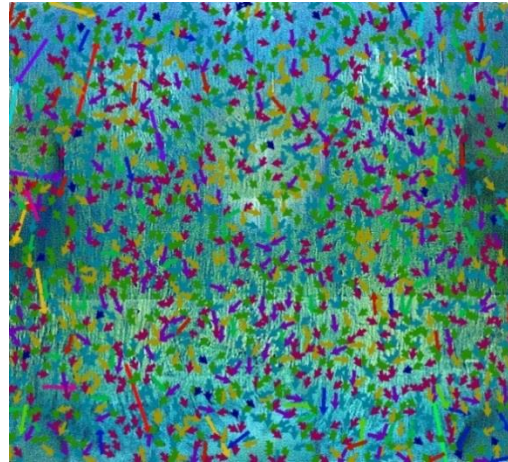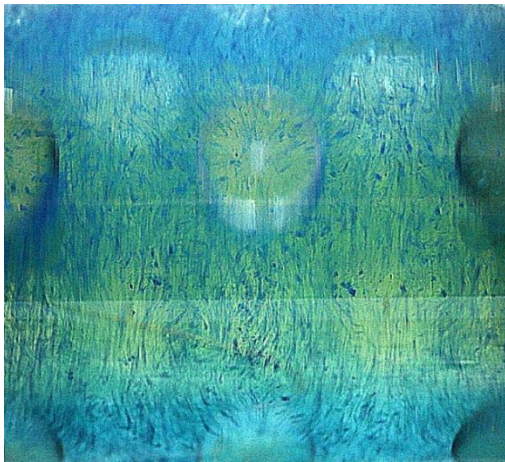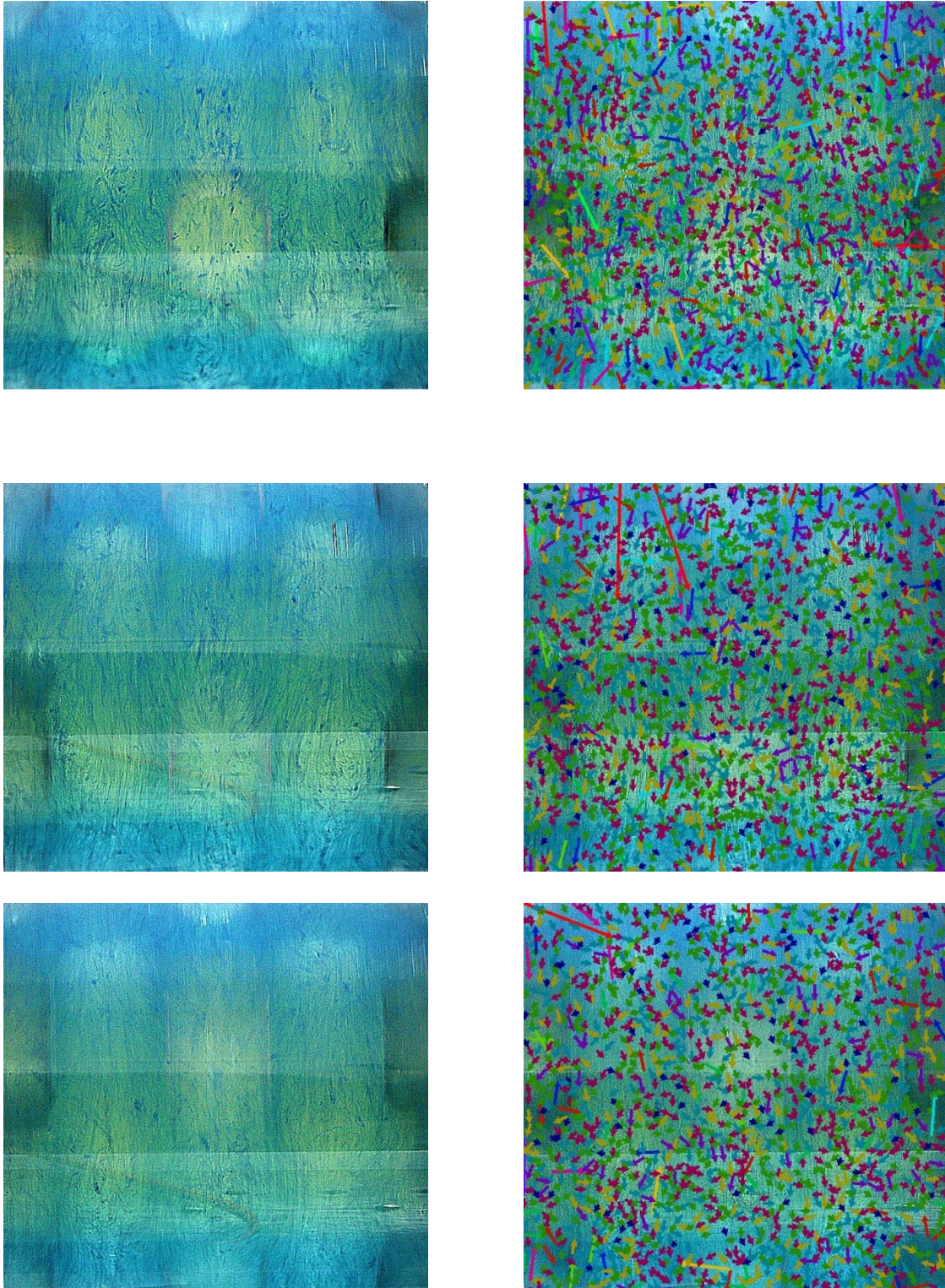
Figure 3.5 – Time-exposure photography (Left) and streak lengths (Right)

(The shutter speed is 1/40s, 1/25s, 1/15s, 1/8 s toward the bottom picture)

The effect of shutter speed on particle streaks will be revealed by Figure 3.5. In the left column of time-exposure photos, the higher shutter speed of the camera, the more clear streaks will be detected. When the shutter speed reaches the minimum value 1/8s, very few streaks can be seen by naked-eye while these can only be identified by the fiber app of Image-Pro software. In the right column showing streak lengths, the number of particle streaks tends to be a little bit smaller with the reduction of shutter speed but the range of streak lengths has no significant change. Meanwhile, this outcome is also reflected in the relevant data of Table 3.3. Based on the log scale histogram in Figure 3.6, the shutter speed has little impact on the percentage of particle streak lengths. 1/40s is thereby chosen as the optimal shutter value in view of much easier recognition of particle streaks.
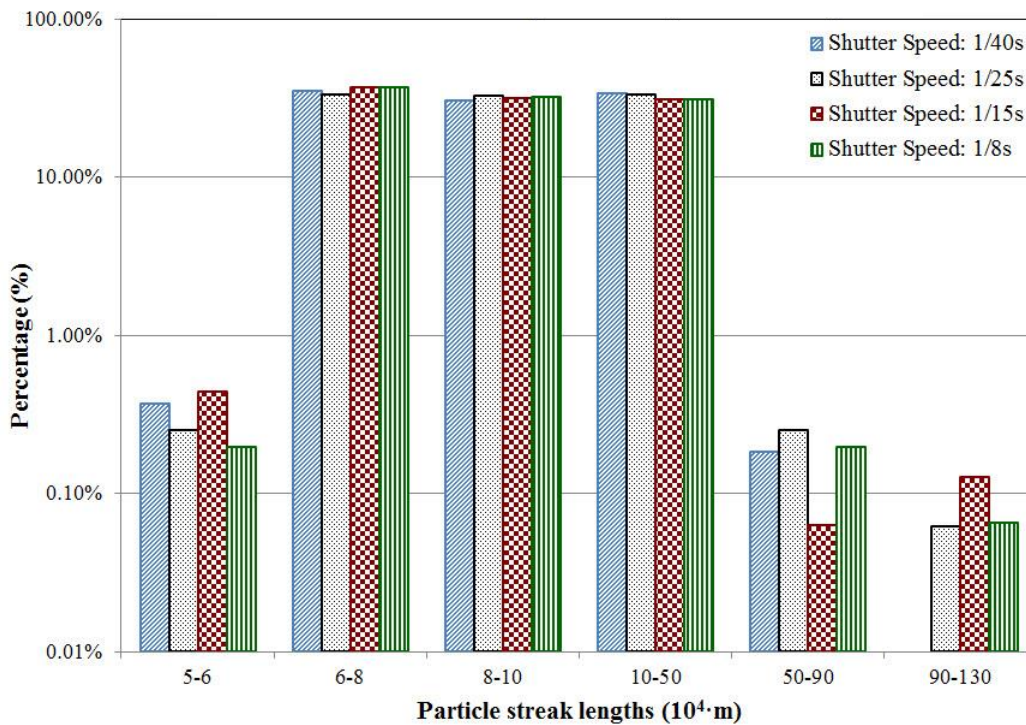
Figure 3.6 – Logarithmic scale histogram of particle streak lengths

Table 3.3 – The data of particle streaks calculated by Image-Pro Premier

Shutter speed (s)	Number of particle streaks	The range of streak lengths (m)
1/40	1628	5.50E-04 ~ 7.12E-03
1/25	1604	5.45E-04 ~ 1.14E-02
1/15	1589	5.52E-04 ~ 1.25E-02
1/8	1533	5.53E-04 ~ 1.03E-02

3.5.3 The effect of shutter speed on histograms of particles velocity

After the length of particle streaks is measured by Image-Pro software, the particle velocity (v) is calculated and then plot in the histograms under different shutter speeds (shown in Figure 3.7). In order to show the percentage of velocity more clearly, the log scale percentage is applied on the vertical axis. In contrast with the histogram of streak lengths, Figure 3.7 indicates that the effect of shutter speed on the percentage of particle velocity cannot be neglected. The value 0.01m/s is considered as the watershed to divide velocity zones into two parts: low velocity zone (LVZ) if v ≤ 0.01m/s and high velocity zone (HVZ) if v > 0.01m/s. When the shutter speed is controlled under higher value 1/40s or 1/25s, the velocity is all located in HVZ. However, the lower shutter 1/15s or 1/8s will cause the distribution of velocity to move towards LVZ. Most of the velocity is distributed between 0.01 and 0.05 m/s. The percentage of velocity in this range is about 86 to 96 per cent.
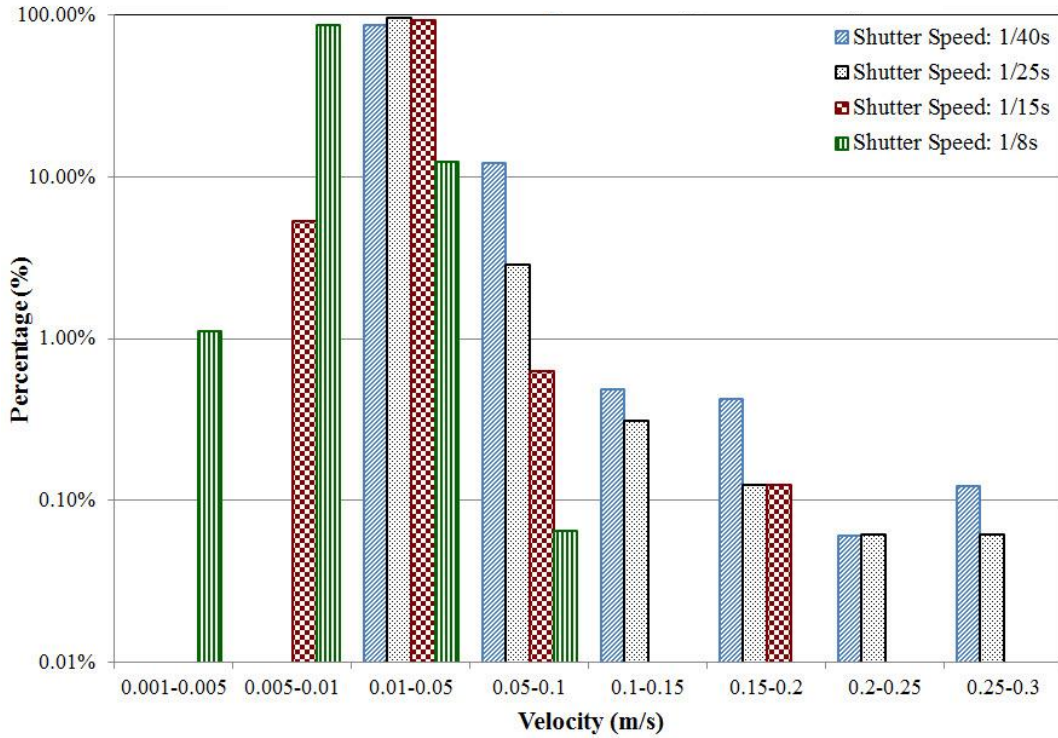
Figure 3.7 – Logarithmic scale histogram of velocity

3.5.4 The numerical calculation of relative velocity

The double wall rotation speeds controlled at 50 rpm are adequate for holding the stained tissue particles in suspension. So, $\omega_s = \omega_c = 50$ rpm = 5.236 rad/s. The relative velocity of single particle $v = \omega_s r_s \pm \omega_c r_c = 5.236*(r_s \pm r_c)$. In which, ω_s is rotation speed for outer shell; ω_c is rotation speed for inner core; r_s is radius of the shell; r_c is radius of the core.

The relative velocity reaches the maximum v_{max} if two particles collide in the same direction while it will be reduced to be minimum v_{min} if two particles collide in opposite directions. Based on the data information in Figure 3.2, v_{max} and v_{min} can be calculated below:

$$v_{max} = 5.236*(r_s \pm r_c) \big|_{max} = 5.236*(r_s \big|_{max} + r_c \big|_{max}) = 5.236*(R + r_1) = 0.20 \text{m/s};$$

$$v_{min} = 5.236*(r_s \pm r_c) \big|_{min} = 5.236*(r_s \big|_{min} - r_c \big|_{min}) = 5.236*(r_2 - r) = 0.01 \text{m/s}.$$

Theoretically, the velocity range of particles should be between 0.01 m/s and 0.2 m/s.

3.5.5 The comparison of experimental results with numerical calculation

In the time-exposure experiment, the particle velocity is calculated and listed in Table 3.4.

Table 3.4 – The data of velocity percentage under different shutter speeds

Velocity (m/s)	Percentage			
0.001-0.005	0.00%	0.00%	0.00%	1.11%
0.005-0.01	0.00%	0.00%	5.35%	86.4%
0.01-0.05	86.7%	96.6%	93.9%	12.4%
0.05-0.1	12.2%	2.87%	0.629%	0.0652%
0.1-0.15	0.491%	0.312%	0.00%	0.00%
0.15-0.2	0.430%	0.125%	0.126%	0.00%
0.2-0.25	0.0614%	0.0623%	0.00%	0.00%
0.25-0.3	0.123%	0.0623%	0.00%	0.00%
Shutter speed (s)	1/40	1/25	1/15	1/8

By comparing with the numerical velocity range 0.01m/s–0.2m/s, the percentage of velocity (P_v) determined by the experiment in this range is calculated below:

P_v = 86.7% + 12.2% + 0.491% + 0.430% ≈ 99.8% if shutter speed is 1/40s;

P_v = 96.6% + 2.87% + 0.312% + 0.125% ≈ 99.9% if shutter speed is 1/25s;

P_v = 93.9% + 0.629% + 0.00% + 0.126% ≈ 94.7% if shutter speed is 1/15s;

P_v = 12.4% + 0.0652% + 0.00% + 0.00% ≈ 12.5% if shutter speed is 1/8s.

In the higher shutter speed 1/40s and 1/25s, almost 100 per cent of velocity determined by the particle test is distributed in this numerical range which indicates the good agreement between experimental and numerical results. Finally, the value 1/40s is selected as the optimal shutter speed on the basis of above calculation results and relevant velocity percentage is shown as a log scale histogram in Figure 3.8.
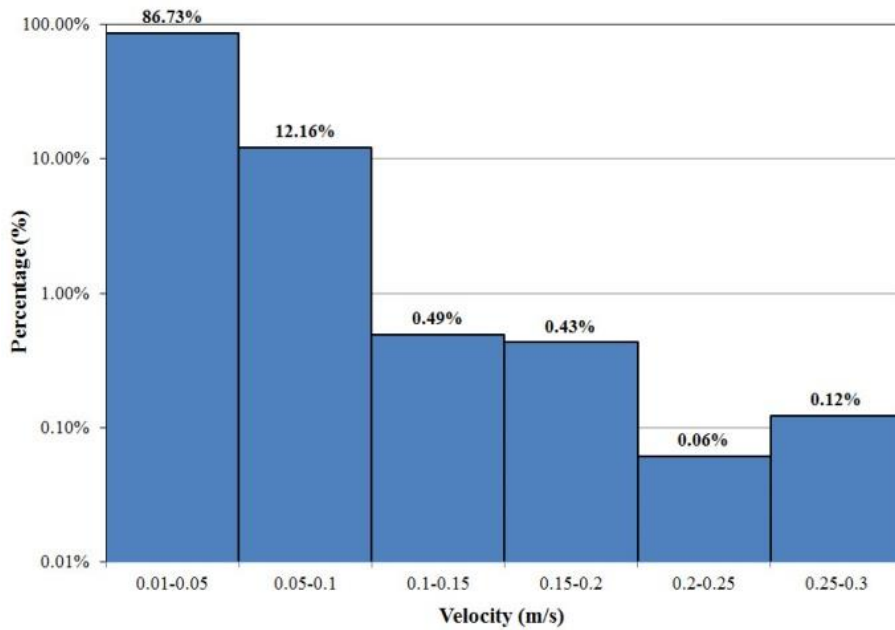
Figure 3.8 – The logarithmic scale histogram of particle velocity

3.6 - Conclusions

The capability of particle mixing in MDR is confirmed by cultispher dispersion test. The methylene blue-stained fixed acinar tissue is superior to cultispher particles in the time-exposure experiment. The purpose of this experiment is to form the particle streaks by reducing the normal shutter. As the sophisticated image processing software, Image-Pro Premier is successfully used to measure the length of particle streaks for further calculation of velocity. The most important image post-processing is to use the 2D filters High-Gaussian to make the streaks

easier to recognize. Relative to streak lengths, the shutter speed has more impact on the distribution of particle velocity. Finally, the parameter shutter speed is optimized to be 1/40s based on the visibility degree of particle streaks and the validation performed by the comparison of numerical results with experimental velocity data.

3.7 - References

Bahnson A, Athanassiou C, Koebler D, Qian L, Shun T, Shields D, Yu H, Wang H, Goff J, Cheng T, Houck R, Cowsert L. 2005. Automated measurement of cell motility and proliferation. BMC Cell Biology 6: 19.

Meijering E, Dzyubachyk O, Smal I. 2012. Methods for cell and particle tracking. Methods in Enzymology 504 (9): 183-200.

http://www.ikotech.com/HD-MPTV.html

http://www.mediacy.com/index.aspx?page=IP_Premier

http://www.mediacy.com/index.aspx?page=App_FiberSeparation

Qian H, Sheetz MP, Elson EL. 1991. Single particle tracking: Analysis of diffusion and flow in two-dimensional systems. Biophysical Journal 60: 910–921.

Smal I, Loog M, Niessen W, Meijering E. 2010. Quantitative comparison of spot detection methods in fluorescence microscopy. IEEE Transactions on Medical Imaging 29: 282–301.

Wereley ST, Meinhart CD. 2001. Second-order accurate particle image velocimetry. Experiments in Fluids 31: 258-268.

4. Porcine Pancreas Digestion Test Using the MDR Digester

4.1 - Abstract

Large quantities of pure viable islets are necessary to treat diabetes. The primary step to realize this goal is the dissociation of the pancreas organ in preparing the islets that are isolated from exocrine tissue. A pig pancreas infused intraductally with collagenase enzyme blend was digested by using both modified Dynacult reactor (MDR) and Ricordi chamber in a parallel test in order to compare the islet yield and other relevant parameters between them.   The experimental data such as mean islet diameter and islet equivalent quantification (IEQ) were categorized within different ranges and plotted in two-series histograms for further analysis and comparison. In this particular case, the donor sow had an exceptionally large pancreas and smaller islets than typical (many of them were less than 100 μm). In the MDR digestion, the 50 rpm rotation rate is adequate for holding the tissue fragments in suspension.   The MDR proceeded more rapidly and uniformly than Ricordi chamber, although there is clear evidence that some excessive digestion occured in the MDR. In addition, the whole process in the MDR is more complete than in Ricordi chamber. Exocrine tissue is digested to smaller fragments and there are no islets attaching with exocrine tissue in MDR while 33 per cent of islets are still embedded/mantled into exocrine tissue pieces by using Ricordi chamber. The main advantage of MDR digester is to recover the smaller size islets that are generally more difficult to isolate from the surrounding tissue when using the Ricordi chamber. The MDR yields a much more uniform digestion of the pancreas with shorter digestion times.

Keywords: **tissue digester, islets of Langerhans, uniform digestion, Ricordi chamber, collagenase dissociation technology, islet equivalent quantification (IEQ)**

4.2 - Introduction

Pancreatic digestion is the primary step in preparing islets of Langerhans for clinical transplantation. Although swine appeared to be a potential source for pancreatic islet transplantation and could resolve the major problem of pancreas donor shortage (Cooper 2002), pig pancreas digestion remained a critical event because of the tight connection between exocrine tissue and islets. In current work, the crucial factors that had a direct impact on islet release have been assessed and compared such as the isolation technique (automated or non-automated), the activity and concentration of enzymes (Ricordi 1986 and O'Neil 2001), warm ischaemia time (WIT), preservation solutions as well as histomorphometry before and after isolation (Dufrane 2006). In addition, some studies suggested that breed-attributed differences may also influence the results of porcine islet isolation (Kirchhof 1994 and Ulrichs 1995).

Of all the factors, islet isolation technology was the most critical step providing a sufficient number of high quality islets for transplantation (Kenmochi, 2000). Firstly, intraductal collagenase technique was used to inject pre-warmed collagenase with calcium into the pancreatic duct. The following procedures involved in mechanical disruption of pancreas into several pieces, the collagenase digestion of tissue and density gradient centrifugation for purification, which was firstly used in rodents by Lacy and Kostianovsky. Gotoh et al. have applied a similar technique to the mouse, significantly improving islet yields, and Sutton and coworkers used this method in the rat. Finally, Ricordi et al's continuous dedication has contributed to the development of collagenase and to the application of the procedure in pancreas of large animal species such as pig (Ricordi 1988).

At the same time, the technique for human islet isolation has been repeated and modified by several groups. Rajotte and colleagues combined collagenase perfusion via the pancreatic

ducts, mechanical disruption, and serial sieving through filters to obtain clean islets from the adult cadaver pancreas. They concluded that islet yields were significantly better with the perfusion technique than with simple injection. Warnock et al., from the same group in Edmonton, compared the method of perfusion versus single intraductal injection, with a Ficoll purification step. They reported that the best yield of large intact islets as from those organs perfused for ten minutes at 4ºC, followed by gradual warming to 37ºC. However, the weakness of perfusion technique was tiresome human intervention during digestion, which would increase the risk of bacterial contamination (Teruya, 1994).

The subsequent development of a semi-automated standardized method by Ricordi, et al. has made the technique more efficient and practical for pancreas digestion (Gray 2004). Several laboratories improved this method, but the basic concept remained unchanged. In the Ricordi method (Figure 4.1), pancreas pieces and glass balls were placed into a cylindrical vessel to form a closed-loop recirculation and dissociation system, operated by intermittent manual shaking of the vessel. This process enabled the balls to interact with the pancreatic tissue and assisted in breaking down the interlobular fibrous tissue to release the islets (Gray, 2004). This group obtained a yield of 2279 islets per gram pancreas with 79 per cent purity, a definite improvement on existing methods. Admittedly, this method succeeded in a large-scale isolation of islets from human and porcine pancreas with the technical advancement. However, the yield of islets from this technique tends to be variable and depends on several factors (Iwashita, 1996). One of the most important reasons was collagenase-containing enzyme blends used for releasing islets from the exocrine tissue produce variable results and can cause damage to islets. The problem was further compounded by the variable activation degree of native proteolytic enzymes within acinar cells. The subjective determination of digestion quenching time, when maximum portion

of islets was released from the exocrine pancreas before they were damaged by the collagenase activity, was another problem worth considering. The digestion termination was actually difficult to control accurately, on the contrary, partial pancreas were still undigested while other portions were over-digested at this time. Additionally, operator function (manual shaking) also produced variability from case to case. Hence, an automated digestion unit capable of producing reproducible operating parameters is needed for the consistent preparation of islets.
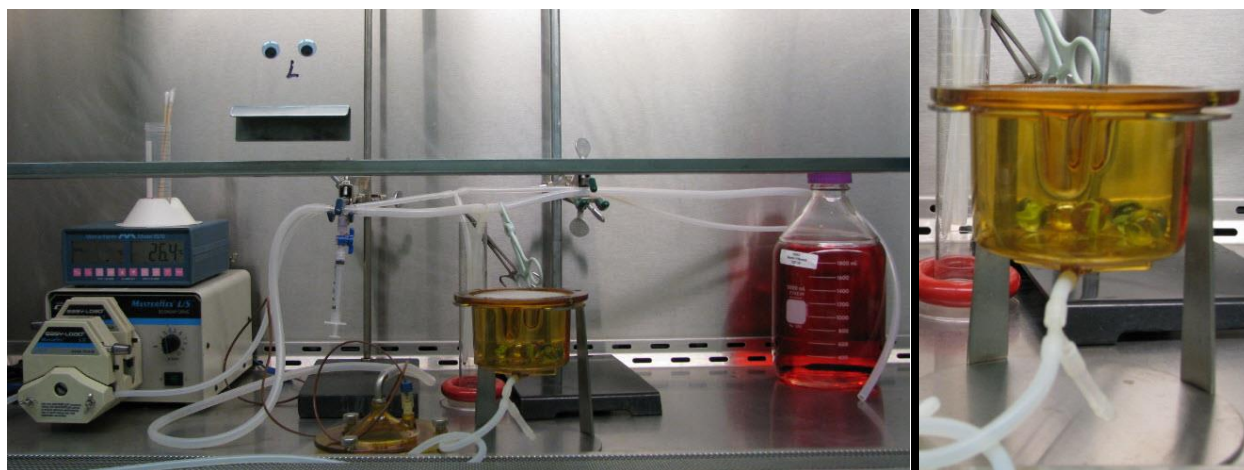
Figure 4.1 – Ricordi chamber digestion system used in VitaCyte, LLC.

The digestion tests are performed by using a reproducible, controllable MDR digester combined with high effective collagenase dissociation system. The preliminary experiment should be performed in the optimal condition on the basis of CFD analysis. As a differential digestion method, the rotation of the inner core is adjusted for optimum dissociation, and independently the exterior wall rotation is optimized to maintain particles in suspension without centrifuging them. As the double walls turn, the tissue fragments continually fall through the solution and, over a period of time, the tissue pieces are dissociated to form 3D particulates. The details of pancreas digestion test and validation of the new MDR model will be discussed in this paper.

4.3 - Materials and Methods

4.3.1 Pancreas procurement and infusion

For decades, patients with diabetes have been treated with porcine insulin, and the pig is regarded as the ideal source of islet cells for clinical xenotransplantation. Porcine tissue has advantages for islet transplantation not only because a large amount of tissue is available, but also because porcine insulin has been proven to work in humans by long-term experience. Besides, the swine model offers a unique advantage when compared to humans: the possibility of standardization of the isolation procedure. It is possible to use pigs of the same age group, always with the same pancreas retrieval procedure. However, the availability of organs is very limited for our digestion tests due to the high cost of porcine pancreas. In view of this problem, VitaCyte LLC, our cooperation company with significant research experience developing enzyme blends, provides a relatively cheaper organ procurement (Figure 4.2) and provides digestion manipulation for us.

Figure 4.2 – The pancreas of donor sow

Before the digestion process, the pancreas is trimmed by careful dissection of the surrounding fat tissue, lymph nodes, and membranes. Hanks' balanced salt solution (HBSS) is then injected through the pancreatic duct at a low flow rate (Figure 4.3). The infused tissue is chopped into smaller pieces and loaded in MDR and Ricordi chamber which are filled with additional collagenase solution for a parallel test.

Figure 4.3 – The pancreas infused intraductally with collagenase enzyme blend

4.3.2 The operation of MDR digestion system

Sterilization process is a required step before the digestion test. For MDR device, the diluted bleach (The dilution ratio is about 1 laundry bleach to 9 water) is used to sterilize the inner surface of cylinder walls because the autoclave will cause damage to the walls. Firstly, PH value of the prepared bleach solution is measure by PH test paper. Then, the bleach is pumped into MDR and the power supply is also turned on for rotation. After 10min, the wall rotation is

stopped by switching off power supply. But we keep pumping into the bleach for 20min (Total sterilization time is 30min). Finally, the MDR is rinsed with sterilized water for enough time until PH of the effluent reaches that of pure water.

The digestion procedure is as follows. The system is inspected to make sure no leaks are evident. The perfused pancreas tissue and collagenase solution are placed in MDR digester. In the digestion process, the dissociated tissue particles settle on the surface of the filter, resulting in the clogging and the pressure increasing inside the chamber. The check valve (Figure 4.4) plays an important role in minimizing the pressure build-up by opening for a short time to vent the excess fluid. In the phase of batch dissociation, valves (1) and (2) are shut off to form a closed circulation loop. Subsequently, both valve (1) and (2) should be open to pump in fresh HBSS to elute the islets in the islets collection process. Since the tissue particle is denser than the surrounding buffer solution, certain rotation speed is required to suspend the particles. The whole device is illustrated in Figure 4.4.
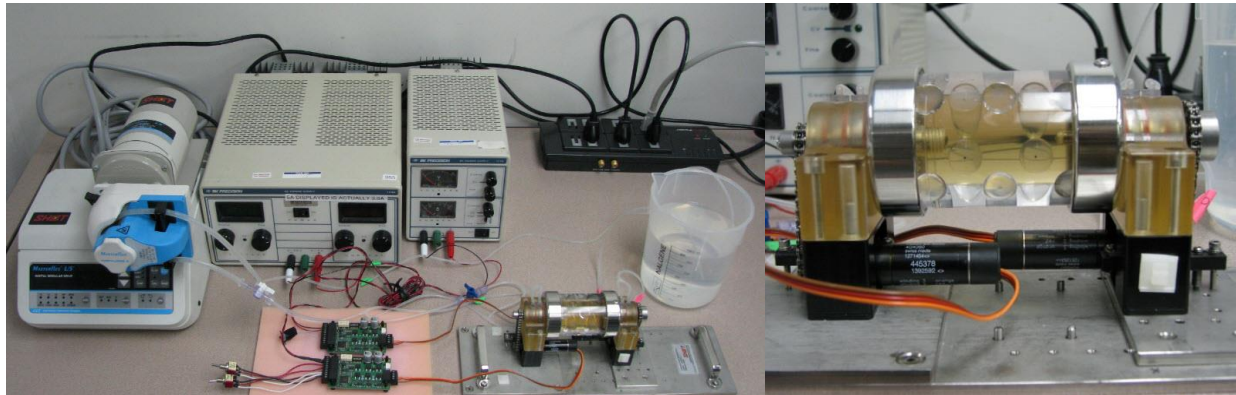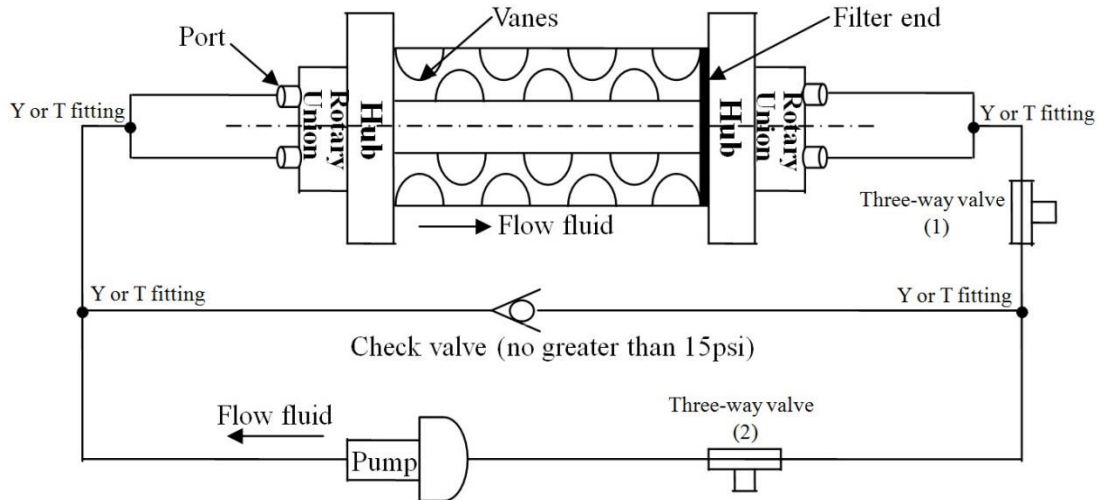
Figure 4.4 – MDR digestion unit and the relevant accessory parts

(Top: the diagram of digestion system; Bottom: the picture of real assembled device)

4.3.3 Pancreas digestion test by both MDR and Ricordi chamber

A single pig pancreas (from a sow) was infused intraductally with VitaCyte collagenase enzyme blend and chopped into typical size pieces as used for the digestion test. About 40 g of infused pancreas, which is set aside for MDR digestion experiment, was chopped into smaller pieces and suspended in the same reagent solution bringing the total internal volume to 82 mL. The suspension is then poured into an open end of the MDR vessel which is sealed by attachment of the hub. The vessel is then mounted to its stand, and 20 mL HBSS at 42°C are added to raise the temperature to maintain enzyme activity at around 33°C. Shell and core

rotation is initiated in opposite directions at 50 rpm without pumping. Based upon gross observations within the MDR vessel, when fragments become less than about 1 mm in average diameter (milky white suspension), pumping of buffer into the reactor vessel initiates collection of suspended particles into the enzyme-quenching buffer (an ice-cold, serum-containing buffer which inactivates the enzymes) until the MDR fluid becomes clear, then the contents of the beaker are weighed. Each collected sample is centrifuged, re-suspended in a predetermined volume of buffer, and analyzed for microscopy to determine the following data: number of islets per mL, number of islets per gram tissue (yield of islets), percent of islets with attached tissue, percent of undigested tissue and mean islet size. In a parallel test, 133 g of the same infused pancreas (the collagenase blend is also the same) and seven glass marbles are loaded into a 500-mL plastic Ricordi chamber for a standard digestion test. The assembly of the tubing system creates a closed-loop recirculation and dissociation system, operated by intermittent manual shaking of the vessel. The same data were obtained on the digest prepared by the Ricordi method for quantitative comparison with the MDR digest.

4.3.4 Islets identification

The precise identification of islets is determined by dithizone staining. At first, 39 mmol/L dithizone solution is prepared by dissolving 100 mg dithizone in a mixture of 10 mL of dimethyl sulfoxide (DMSO) and 20 mL of absolute ethanol, and then filtered, aliquoted, stored at -15°C (Shewade, 1999). The dithizone solution is then used to stain 1 mL sample of the islet suspension taken after the MDR digestion test in a Petri dish. Dithizone complexes with the zinc in β-cell granules and turns a dark red and has allowed the accurate monitoring of the digestion process (London NJM, 1994). The staining process is carried out by adding 10 µl dithizone

solution to islets which is suspended in 1 mL Krebs-Ringer Bicarbonate buffer (pH 7.4) with HEPES (10 mmol/L) and incubate at 37°C for 10 to 15 minutes (Y.M. Shewade, 1999). The pictures of islets are taken by a digital camera attaching with an inverted phase contrast microscope with a calibrated grid in the eyepiece at 10X magnification. The images taken are saved and estimated for size distribution and numbers of the stained islets.

4.4 - Quantification of islet preparations

Substantial heterogeneity exists in islet size within a porcine pancreas. In order to measure the quantity of islets in an islet preparation, both the number of islets and size distribution should be taken into consideration. The diameter of each islet within the sample aliquots is categorized within a size range: 0–40 μm, 41–80 μm, 81–120 μm, 121–160 μm, 161–200 μm, 201–240 μm, and over 240 μm. The number of islets is counted and the percentage of islets is calculated in each category and plotted in a histogram. An "islet equivalent quantification" (IEQ) is defined as an islet with a diameter of 150 μm. The value of each IEQ is calculated by the following formula:

$$\text{IEQ} = \frac{\text{Volume of each islet}}{\text{Volume of islet with 150μm diameter}} = \frac{\frac{1}{6}\pi d_{min}d_{max}d_{mean}}{\frac{1}{6}\pi(150)^3} = \frac{\frac{1}{6}\pi d_{min}d_{max}d_{mean}}{1766250} \quad (4\text{-}1)$$

In which, d_{min} is minimum diameter of each islet

$\quad\quad d_{max}$ is maximum diameter of each islet

$\quad\quad d_{min}$ is mean diameter of each islet, $d_{mean} = \frac{1}{2}(d_{min} + d_{max})$

The amount of total IEQs in one tissue sample is the sum of the IEQ for each islet, then the IEQs/mL and IEQs/gram tissue can be calculated to estimate the yield of islets.

4.5 - Results and Discussion

4.5.1 Analysis of MDR digestion test video

The pancreatic digestion test should be performed in the optimal condition on the basis of CFD analysis. The double-wall rotation rate of 50 rpm in opposite directions was determined to be adequate for holding the tissue fragments in suspension. Observations of fragments motion are videoed or photographed by using a quality digital camera. The process of pancreas digestion is recorded as a still photo in Figure 4.5.
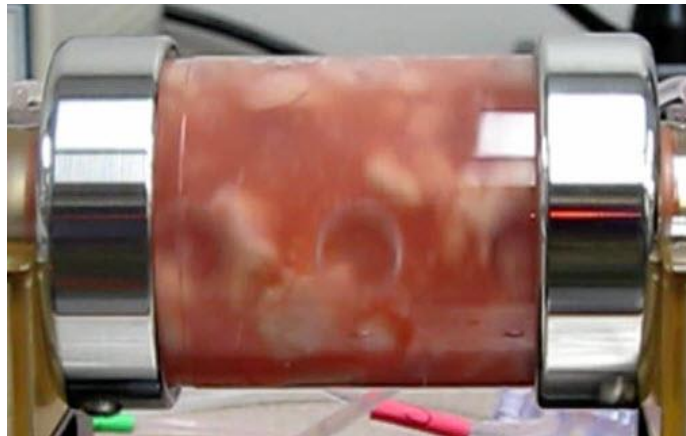
Figure 4.5 – Suspension of tissue fragments in the MDR digestion

At the same time, the particle streaks are formed by using time-exposure photography, that means the shutter of camera opens longer time than normal (Figure 4.6). Then, the Image-Pro software is used to identify and measure the length of streaks (Figure 4.7). Please note: the arrows shown in this picture do not represent velocity directions; they are automatically generated as scalar lengths by the fiber-length software.

Figure 4.6 – Time-exposure photography

of tissue fragments

Figure 4.7 – Streaks length distribution

Based on the data of streak lengths, we calculate the velocity of tissue fragments and plot it in the histograms illustrated in Figure 4.8. In order to show the percentage of velocity more clearly, the logarithmic scale axis is used on the right histogram. The histograms indicate 82 per cent of velocities are less than 0.1 m/s in digestion test while 99 per cent are less than this value in the particle test (Chapter 3). By comparing the histograms between both of two tests, we can figure that the fragments move faster in the digestion test than in the particle test. Uniform suspension of tissue fragments is verified by comparison of the similar velocity distribution between Figure 4.8 and Figure 3.8 (in chapter 3) of stained particle experiment.
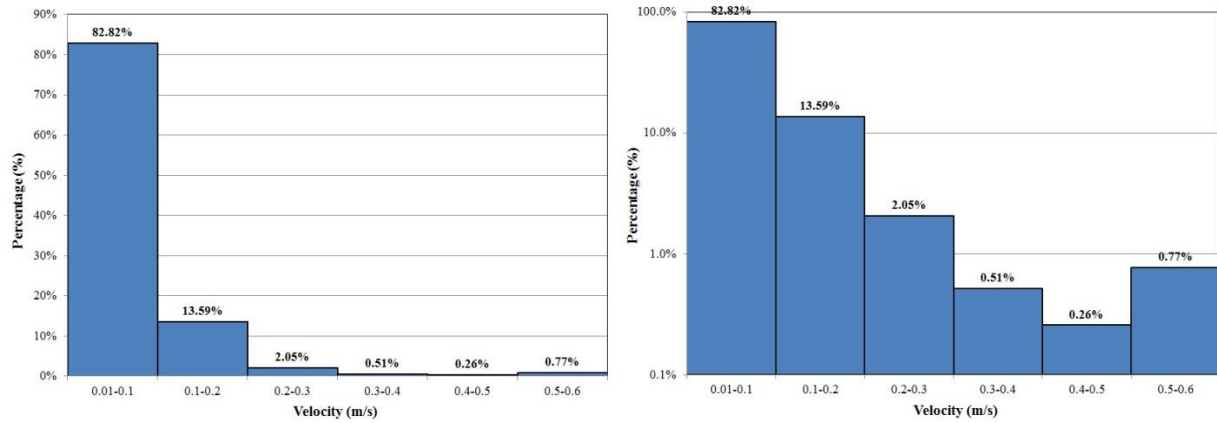
Figure 4.8 – Velocity histogram (left)   and   Logarithmic scale velocity histogram (right)

4.5.2 Observation of islets stained by dithizone

At first, the pancreas has to be digested by using both MDR and Ricordi chamber in a parallel test so the organ is from the same donor; the collagenase blend is also the same. Then, the islets are collected and stained by dithizone for microscope observation. Figure 4.9 and figure 4.10 show the bright red spots that are islets isolated by the MDR (islets-M) and by using the 500 mL Ricordi chamber (islets-R), respectively.
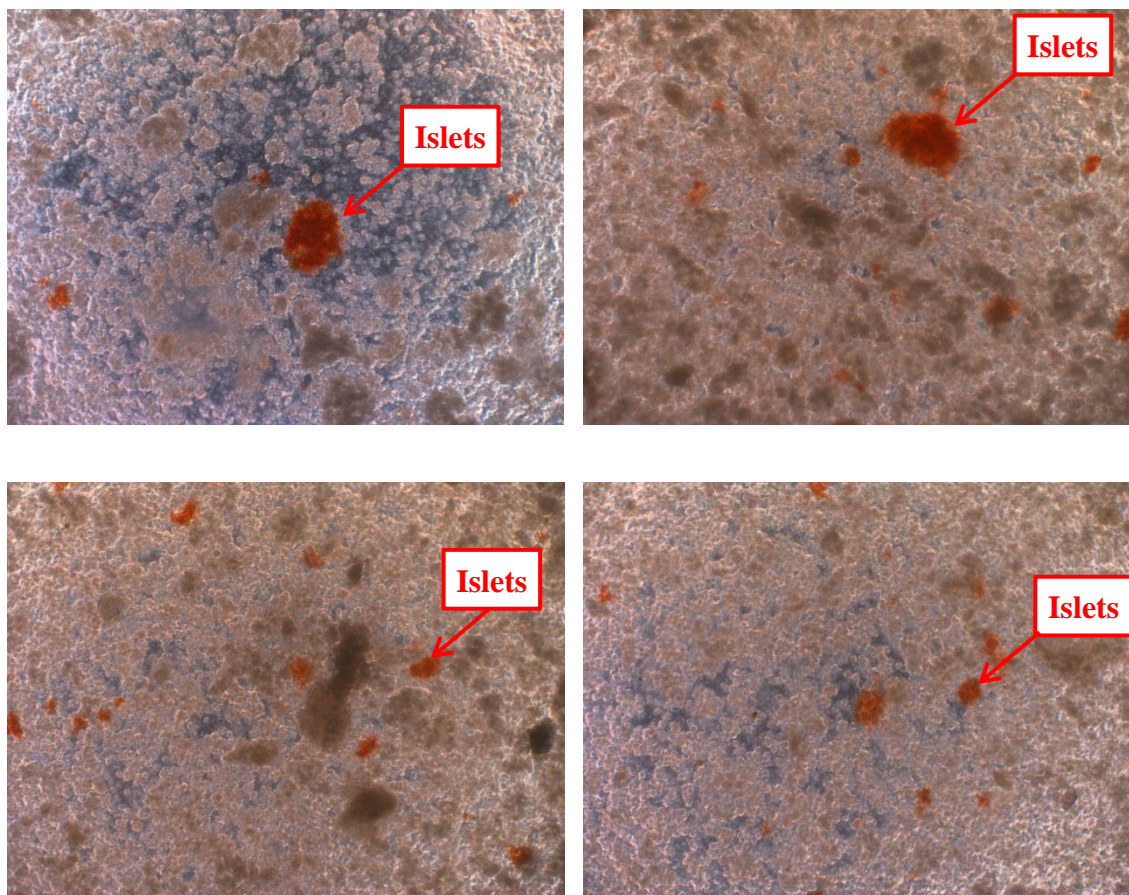
Figure 4.9 – Images of dithizone-stained islets taken under microscope at 10X magnification in MDR digests (Note: absence of large fragments).
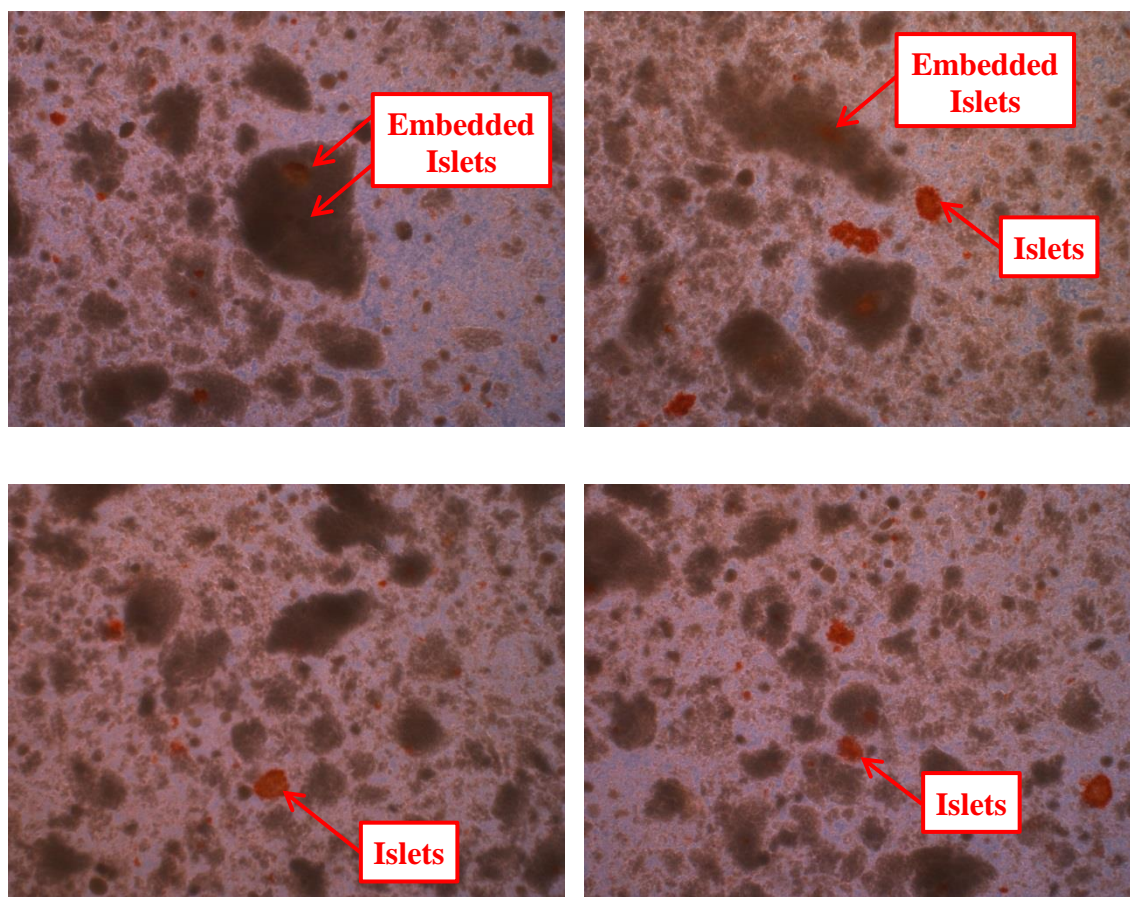
Figure 4.10: Images of dithizone-stained islets taken under microscope at 10X magnification in Ricordi chamber digest (Note: islets are embedded in large fragments of exocrine tissue)

In this particular case, the donor sow had an exceptionally large pancreas that contained smaller islets than typical ones (most of islets were less than 100 µm), but generally the average diameter of islets should be around 160 to 170 µm. The above two groups of images indicate that exocrine tissue is reduced to smaller size level in MDR than in Ricordi chamber, and most of islets-M are detached from the surrounding tissue while some of islets-R are still embedded in the non-islet tissue pieces. Especially in the upper left image of Ricordi group, one islet is

embedded in large tissue piece. This is considered undesirable and actually does not occur in MDR digest. Hence, the MDR digestion process is more complete.

4.5.3 Quantity assessment of islets

After analyzing the images of stained islets, we compare islet size histograms between the two digest methods in Figure 4.11. The number of islets-M is much less than that of islets-R for diameter range over 40 micron while opposite outcome can be seen for the diameter less than 40 micron. The distribution of islets-M diameter is highly focused on the range 0 to 40 and 41 to 80 micron, the number of islets-M in both ranges is 30 and 48 respectively. However, the diameter of islets-R has a more extended distribution between 40 and 160 micron. Most of the diameter is between 40 and 80 micron including 83 islets-R.
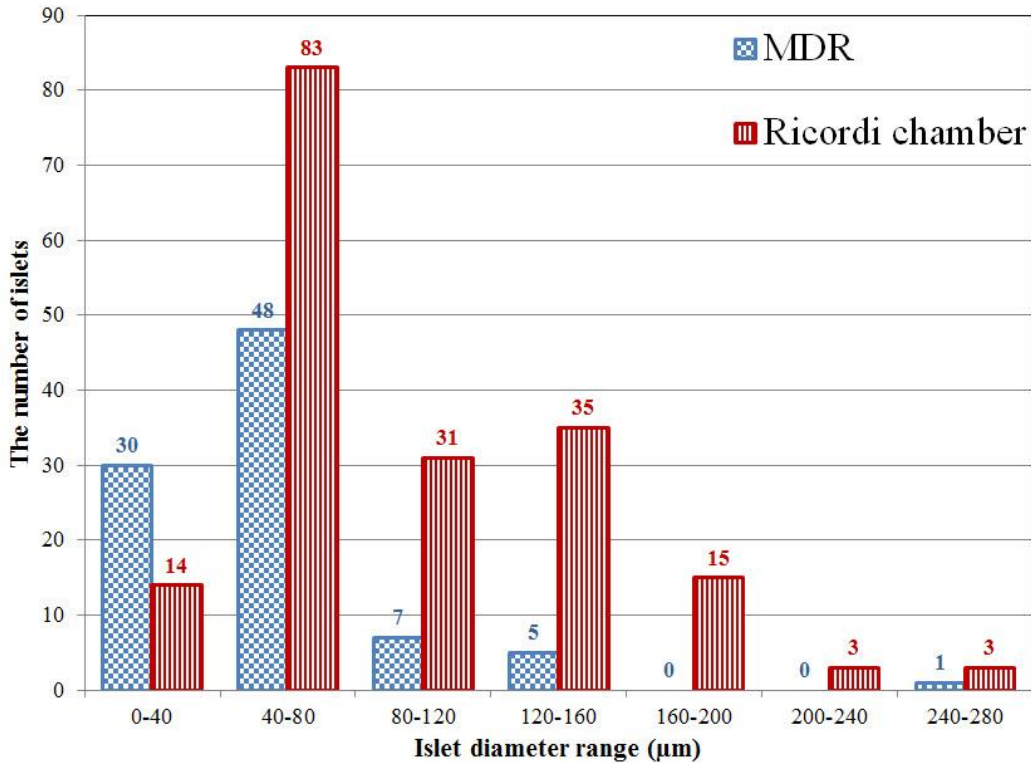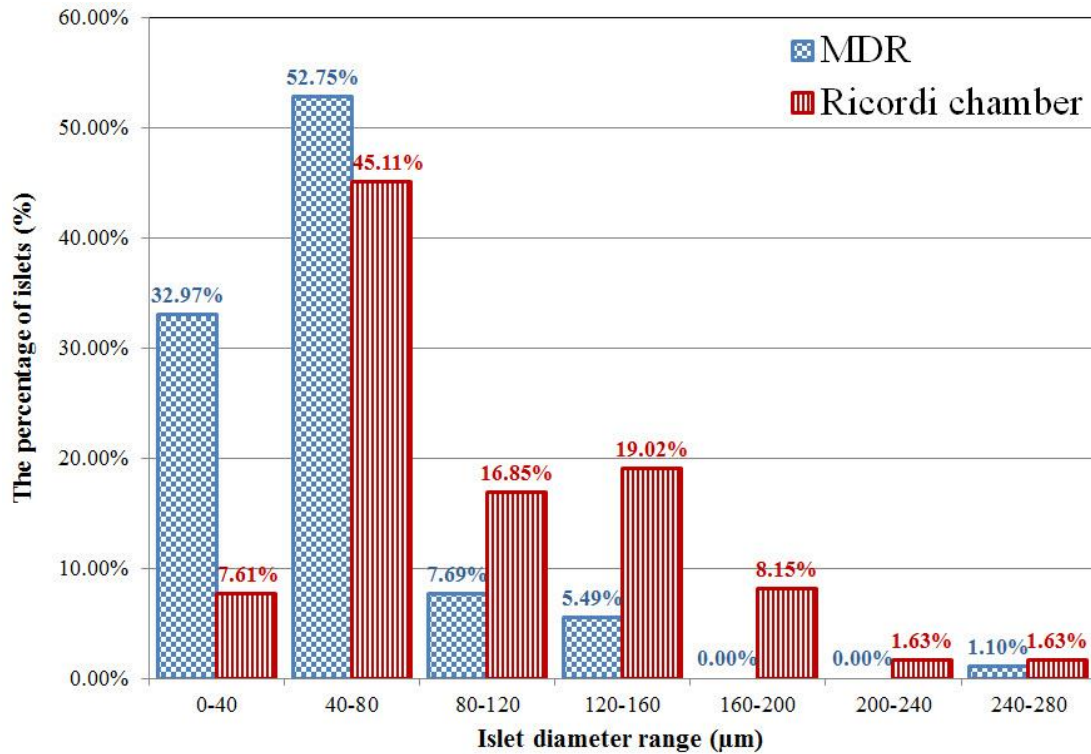
Figure 4.11 – Histograms of islet sizes plotted in frequency (top) and percentage (bottom)

Based on the data of islets size percentage, most of islets isolated by both MDR and Ricordi chamber have the diameter between 40 to 80 microns, which indicates the donor sow has a pancreas containing much smaller islets (less than 100 microns), the corresponding percentage is 53 and 45 per cent. Then for the MDR, percentage of smaller islets with the diameter less than 40 micron is much higher while percent of larger diameter in the range 80 to 200 micron is lower than for Ricordi chamber. The mean islets-M diameter is smaller than islets-R. But the smaller islets are not bad at all in view of the particular donor pancreas. The main advantage of MDR is to recover the smaller size islets that are generally more difficult to isolate from the surrounding tissue when using the Ricordi chamber.

The quantity of islets is also calculated using IEQ that is equal to the ratio of each islet volume to the volume of islet with 150 μm diameter. The value of IEQ is divided into two sections: islets with the mean diameter less than 150 μm if IEQ < 1; islets with the mean

diameter more than 150 μm if IEQ > 1. When the mean diameter is equal to 150 μm, the value

of IEQ is 1 in most cases except the irregular shape. Generally speaking, the diameter of large

islets should be no less than 150 μm. Hence, the IEQ frequency or percentage shown in

histograms (Figure 4.12) further demonstrates that very few large islets (only one in our sample,

the percentage is 1.1 per cent) are recovered from MDR digest and only small percent of 12.50

per cent large islets (counted to be 23) are collected using Ricordi method. Then, the comparison

of IEQ histograms is performed between the two digest methods. The number of islets-M is

much less than that of islets-R if IEQ > 0.04, and vice versa. Similarly, the distribution of IEQ is

also highly focused on a certain range 0-0.2 for islets-M. The IEQ of islets-R has a more

extended distribution between 0.02 and 0.4.
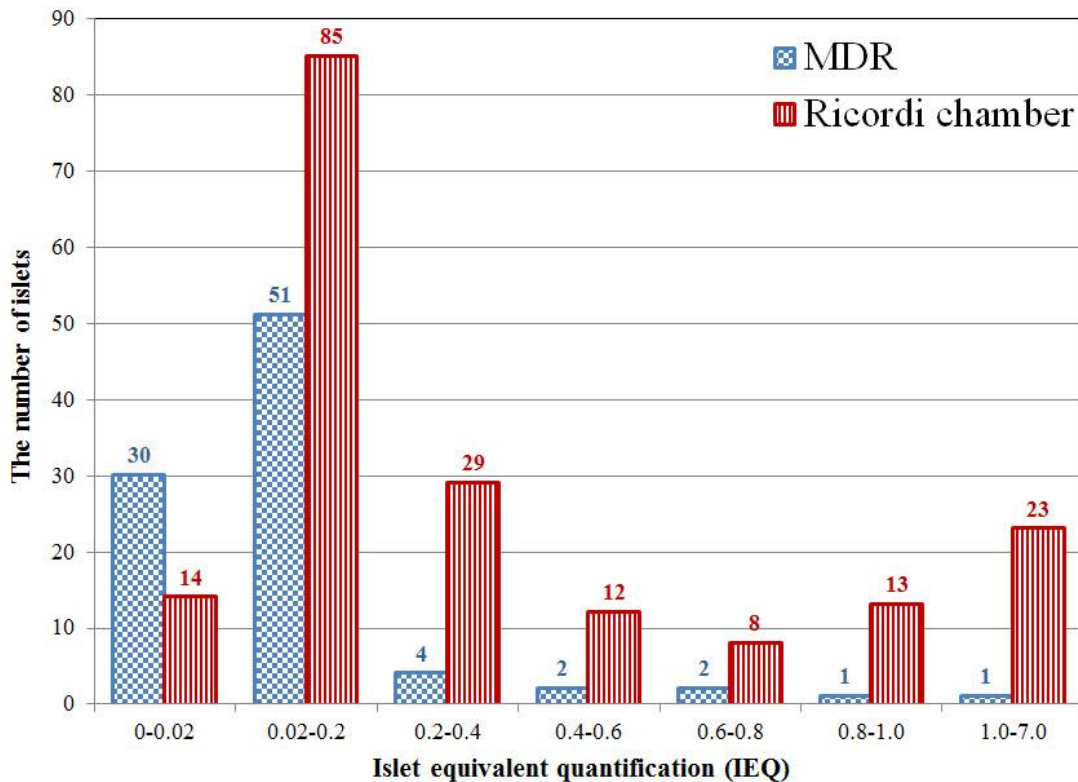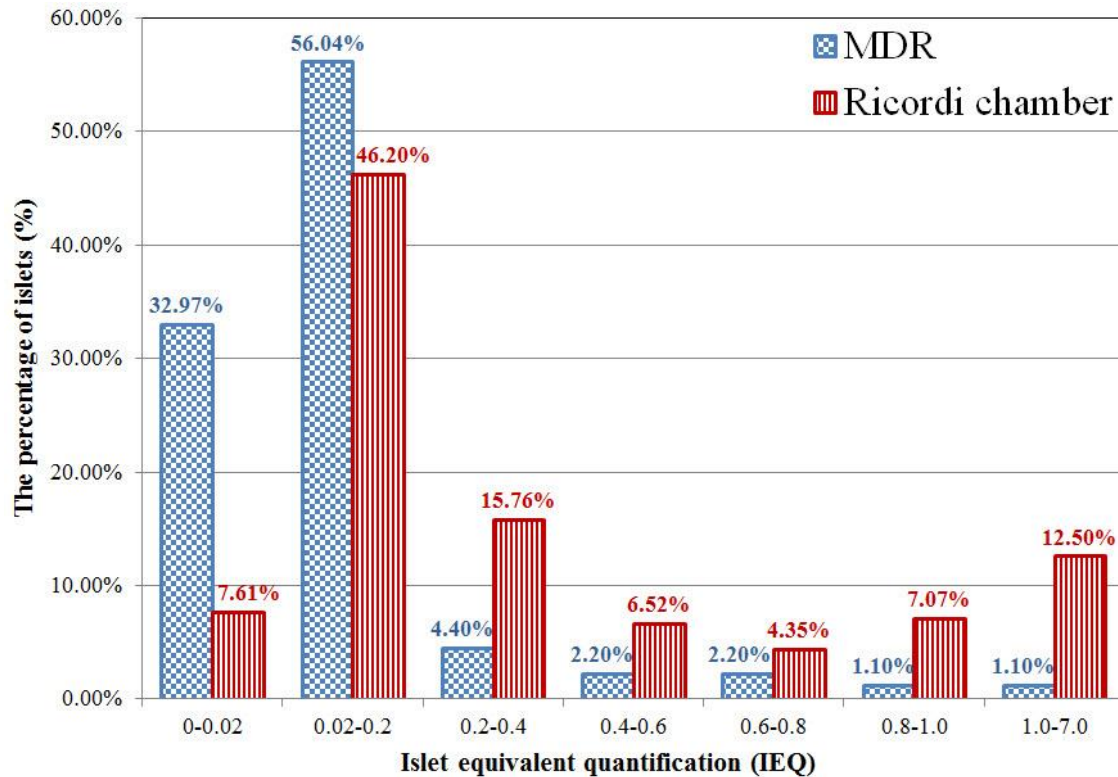
Figure 4.12 – Histograms of IEQ plotted in frequency (top) and percentage (bottom)

To sum up, the tendency of IEQ histograms in Figure 4.12 is very similar to that of islet sizes histogram shown in Figure 4.11. So IEQ is an alternative criterion used to assess the quantity of islets. The comparison of IEQ histograms between MDR and Ricordi chamber also indicates the mean islets-M diameter is smaller than islets-R.

4.5.4 Comparison of digestion results between MDR and Ricordi chamber

The yield of islets and other important parameters are summarized in Table 4.1 for the comparison of MDR with Ricordi chamber. Then the pros and cons for MDR digest will be discussed respectively. The pros are MDR digestion proceeds more rapidly and uniformly than Ricordi chamber in preliminary testing. There are no islets attaching with exocrine tissue in MDR while 33 per cent islets are still embedded and mantled into larger tissue pieces by using

Ricordi chamber. More of smaller size islets are recovered through MDR digest. In addition, the percent of undigested tissue is reduced by 29 per cent in the MDR. The cons are the lower yield of islets that are somewhat discouraging. This weakness is probably caused by the higher-than-expected digestion rate caused by improved mixing, also typically do not "quench" the digestion but rather only slowly dilute the suspension thereby reducing the rate of enzyme inhibition in the effluent.

Table 4.1 – Comparison of pancreatic digestion results between MDR and Ricordi chamber

Parameters in digestion test	MDR	Ricordi chamber
Shell/core rotation speed (rpm)	50	N/A
Starting tissue mass (g)	40.7	162
Digestion time (min)	30	25.9
Rotation time (min)	10.8	N/A
Number of islets/ml	91	368
Number of islets/g	112	227
% Islets with tissue attached (n/n)	0%	33%
% Islets diameter < 50µm (n/n)	37%	9%
Mean islet size (µm)	71	100
% Undigested tissue (w/w)	39%	54%

**Note: All the images of islets and data on islet percent/yield are provided by Dr. Mike Green,

VitaCyte, LLC.

We divide the tissue-attached islets into three types, and then summarize in Table 4.2.

Embedded islets that are fully wrapped by exocrine tissue (e);

Mantled islets that are partially wrapped by exocrine tissue (m);

Fragmented islets that are actually broken by mechanical forces or collagenase dissociation (f).

Table 4.2 – The percent of different types of tissue-attached islets

The type of islets with tissue attached	Percent in islets-M	Percent in islets-R
e	0%	24%
m	0%	8%
f	0%	0%

The above results in Table 4.2 for both digestion methods are acceptable without any damaged islets (f=0%). Apart from the preliminary tests listed in Table 4.1, two extra tests were also performed in parallel by MDR. However, there is clear evidence that excessive digestion occured in both tests (not listed in the table), and fragmented islets were found. The exocrine tissue is reduced to nearly single-cell level, fragment clumping is formed due to release of small amounts of DNA, and "membrane balls" are also present in a test with the longest digestion time. The IEQ value tends to be lower because of higher degree of fragmentation. Hence, as a key point for intelligent parameter changes, shorter digestion time of MDR test will be required for further process optimization. Alternatively, the damage to the islets might be addressed by other modifications. For example, a sampling port used to take the sample and assess the digest microscopically may be valuable at least for the preliminary tests. On the other hand, some sort of temperature control accessories would be preferred as well. In summary, the MDR device yields a much more uniform digestion of the pancreas but also appears to digest more rapidly.

4.6 - Conclusions

Based on all the simulation, calculation and digestion analysis, it is concluded that the newly designed MDR digester mimics features of Ricordi chamber while overcoming the deficiency of manual operation. In preliminary testing MDR digestion proceeds more rapidly and uniformly than Ricordi chamber. The main advantage of MDR is to recover the smaller size islets that are generally more difficult to isolate from the surrounding tissue by using Ricordi chamber. Exocrine tissue is digested to smaller fragments in MDR than those in Ricordi chamber. Process optimization will require a shorter digestion time relative to that of the Ricordi chamber.

4.7 - References

Cooper DK, Gollackner B, Sachs DH. 2002. Will the pig solve the transplantation backlog? Annual Review of Medicine 53: 133.

Dufrane D, D'hoore W, Goebbels R-M, Saliez A, Guiot Y, Gianello P. 2006. Parameters favouring successful adult pig islet isolations for xenotransplantation in pig-to-primate models. Xenotransplantation 13: 205.

Gotoh M, Maki T, Kiyoizumi T, et al. 1985. An improved method for isolation of mouse pancreatic islets. Transplantation 40: 437-438.

Gray DWR, Sudhakaran N, Titus TT, McShane P, Johnson P. 2004. Development of a Novel Digestion Chamber for Human and Porcine Islet Isolation. Transplantation Proceedings 36: 1136.

Iwashita C, Asano T, Kenmochi T, Jingu K, Uematsu T, Nakagohri T, Hasegawa M, Maruyama M, Miyauchi H, Isono K. 1996. Combined method of mechanical chopper and automated two-step digestion technique for islet isolation from canine pancreas. Transplantation Proceedings 28(1): 337.

Kenmochi T, Asano T, Jingu K, Iwashita C, Miyauchi H, Takahashi S, Saito T, Ochiai T. 2000. Development of a Fully Automated Islet Digestion System. Transplantation Proceedings 32: 341.

Kirchhof N, Hering BJ, Geiss V, Federlin K, Bretzel RG. 1994. Evidence for breed-dependent differences in porcine islets of Langerhans. Transplantation Proceedings 26: 616.

Lacy PB, Kostianovsky M. 1967. Method for the isolation of intact islets of Langerhans from the rat pancreas. Diabetes 16: 35.

London NJM, Robertson GSM, Chadwick DR, Johnson PRV, James RFL, Bell PRF. 1994. Human pancreatic islet isolation and transplantation. Clinical Transplantation 8: 438.

O'Neil JJ, Stegemann JP, Nicholson DT et al. 2001. The isolation and function of porcine islets from market weight pigs. Cell Transplantation 10: 235.

Rajotte RV, Warnock GL, Evans MG, et al. 1987. Isolation of viable islets of Langerhans from collagenase-perfused canine and human pancreata. Transplantation Proceedings 19: 18-922.

Ricordi C, Finke EH, Lacy PE. 1986. A method for the mass isolation of islets from the adult pig pancreas. Diabetes 35: 649.

Ricordi C, Lacy PB, Finke EH, Olack BJ, Scharp DW. 1988. Automated method for isolation of human pancreatic islets. Diabetes 37: 413.

Shewade YM, Umrani M, Bhonde RR. 1999. Large-scale isolation of islets by tissue culture of adult mouse Pancreas. Transplantation Proceedings 31: 1721-1723.

Sutton R, Peters M, McShane P, et al. 1986. Isolation of rat pancreatic islets by ductal injection of collagenase. Transplantation 42: 689-691.

Teruya M, Idezuki Y, Bandai Y, Kubota K, Kosuge T, Sakamoto H, Terada M. 1994. New digestion chamber for the automated isolation method of pancreatic islets. Transplantation Proceedings 26(4): 2279.

Ulrichs K, Bosse M, Heiser A et al. 1995. Histomorphological characteristics of the porcine pancreas as a basis for the isolation of islets of Langerhans. Xenotransplantation 2: 176.

Warnock GL, Ellis D, Rajotte RV, et al. 1988. Studies of the isolation and viability of human islets of

Langerhans. Transplantation 45: 957-963.

5. Summary and Future Work

A newly designed automated digestion unit is successfully created for the preparation of pancreatic islets with a shorter time and more complete digestion process. In the pancreatic digestion test, the MDR digester can be used to recover the smaller size islets that are generally more difficult to isolate from the surrounding tissue, and exocrine tissue is digested to smaller fragments without any embedded islets. The MDR device is more flexible in operation because the rotation of the inner core is adjusted for optimum dissociation, and independently the exterior wall rotation can maintain particles in suspension without centrifuging them. CFD simulations are successfully developed as an optimization tool to confirm a more uniform and lower shear environment in the MDR. As the sophisticated image processing software, Image-Pro Premier is introduced to identify and measure the length of particle streaks automatically and used for further calculation of velocity.

The new MDR digester mimics features of Ricordi chamber while overcoming the deficiency of manual operation by incorporating an automated horizontally rotating bioreactor consisting of a rotating outer cylindrical shell and a counter-rotating core both with hemispherical baffles. This configuration is designed to enhance the turbulent effect and contact area between tissue fragments and walls. The discrete phase model (DPM) in the FLUENT computational fluid dynamics (CFD) package is used to predict the flow patterns and shear environment in the MDR and Ricordi chamber. CFD analysis and comparison of flow variable contours indicate that MDR has predictable, controllable fluid shear environment and optimized differential rotation mode.

The capability of particle mixing in MDR is confirmed by cultispher dispersion test. The particles move along a path controlled by the action of different hydrodynamic forces. The

complete mixing process occurs in the intermediate region between adjacent vanes and double walls without any sedimentary particles. The methylene blue-stained fixed acinar tissue is superior to cultispher particles in the time-lapse experiment. The particle streaks are formed using time-lapse photography by means of opening the shutter of camera longer time than normal. The shutter speed has little impact on the percentage of streak lengths while the lower shutter speed will cause the distribution of particle velocity to move towards low velocity zone in the log scale histogram. The shutter speed is optimized to be 1/40 s based on the visibility degree of particle streaks and the validation performed by the comparison of numerical results with experimental velocity data.

The current project realizes the preliminary goal for automatic digestion process, which lays a good foundation for the further research and development of tissue digestion to achieve large-scale production of pancreatic islets. More energy should be spent on the process optimization to fulfill the ultimate requirement. The future research plan will focus on the following research area as a supplement:

1. The current MDR dimension will be scaled-up to develop a superior digestion system capable of processing multiple pancreases for improving the islets production. Initial scale-up process will be based on CFD simulation to assess the shear environment. At the same time, the relevant important parameters such as reactor proportionality, gap sizes and flow rate ranges should also be optimized.

2. The further research will be developed to integrate a series of MDR chambers into an entity, which is an alternative method used to obtain more islets. In addition, the combination of MDR digester with Quadrupole Magnetic Sorter (QMS) for islet separation

could greatly improve islet recovery and viability and provide a fully-automatic process of islet production and purification.

3. In order to further optimize the digestion process, additional testing is required to optimize the digestion time and prevent any overdigestion of the islets. Additional modifications, such as a sampling port and temperature control, would improve reproducibility of results and facilitate overall operation.

In addition to the improvements of engineering process as described above, some scientific issues still need to be considered and resolved in the future study:

4. To prevent any immune-mediated damage to islets, the design of new multifunctional coatings is very important for the support of extracellular matrix and maintenance of the physiological function of the islets. For example, multifunctional biologically-active polymers can be used as novel immune-protective and anti-inflammatory coatings which are necessary for maintaining islet viability and functions.

5. A standardized methodology for characterizing collagenase and neutral protease enzymes used in human islet isolation should be developed to achieve the correlation of biochemical characteristics of tissue dissociation enzymes with the viability, function and yield of islets. This is also a crucial step capable of implementing a consistent, cost effective treatment for the patients with type-1 diabetes.

6. Islet viability assessment is also a problem because in vitro testing does not always successfully predict the results of post-transplantation. During the static incubation, the insulin secretion will be measured in two critical conditions when the islets are exposed to low and high concentration of glucose, then a stimulation index will be formulated.

# Appendix A: The Prototype of MDR Vessel Structure*
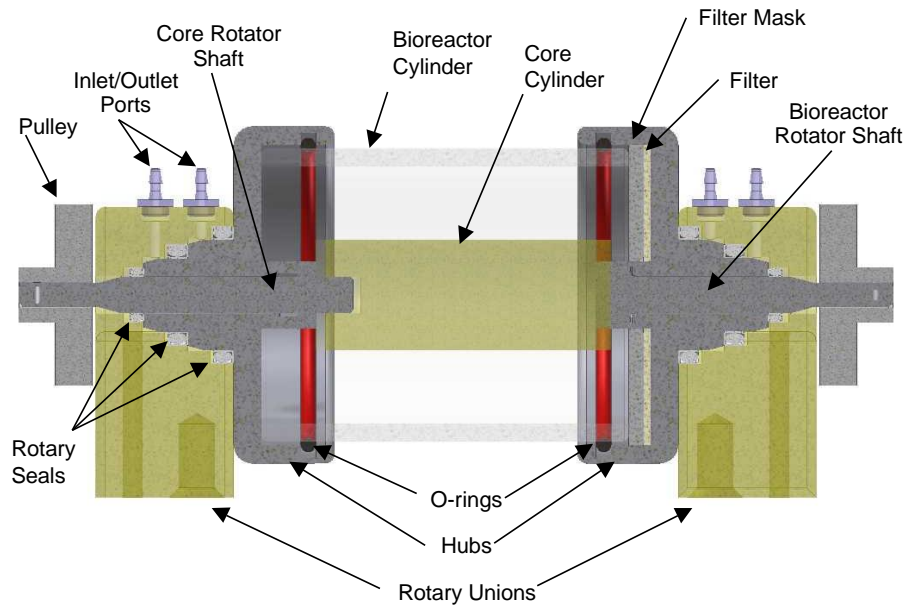
Figure A.1 – Front view of assembled Dynacult bioreactor.
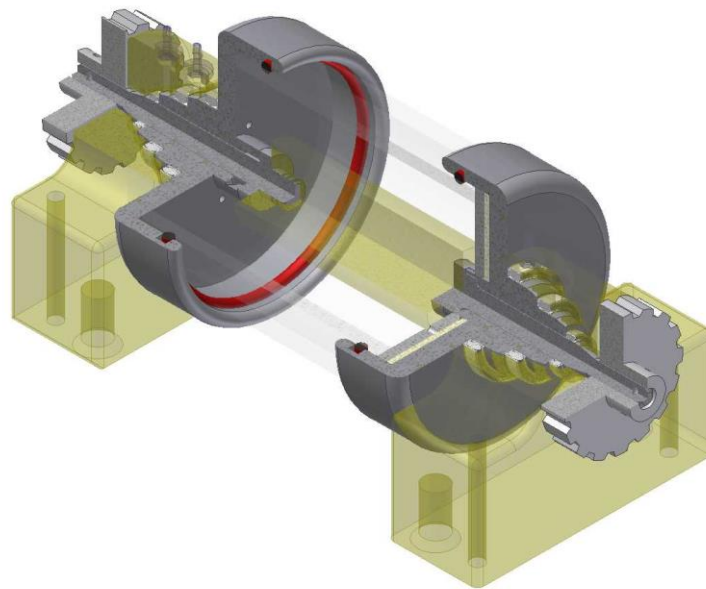
Figure A.2 – Cutaway view of assembled Dynacult bioreactor.

(Todd, P., Hodapp, l., Jones, A., Kennedy, D., Popson, T., Taylor, E. 2004. Robotic Bioreactor

for Cell Culture in Space Applications (Dynacult). Final Progress Report: 1-119)

A.1 - MDR Digester Removal

1) Loosen the two screws on either end that tighten the chains.

2) Pull the chains off of the sprockets, but do not yet remove the chains from the bioreactor pulley.

3) Remove the two Philips-head screws in each pillow block.

4) Lift the bioreactor vertically and level off of the alignment pins on the motor mounts.

A.2 - MDR Digester Disassembly

1) Make sure that you allow an air opening into the MDR via one of the fluid ports and/or one of the self-sealing screw bleed ports prior to disassembling the bioreactor (failure to do so may result in significant spillage during disassembly).

2) Turn the MDR up so that the vessel is vertical, like a coke can, with the core side facing up (the core side is the end that also contains the filter and filter mask). Grasp the lower hub and shell with one hand, and grasp the upper hub with the other hand. Gently twist and rock the upper hub until it comes off.

3) If necessary, pour out any contents into a specimen container using appropriate biohazard safety measures as dictated by OSHA and/or your facility regulations.

4) Continue to dissemble the remainder of the MDR as necessary for further operations (i.e. to replace the filter, replace the seals, change out the core and shell, etc.).

A.3 MDR Digester Assembly

1) Place the filter on the filter (right) end hub. Push the filter mask over the top of the filter, followed by the spring. Install the o-ring into the gland on the hub.

2) Push the filter (right) end hub through the Teflon shim and into the filter (right) end pillow block.

3) Put the threaded shaft through the right end hub, and pillow block such that the threads are facing the center. Install appropriate number of washer spacers outside of the pillow block on the shaft.

4) Install the gear outside of the spacers. Using appropriate tools, space the gear approximately 0.010" off of the washers. Tighten the set screws.

5) Install the o-ring into the left end hub.

6) Push the left end hub through the Teflon shim and into the left end pillow block.

7) Push the shaft through the hub and pillow block, making sure that the locking feature is engaged between shaft and the hub. Install appropriate number of washer spacers outside of the pillow block on the shaft.

8) Install the gear outside of the spacers. Using appropriate tools, space the gear approximately 0.010" off of the washers. Tighten the set screws.

9) Install the spacer in the left side hub and push the selected MDR shell into the o-ring.

10) Screw the selected core onto the threaded shaft. Push the shell into the right side hub to enclose the MDR vessel.

11) Install the ultem optical sensor mounts with optical rings onto the shafts on each end of the bioreactor.

A.4 - MDR Digester Installation

1) Place the chains onto the two pulleys on either end of the MDR.

2) Lower the vessel vertically and level onto the alignment pins on the motor mounts.

3) Install the two Philips-head screws in each pillow block just to snug.

4) Pull the two drive chains onto the drive sprockets.

5) Tighten the two screws on either end of the MDR that tighten the chains. Raise the set screws then drop the sprockets down by tightening the tuning screws until the chain is slightly slack (neither tight nor loose). Once the pinions are in place, gently snug the set screw (make sure that the motor is not being pulled or cocked at an angle due to loading).

Appendix B: Minimum External Wiring*
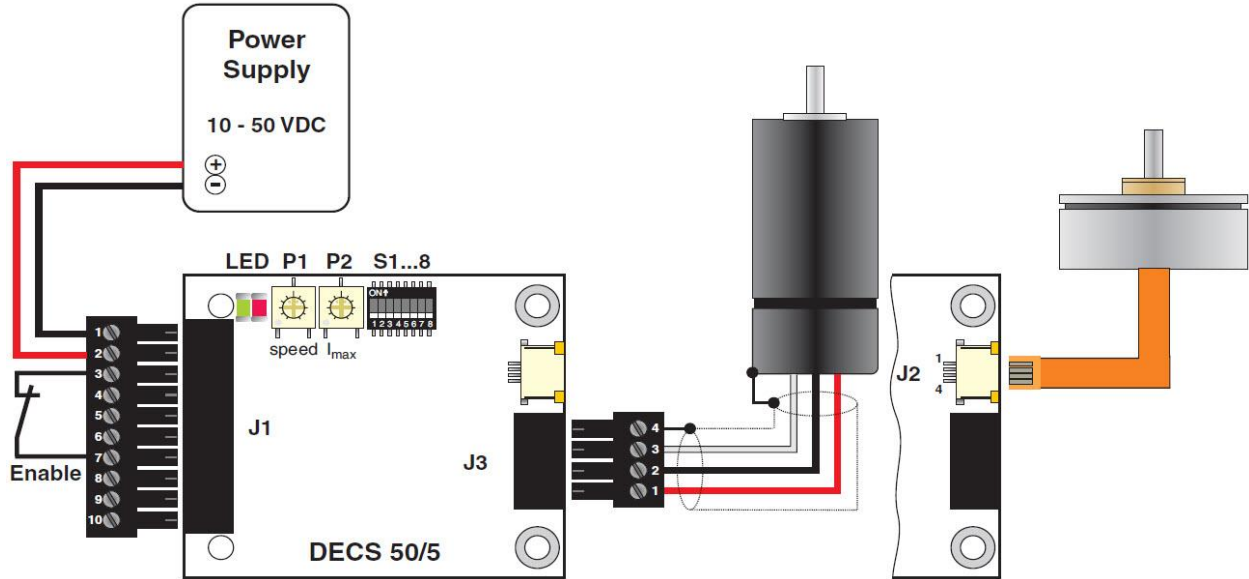
Pin assignment J1:

1. Power GND
2. +Vcc 10...50 VDC
3. Enable
4. Direction
5. Brake
6. Set value speed
7. +5 VDC OUT
8. Gnd
9. Monitor n
10. Ready

Pin assignment J3:

4. Cable shield
3. Motor winding 3
2. Motor winding 2
1. Motor winding 1

Pin assignment J2:

1. Motor winding 1
2. Motor winding 2
3. Motor winding 3
4. Neutral point Y (not used)

Figure B.1 – The diagram of Maxon motor connecting with motor control board.

(http://www.maxonmotorusa.com/maxon/view/product/control/1-Q-EC-Verstaerker/343253)

# Appendix C: The Interface of Fluent Simulations
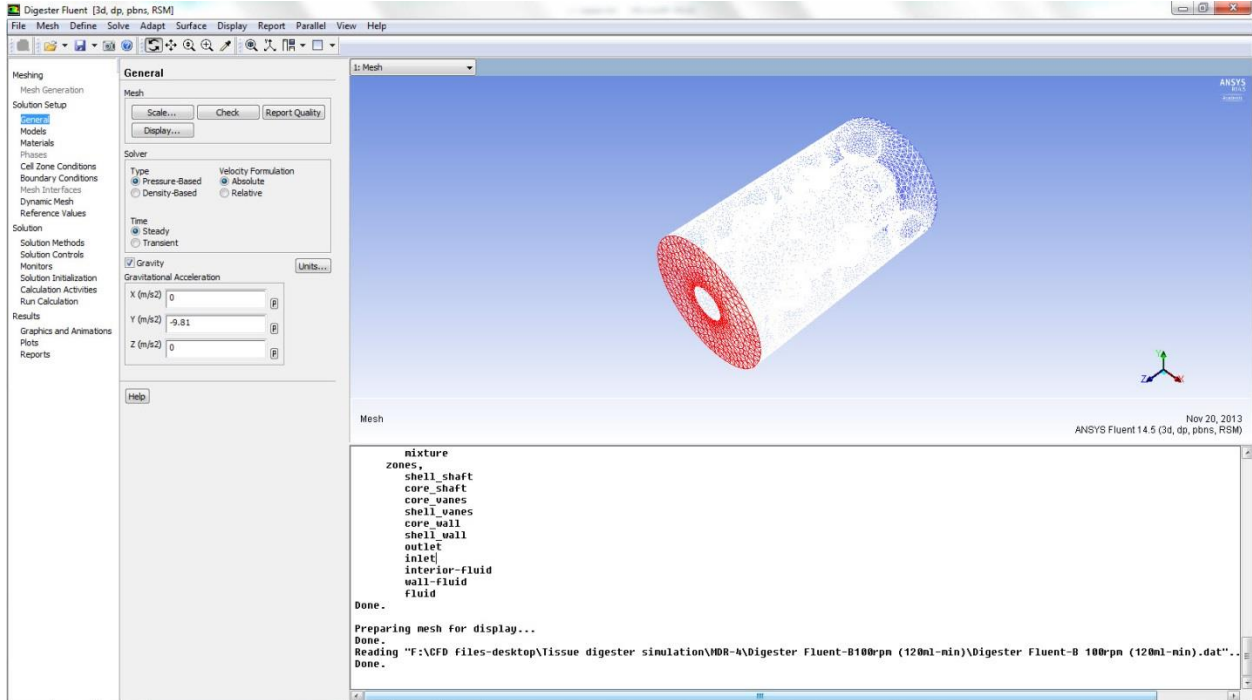
Figure C.1 – Screenshot of ANSYS Fluent 14.5 software.
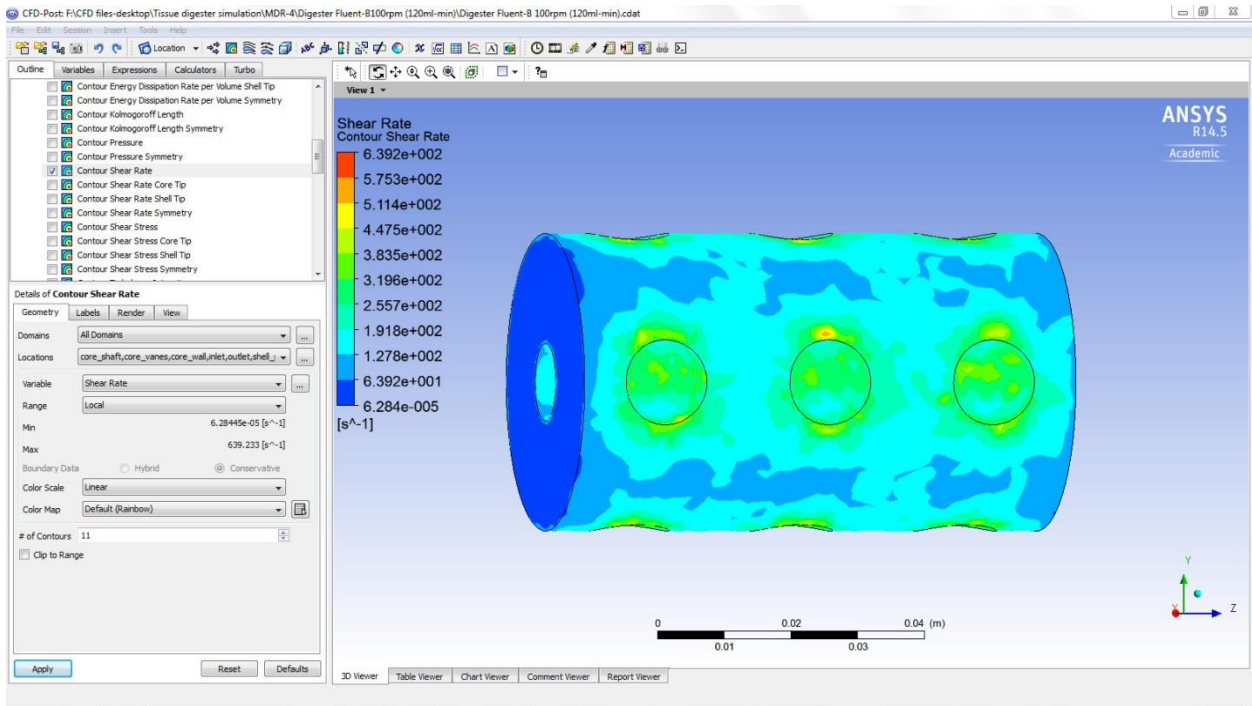
Figure C.2 – Screenshot of ANSYS CFD-Post 14.5 software.

Appendix D: Particle Tracking Test
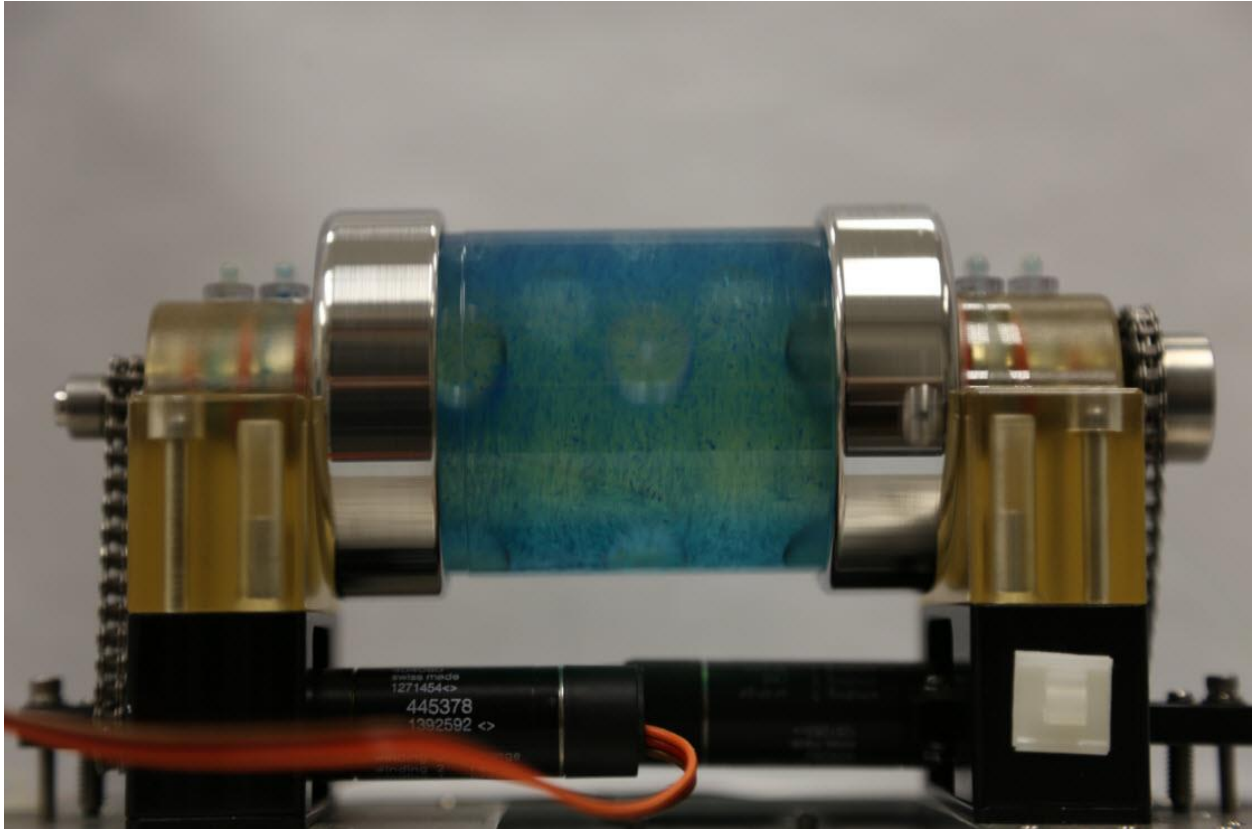
Figure D.1 – The original time-exposure photography of stained tissue fragments.

Figure D.2 – Screenshot of Image-Pro Premier software (Media Cybernetics internet source).

Appendix E: Product Information - Cultispher-G*

E.1 - Product Description

Cultispher-G is designed to be used in stirred systems, for small scale spinners and in large scale tank reactors. Cultispher-G microcarriers can be used in virtually any type of traditional culture vessel. The best results are obtained when using vessels which give even suspension of the microcarriers with gentle stirring. Suitable vessels for small scale culture include those based on rod-stirring (Techne Ltd., Cambridge, UK) or a suspended Teflon-coated bar magnet (Bellco Glass Inc., Vineland, NJ, USA; Wheaton Scientific, Millville, NJ, USA). Equipment for large scale culture, especially designed for microcarriers, is available from most fermenter manufacturers. Cultispher-G is based on a highly cross-linked gelatin matrix which results in excellent mechanical and thermal stability.

E.2 - Preparation

Rehydration: The dry microcarriers are swollen and hydrated in calcium and magnesium free PBS (50 ml/g dry Cultispher-G) for at least 1 hour at room temperature. Some of the beads might float at first, but autoclaving will expel any air trapped in the beads allowing them to settle.

Sterilization: Without removing the PBS, the microcarriers are sterilized by autoclaving (for instance 121 °C, 15 min, 15 psi).

Washing: Remove the PBS by suction, add new PBS (50 ml/g dry Cultispher-G) and mix. Repeat the washing twice with culture medium.

Storage: Sterilized microcarriers may be stored at 4 °C for 1 month.

(http://www.sigmaaldrich.com/catalog/product/sigma/m9418?lang=en&region=US)

References

Andereck CD, Liu SS, Swinney HL. Flow regimes in a circular Couette system with independently rotating cylinders. Journal of Fluid Mechanics. 1986, 164: p155–183.

Armenante, P. H., Chang, G. M. Industrial and Engineering Chemistry Research. 1998, 37: p284.

Begley, C. M., Kleis, S. J. The fluid dynamic and shear environment in the NASA/JSC rotating-wall perfused-vessel bioreactor. Biotechnology and Bioengineering [J]. 2000, 70(1): p32-40.

Begley, C. M., Kleis, S. J. RWPV bioreactor mass transport: earth-based and in microgravity. Biotechnology and Bioengineering. 2002, 80 (4): p465-476.

Buchs, J., Maier, U., Milbradt, C., Zoels, B. Power Consumption in Shaking Flasks on Rotary Shaking Machines: I. Power Consumption Measurement in Unbaffled Flasks at Low Liquid Viscosity. Biotechnology and Bioengineering [J]. 2000, 68(6), p590.

Buchs, J., Maier, U., Milbradt, C., Zoels, B. Power Consumption in Shaking Flasks on Rotary Shaking Machines: II. Nondimensional description of specific power consumption and flow regimes in unbaffled flasks at elevated liquid viscosity. Biotechnology and Bioengineering [J]. 2000, 68(6), p596.

Chiampo, F., Guglielmetti, R. Manna, L. Conti, R. Proceedings of 7th European Congress on Mixing, Brugge, Belgium, 1991, p333.

de los Santos, B., Shiragami, N., Unno, H., Kariya, M. A model for microcarrier motion inside a horizontally rotating bioreactor for animal cell culture. Bioprocess Engineering 1994, 11, p115-120.

Dubois, C.; Thibault, F.; Tanguy, P. A.; Ait-Kadi, A. Institution of Chemical Engineers Symposium Series. 140 (1996) pp. 249-258.

Gao, H. Ayyaswamy, P. S., Ducheyne, P. Dynamics of a microcarrier particle in the simulated microgravity environment of a rotating wall vessel, Microgravity Science and Technology. X/3 (1997) 154–165.

Gill, N. K., Appleton, M., Baganz, F., Lye, G. J. Quantification of power consumption and oxygen transfer characteristics of a stirred miniature bioreactor for predictive fermentation scale-up. Biotechnology and Bioengineering. 2008, 100 (6): p1144-1155.

Goodwin TJ, Prewett TL, Wolf DA, and Spaulding GF. Reduced shear stress: a major component in the ability of mammalian tissues to form three-dimensional assemblies in simulated microgravity. Journal of cellular biochemistry.1993, 51: p301–311.

Goodwin TJ, Wolf DA, Spaulding GF, and Prewett TL (Inventors). Method for Producing Non-Neoplastic, Three-Dimensional Mammalian Tissue and Cell Aggregates Under Microgravity Culture Conditions and the Products Produced Therefrom. US patent 5496722. 5 March 1996.

Gray DWR, McShane P, Grant A, Morris PJ. A method for isolation of islets of Langerhans from the human pancreas. Diabetes 33: 1055-1061, 1984.

Guezennec YG, Brodkey RS, Trigui N, Kent JC. Algorithms for fully automated three-dimensional particle tracking velocimetry. Experiments in fluids [J]. 1994, 17: 209-219.

Hammond, T. G., and Hammond, J. M. Optimized suspension culture: the rotating-wall vessel (Invited review). American Journal of Physiology. Renal Physiology. 281: F12–F25, 2001.

Harrison, R. G., Todd, P. W., Rudge, S. R. Bioseparations Science and Engineering, 2nd Ed. Oxford, 2003, p250-255.

Horaguchi A, Merrell RC. Preparation of viable islet cells from dogs by a new method. Diabetes 30: 455-458, 1981.

http://www.ikotech.com/HD-MCTV.html

Hudcova, V., Machon, V., Nienow, A. W. Biotechnology and Bioengineering. 1989, 34: p617.

Iwashita, C., Asano, T., Kenmochi, T., Jingu, T., Uematsu, T., Nakagohri, T., Hasegawa, M. Maruyama, M., Miyauchi, H., and Isono, K. Combined method of mechanical chopper and automated two-step digestion technique for islet isolation from canine pancreas. Transplantation Proceedings. 1996, 28(1), p337.

Kleis SJ, Schreck S, and Nerem RM. A viscous pump bioreactor. Biotech Bioeng 36: 771–777, 1990.

Lacy PE, Kostianovsky M. Method for the isolation of intact islets of Langerhans from the rat pancreas. Diabetes 16: 35-39, 1967.

Liu, T., Li, X., Sun, X., Ma, X., Cui, Z. Analysis on forces and movement of cultivated particles in a rotating wall vessel bioreactor [J]. Biochemical Engineering 18 (2004): p97-104.

Markopoulos, J., Kontogeorgaki, E. Chemical Engineering and Technology. 1995, 18: p68.

Markopoulos. J. Chemical Engineering and Technology. 1996, 68: p796.

Markopoulos, J. Pantuflas, E. Chemical Engineering and Technology. 2001, 24: p1147.

Moskalewski S. Isolation and culture of the islets of Langerhans of the guinea pig. General and comparative endocrinology 5: 342-353, 1965.

Nakamura, M. Zborowski, M., Lasky, L. C., Margel, S., Chalmers, J. J. Theoretical and experimental analysis of the accuracy and reproducibility of cell tracking velocimetry. Experiments in Fluids [J]. 2001, 30: 371-380.

Noel J, Rabinovitch A, Olson L, et al. A method for large scale high-yield isolation of canine pancreatic islets of Langerhans, Metabolism 31: 184-187, 1982.

Papoutsakis, E. T. Fluid-mechanical damage of animal cells in bioreactors. TBTECH December, 1991, Vol 9, p428.

Qiu, Q. Q., Ducheyne, P., Ayyaswamy, P. S. Fabrication, characterization and evaluation of bioceramic hollow microspheres used as microcarriers for 3D bone tissue formation in rotating bioreactors, Biomaterials 20 (1999) 989–1001.

Ricordi C, Lacy PE, Finke EH, et al. Automated method for isolation of human pancreatic islets. Diabetes 37: 413-420, 1988.

Rivera-Solorio, I., Kleis, S. J. Model of the mass transport to the surface of animal cells cultured in a rotating bioreactor operated in micro gravity. Biotechnology and Bioengineering [J], 2006, 94(3), p496.

Robert CM, Andrew GB, Michael LG, Francis ED. Tissue dissociation enzymes used for isolating islets for clinical transplantation: factors to consider in setting acceptance criteria. VitaCyte report.

Rousseaux, J. M., Muhr, H., Plasari, E. The Canadian Journal of Chemical Engineering. 2000, 78: p650.

Sanchez Perez, J. A., Rodriguez Porcel, E. M., Casas Lopez, J. L., et al. Shear rate in stirred tank and bubble column bioreactors. Chemical Engineering Journal [J]. 2006, 124, p2.

Tatterson, G. B., Scale-up and Design of Industrial Mixing Processes, McGraw-Hill, New York 1994, pp. 53-90, 114-124, 191.

Todd P, Klaus DM, Stodieck LS, Smith JD, Staehelin LA, Kacena M, Manfredi B, and Bukhari A. Cellular responses to gravity: extracellular, intracellular and in-between. Adv Space Res 21: 1263–1268, 1998.

Todd, P., Hodapp, L., Jones, A., Kennedy, D., Popson, T., Taylor, E. Robotic Bioreactor for Cell Culture in Space Applications (Dynacult). Final Progress Report. 2004, p1-119.

Vosscheperkeuter GH, Vansuylichem P.T.R, Vonk M.W.A, Wolters G.H.J, and Vanschilfgaarde R. Histochemical analysis of the role of class I and class II clostridium histolyticum collagenase in the degradation of rat pancreatic extracellular matrix for islet isolation. Cell Transplantation 6: 403-412, 1997.

Warnock GL, Ellis D, Rajotte RV, et al. Studies of the isolation and viability of human islets of Langerhans. Transplantation 45: 957-963, 1988.

Wolters G.H., Vos-Scheperkeuter G.H., Van Deijnen J.H., and Van Schilfgaarde R. An analysis of the role of collagenase and protease in the enzymatic dissociation of the rat pancreas for islet isolation. Diabetologia. 35: 735-742, 1992.

Yu, P., Lee, T. S., Zeng, Y., Low, H. T. Fluid dynamics of a micro-bioreactor for tissue engineering. Tech Science Press [J]. 2005, 1(3), p243.

Vita

Zhongliang Lu was born in Dalian, China, the only son of Wei Lu and Shu Zou. He graduated from Dalian University of Technology, Dalian, China, in the summer of 2005 obtaining his bachelor's degree of bioengineering. In fall 2005 he was awarded the Yungen Zhuang Scholarship to attend Zhejiang University in Hangzhou, China. While pursuing a master's degree of biochemical engineering, he was involved in a team-oriented project "Studies on Preparation and Application of γ-Poly Glutamic Acid" and collaborated with team members to achieve the encouraging results: the yield of targeted products was increased by 80 per cent by establishing the effective separation of γ-poly glutamic acid from highly viscous culture broth. The ultrafiltration technology is the key point applied to the polymer concentration thereby reducing the amount of precipitant for polymer extraction and the cost of separation process.

In the fall of 2008, Zhongliang entered the Ph. D. program at Auburn University. He accepted a graduate research assistantship in Dr. Thomas Hanley's research group and was selected for a multidisciplinary project, collaborating with Dr. Paul Todd at Techshot Inc., Greenville, Indiana. He completed a new tissue digester design for automatic digestion process applying the knowledge of chemical engineering to solve biomedical issues. He was a speaker at the AIChE conferences in 2012 and in 2013. He will graduate with a PhD degree in chemical engineering in the fall of 2013.